Studies of the Hydrides of the Heavier Group 14 Elements

Daniel Hugh Brown

A thesis submitted in fulfilment of the requirements
for the degree of Doctor of Philosophy
to the
University of Edinburgh
1998

Declaration

This thesis has been composed by myself and it has not been submitted in any previous application for a degree. The work reported within was executed by myself, unless otherwise stated.

May 1998

Abstract

The chemistry of some simple tin hydrides $(CH_3)_{4-x}SnH_x$ (x = 1–4) has been investigated with particular reference to their reactivity towards the reagents NaH, KH, alkyl lithium compounds, and the ylids Me_3PCH_2 and Ph_3PCH_2. It has been found that the reaction between the stannanes and alkali metal hydrides or the ylids produces salts containing the respective stannyl anions, $[Sn(CH_3)_{3-x}H_x]^-$ (x = 0–3). These salts have been characterised by low temperature infrared spectroscopy, the results of which are in good agreement with the results of *ab initio* calculations. In contrast, reactions involving alkyl lithium compounds proceed by transmetallation with elimination of LiH and alkylation of the tin centre.

The technique of *in situ* crystal growth at low temperatures has been used to obtain X-ray crystal structures of Me_3PCH_2, Me_2SnH_2 and Me_3SnH. The structure of the ylid in the solid phase has been shown to resemble the calculated structure of a transition state involving rotation of the CH_2 group about the P-C axis.

The reaction between monochlorostannane and sodium metal produced small quantities of Sn_2H_6, detected by mass spectrometry. Attempts to increase the scale of this preparation were unsuccessful. Gas phase electron diffraction data were recorded for monochlorostannane but subsequent refinement showed that some decomposition of the sample had occurred giving rise to SnH_2Cl_2.

The structure of Me_3PbH was investigated by powder neutron diffraction and gas phase electron diffraction. Rietveld refinement of the neutron diffraction data based on an extant single crystal structure of Me_3PbH was unsuccessful owing to inconsistencies between the two data sets, most probably stemming from the different temperatures at which they were collected. The gas phase experiment was partially successful, but data collected at the short camera distance, and crucial to an accurate structural determination, could not reasonably be refined in conjunction with that collected at the long camera distance. No reliable gas phase structure of Me_3PbH has yet been determined.

To Mum and Dad

Acknowledgments

I should like to thank the following for their contributions to this thesis, and all that lead up to it,

My supervisor, Dr. Colin Pulham, for his advice, wisdom, and willingness to let me follow my own route through the wilds of this doctorate.

Professor David Rice and Dr. Elizabeth Page for their hospitality in Reading.

Drs. Bruce Smart, Paul Brain, and Simon Parsons for their patient guidance through the worlds of *ab initio* calculation, electron diffraction, and X-ray crystallography.

Members past and present of the Pulham and Rankin groups, for being there, just in case.

This thesis was written and typeset using LaTeX2e on an Acorn RiscPC running NetBSD 1.2, RiscOS 3.7, and Windows 3.11.

Notes

1 Torr = 1mmHg = 133.3 Pa

1 atmosphere = 101325 Pa

1 Hartree, $E_H \approx 4.36 \times 10^{-18}$ J

The following abbreviations are used in the text:

Me: Methyl, -CH_3

Et: Ethyl, -CH_2CH_3

^{i}Pr: Isopropyl, -$CH(CH_3)_2$

Bu: Butyl, -$CH_2CH_2CH_2CH_3$

Ph: Phenyl, -C_6H_5

Bz: Benzyl, -$CH_2C_6H_5$

TMEDA: Tetramethylethylenediamine, $(Me_2NCH_2)_2$

PMDETA: Pentamethyltriethylenediamine, $(Me_2NCH_2CH_2)_2NMe$

2,2,2-crypt: The cryptand, $N(CH_2CH_2NHCH_2CH_2NHCH_2CH_2)_3N$

NMR: Nuclear Magnetic Resonance

ESR: Electron Spin Resonance

GED: Gas-phase Electron Diffraction

NMR data are expressed in accordance with the chemical shift convention outlined by IUPAC, *i.e.* a positive chemical shift denotes a positive frequency and *vice versa* with respect to the designated reference substance,

^{1}H, ^{13}C NMR spectra referenced to tetramethylsilane

^{31}P NMR spectra referenced to 85% H_3PO_4

^{119}Sn NMR spectra referenced to Me_4Sn

The following abbreviations are used in the tabulation of spectra :

s: strong, m: medium, w: weak, v: very, br: broad.

sh: shoulder, ν: stretching mode, δ: deformation mode, ρ: rocking mode.

Contents

List of Figures

List of Tables

Chapter 1

Introduction

The chemistry of stannane, SnH_4, and its derivatives began in Germany at the close of the First World War, through the experimental ingenuity and remarkable persistence of Fritz Paneth, and co-workers.[1–3] Since then, the use and application of stannane derivatives has become widespread in the chemical industry in such diverse roles as marine antifoulants, poly-(vinyl chloride) stabilisers, and as fungi- and bacteri-cides.[4]

Excellent reviews of the organometallic chemistry of tin have appeared elsewhere,[5,6] and so no attempt shall be made to reproduce such accounts here. Also, as the work presented in this thesis comprises a series of relatively independent investigations into synthetic and structural aspects of tin and lead chemistry, the themes and species explored are best introduced in detail at the beginnings of their respective chapters. Here, we limit ourselves to a presentation of aspects of organotin chemistry of general relevance, and describe the initial aims of the research that culminated in the production of this thesis.

1.1 Stannanes

Stannane, SnH_4, was first synthesised by Paneth by cathodic reduction of aqueous tin(II) sulphate.[2,3] Reaction times between two days and a week were employed to generate sufficient stannane to enable vapour pressure measurements to be performed, and an analysis by decomposition to be attempted. The equipment

required, the large currents employed, and the tiny rate of stannane generation (averaging 0.1 ml per electrolytic cell per hour) were sufficient to discourage others from continuing Paneth's work, leaving a gap of some twenty years before stannane was once again prepared, though this time in high yield through the use of the newly discovered reagent lithium aluminium hydride,[7–9]

$$SnCl_4 + LiAlH_4 \xrightarrow{Et_2O} SnH_4 + \ldots \quad (1)$$

Stannane is a colourless gas at room temperature, boiling at -52°C, and melting at -150°C,[10] and is easily handled by high vacuum line techniques. Its thermal decomposition is catalysed by the presence of metallic impurities, including tin metal itself, and so it must be stored at room temperature in the presence of a small amount of oxygen, or pure as the solid in liquid nitrogen.[7,11]

Organostannanes may be prepared in a similar fashion from the appropriate halide, and organodistannanes by the coupling of halides in the presence of sodium, or through the use of a tin-lithium, or a tin-sodium compound,[5]

$$R_3SnX + LiAlH_4 \longrightarrow R_3SnH + \ldots \quad (2)$$

$$2\ R_3SnX + 2\ Na \longrightarrow R_3Sn\text{–}SnR_3 + 2\ NaX \quad (3)$$

$$R_3SnX + LiSnR'_3 \longrightarrow R_3Sn\text{–}SnR'_3 + LiX \quad (4)$$

The formation of distannane, $H_3Sn\text{-}SnH_3$, was first reported in 1961 by Jolly as a byproduct of an aqueous stannane preparation,[12]

$$SnO_2^- + BH_4^- \xrightarrow{6M\ HCl(aq.)} SnH_4 + Sn_2H_6 + \ldots \quad (5)$$

Recently, distannane has also been detected mass spectrometrically after UV irradiation of stannane in the gas phase.[13] Neither preparation gave significant yields, and therefore little structural information is currently available concerning the simplest isolable compound containing a Sn–Sn bond.

However, compounds containing a tin–tin bond are well represented. Cyclic species containing $(R_2Sn)_n$ where n = 3,[14] 4,[15–18] and 6,[19] are well characterised, as are species containing Sn–Sn chains.[20,21] Recently, the first tin propellane was prepared,[22,23] and polystannides, containing the Sn_5^{2-} and Sn_9^{4-} anions,

are also known.[24,25] Estimates for the tin–tin bond enthalpy range from around 220 kJ mol^{-1} to 35 kJ mol^{-1} depending upon the degree of steric hindrance about the tin atoms.[6] The extreme thermal instability of distannane[13] is not therefore due to an intrinsic weakness of the tin–tin bond, but more probably to a number of other factors, including the small steric bulk of the hydride ligand, the weakness of the Sn–H bond, and the ease with which H_2 may be eliminated from the molecule.

1.2 The Methylstannanes

The preparation of the first alkyl derivative of stannane was reported by Kraus and Greer[26] in 1922, soon after Paneth established the existence of stannane itself. Trimethylstannane was prepared in liquid ammonia solution by the action of ammonium nitrate on Me_3SnNa,

$$Me_3SnCl + 2\ Na \xrightarrow{\text{liq. } NH_3} Me_3SnNa + NaCl \qquad (6)$$

$$Me_3Sn^- + NH_4^+ \xrightarrow{\text{liq. } NH_3} Me_3SnH + NH_3 \qquad (7)$$

The vapour pressure curve, boiling point, and molecular weight of trimethylstannane were determined and confirmed by Finholt *et al.*, some 25 years later.

The preparations of dimethyl- and methyl-stannane were to wait until lithium aluminium hydride became available, but investigation into the chemistry of the organotin halides continued. In 1925, Kraus and Greer[27] reported the synthesis of Me_2SnNa_2 and $(Me_2Sn)_x$ by reduction of the dihalide by sodium in liquid ammonia.

$$Me_2SnBr_2 + 2\ Na \xrightarrow{\text{liq. } NH_3} (Me_2Sn)_x + 2\ NaBr \qquad (8)$$

$$(Me_2Sn)_x + 2\ Na \xrightarrow{\text{liq. } NH_3} Me_2SnNa_2 \qquad (9)$$

They described the polymer as "a yellow solid, insoluble in organic and inorganic solvents, and oxidising readily", a description confirmed by Kettle[28] in 1959. Since then, a number of cyclic $(R_2Sn)_x$ species have been prepared the colour of which depending significantly on the nature of R, and the number of links in the

Sn–Sn chain. For example, $(Bz_2Sn)_6$ is pale yellow, while $(Ph_2Sn)_6$ is colourless,[19] and $(Ar_2Sn)_3$ and $(Ar_2Sn)_2$, where Ar = $^iPr_3C_6H_2$, are orange and red respectively.[29] The propellane Sn≡$(SnAr_2)_3$≡Sn, where Ar = 2,6-diethylphenyl, can also be regarded as a product of the fusion of 3 four-membered rings, and is deep blue.[22]

Later in 1925, Kraus and Sessions[30] also characterised hexamethylditin, produced by reaction of trimethyltin bromide with just one equivalent of sodium, rather than the two equivalents used to prepare Me_3Sn^-,

$$2\ Me_3SnBr + 2\ Na \xrightarrow{\text{liq. } NH_3} Me_3SnSnMe_3 + 2\ NaBr \qquad (10)$$

They described it as "a mobile liquid above its melting point of 23°C, which cannot be distilled in air since the hot vapours flash in the condenser". Current research[5] confirms their melting point, and estimates the Sn–Sn bond enthalpy at between 210 and 240 kJ mol^{-1}.

The structures of Me_3SnH and Me_2SnH_2 have been investigated in the gas phase by electron diffraction,[31] and that of $MeSnH_3$ by microwave spectroscopy.[32] However, little is known about the solid state structures of these compounds, most probably owing to their very low melting points.

1.3 Stannylmetallic Compounds

Organotin derivatives of the alkali metals have been prepared by reaction of R_3SnX, R_3SnH, or $R_3SnSnR'_3$ with an alkali metal in an electron transfer reaction.[6] RLi also reacts with R'_3SnH or R'_3Sn–SnR'_3 to give R'_3SnLi, where R′ = Bu, Ph.

The crystal structure of Ph_3Sn^- K[18-crown-6]$^+$ has been solved, and found to contain isolated pyramidal Ph_3Sn^- anions.[33] If lithium and PMDETA are used instead, subsequent crystallographic investigation reveals the formation of Ph_3SnLi[PMDETA], containing a Sn–Li bond that has been shown to persist in solution through the observation of a $^{117/119}$Sn-Li coupling by ^{7}Li NMR spectroscopy.[34]

Organotin–lithium compounds have been much exploited in the formation of Sn–C bonds by reaction with organic halides and other electrophiles,[6]

$$RX + R'_3SnM \longrightarrow R'_3SnR + MX \qquad (11)$$

However, the chemistry of H_3Sn^-, RH_2Sn^-, and R_2HSn^- has been little explored.

The decomposition of R_3SnLi in solution has been studied in some detail by Kobayashi *et al.*.[35,36] They noticed that if R_3SnX and lithium metal were combined in tetrahydrofuran solution, yields of R_3Sn^- were low if an excess of the halide was used. This they attribute to the presence of R_3SnSnR_3, formed by the reaction of R_3Sn^- with R_3SnX,

$$R_3SnX + R_3Sn^- \longrightarrow R_3SnSnR_3 + X^- \qquad (12)$$

Mixtures formed by adding R_3SnSnR_3 to R_3SnLi were observed to decompose much more rapidly than solutions containing R_3SnLi only.

1.4 The Methylplumbanes

Of all the hydrides of the Group 14 elements, those of lead are the least studied, and the most poorly characterised. This is in part due to the extreme care with which they must be handled and to the difficulties in preparing them. Trimethyllead hydride, Me_3PbH, is highly thermally fragile and highly toxic, and the dihydride, Me_2PbH_2, also decomposes explosively on warming.[37]

The first synthesis of Me_3PbH was reported in 1959 by Duffy and Holliday,[38] as a product of the reaction of Me_3PbCl and KBH_4 in liquid ammonia,

$$Me_3PbCl + KBH_4 \xrightarrow{NH_3(l)} Me_3PbBH_4.xNH_3 + \ldots \qquad (13)$$

$$Me_3PbBH_4.xNH_3 \xrightarrow{\Delta} Me_3PbH + (x-1)NH_3 + H_3N.BH_3 \qquad (14)$$

Independently, Becker and Cook,[39] and Amberger[37] reported an improved synthesis in the following year using lithium aluminium hydride as the reducing agent. Amberger also detailed the synthesis of the dihydride, Me_2PbH_2,

$$Me_2PbX_2 + LiAlH_4 \xrightarrow{\text{-90 to -110°C, X=Br or Cl}} Me_2PbH_2 + \ldots \qquad (15)$$

Dimethyl- and trimethyl-plumbane were characterised mainly by elemental analysis of their decomposition products, although evidence for a Pb–H bond in trimethylplumbane was gleaned from a proton NMR spectrum obtained by Duffy *et al.*[40] of the liquid at -70°C. A broad singlet was observed and assigned to the three methyl groups in the molecule and two unresolved multiplets at significantly lower field, whose combined intensity was roughly one ninth that of the methyl peak were assigned to the Pb–H proton. They accounted for the presence of two distinct Pb–H resonances by suggesting an equilibrium in the neat liquid in which two distinct environments are created for hydrogen bound directly to lead,

$$2\ Me_3PbH \xrightarrow{-70°C} [Me_3Pb]^- + [Me_3PbH_2]^+ \qquad (16)$$

Amberger also studied the infra-red spectrum of the molecule, although it is not clear for which phase this was recorded, and assigned a band at 1709 cm^{-1} to the Pb–H stretch.[37]

A decomposition study of Me_3PbD was performed by Becker *et al.*,[39] in which the major deuterated products were D_2 and MeD, leaving undeuterated Me_4Pb as the remaining alkyltin species. No HD and MeH were observed, suggesting that decomposition occurred *via* a free radical pathway in which the first step was the homolysis of the Pb–H bond,

$$Me_3PbH \xrightarrow{\Delta} Me_3Pb\cdot + H\cdot \qquad (17)$$

In the following thirty-five years, no other studies of the methyllead hydrides were reported. Although the evidence accumulated for their synthesis was overwhelming, no significant structural study was performed, most probably due to the experimental difficulties inherent in their synthesis and manipulation. No detailed determination of the structure of either hydride was reported, and no information at all was presented on the length of the Pb–H bond.

1.5 Aims of the Present Research

The aims of this research were as follows,

1. To develop a synthesis of distannane of sufficiently high yield to enable a structural investigation of the compound by gas phase electron diffraction.

2. To synthesise and structurally characterise salts containing the stannyl anions $Me_xSnH_{3-x}^-$ (x = 0–3).

3. To investigate the use of these anions in syntheses of compounds containing bonds between tin and other main group elements, such as gallium, indium, and silicon.

4. To determine the structures of the stannanes Me_xSnH_{4-x} (x = 0–3) in the solid state.

5. To begin the structural characterisation of the methylplumbanes by investigating the structure of Me_3PbH in both solid and gas phases.

Chapter 2

Experimental Techniques

This chapter describes the general techniques and the reagents used throughout this investigation. A number of more specialised methods of structural analysis have also been applied in this work and are presented in detail in the text preceding their application.

2.1 The Manipulation of Air Sensitive and Temperature Sensitive Compounds

The majority of the compounds handled in this investigation were sensitive to air, moisture, and sometimes temperature, and so required the use of specialised techniques for their manipulation. A general description of such techniques is not warranted here as a good account may be found elsewhere,[41] and so this account will confine itself to a description of the apparatus used, and the manner of its application.

Air-sensitive solids were handled using a Vacuum/Atmospheres dry box possessing an evacuable port for the introduction and removal of samples. Oxygen and water were removed from the N_2 gas stream by recirculation through a reservoir containing copper(I) oxide and molecular sieves. Schlenk line techniques were used to handle solids and liquids, alternate evacuation and purging of apparatus with dry nitrogen allowing the manipulation of compounds subject to hydrolysis or oxidation.

However, the bulk of the compounds used in this work were highly volatile liquids or gases, more easily handled using high vacuum line techniques. The vacuum line forming the centrepiece of this work is outlined in Figure 2.1. The use of a mercury diffusion pump backed by an oil filled rotary pump allowed an ultimate pressure of around 10^{-4} Torr to be achieved. Ground glass joints permitting the attachment of further apparatus at either end of the line were lubricated with Dow Corning silicone grease, whilst Apiezon 'L' grease was used for attaching the cold trap and for the ground glass stop cocks between the line and the pumps. The remaining taps used within the vacuum line were Young's greaseless taps, chosen to ease the manipulation of materials which were soluble in, or reactive to vacuum grease.

When highly reactive, or thermally sensitive materials (such as trimethyllead hydride) were to be manipulated, glass assemblies were individually constructed with appropriately sited break-seals and constrictions, which could then be heated with a hand torch ("flamed out") under continuous pumping to remove any volatile impurities adsorbed on the inner surfaces of the glassware. Such assemblies reduced the exposure of reactive materials to vacuum grease to a minimum, and could also be cooled by the passage of a stream of cold gas over their surface, minimising the risk of thermal decomposition of the material during manipulation.

Qualititative investigations of the chemistry of materials most easily handled on the high vacuum line were generally performed using Young's tap ampoules (see Figure 2.2). Reactions solely involving volatile species were carried out by condensing solvent and reactants into an ampoule from the high vacuum line. The amounts of reactants used were measured using a combination of a measuring bulb of known volume, a Baratron pressure gauge, and the application of the ideal gas laws. The use of liquid reagents such as butyl lithium solutions required the combination of Schlenk line and high vacuum line techniques, while air sensitive solids were added in the dry box as the first stage of the manipulation.

Reactions and distillations were carried out at low temperatures through the use of 'slush' baths comprising a Dewar vessel containing a solvent cooled to its melting point by careful addition of liquid nitrogen. The slush baths used throughout this work are detailed in Table 2.1.

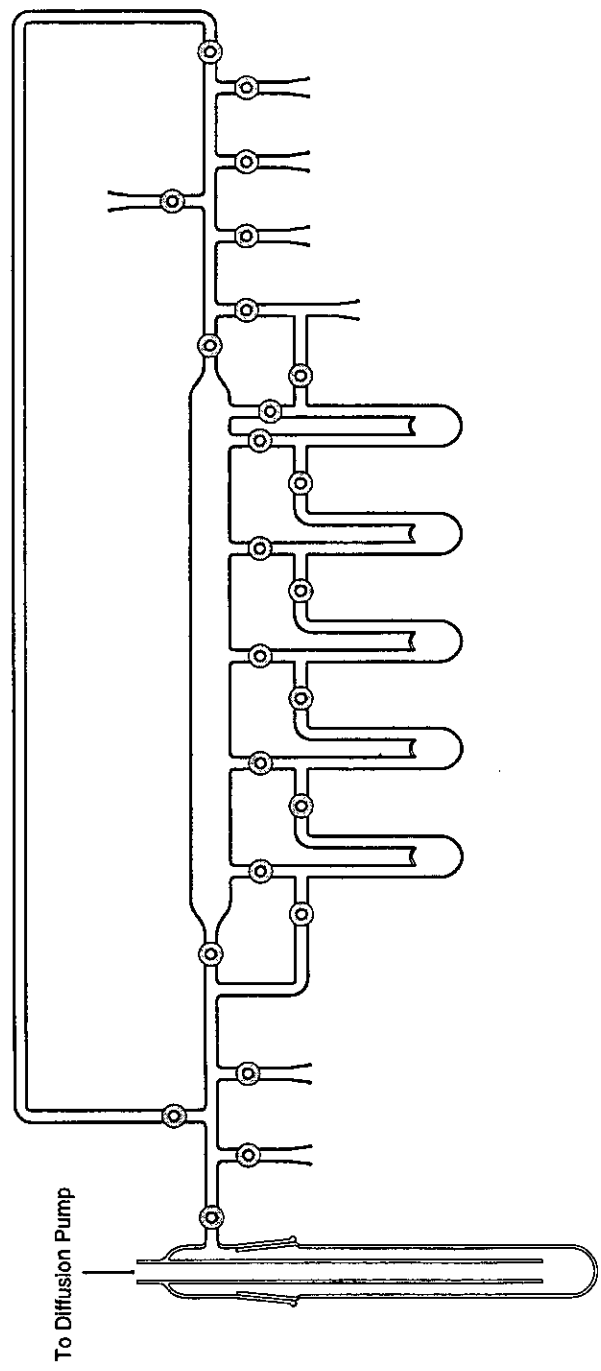

Figure 2.1. A High Vacuum line for the Handling of Air Sensitive, and Temperature Sensitive Compounds.

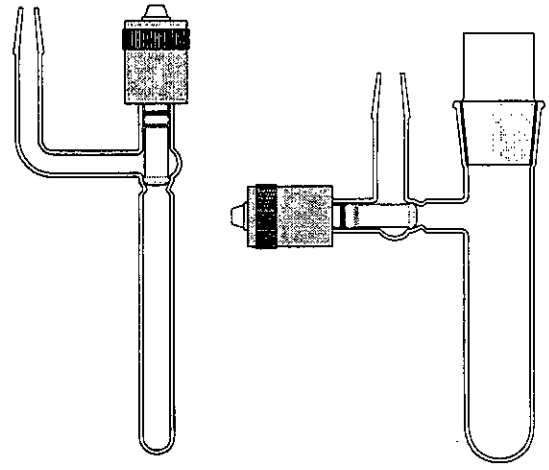

Figure 2.2. Young's Tap Ampoules for High Vacuum Line Manipulations. The smaller was used for qualitative work, and the larger for manipulations on a preparative scale.

Solvent	Temp./°C
Water	0
Bromobenzene	-31
Chlorobenzene	-45
Chloroform	-63
Acetone/dry ice	-78
Ethyl acetate	-83
Toluene	-95
Diethyl ether	-112
Methylcyclohexane	-126

Table 2.1. Solvents used for the Preparation of 'slush' baths

2.2 Analytical and Theoretical Techniques.

2.2.1 Infra-red Spectroscopy

Infra-red spectra were recorded on a Perkin Elmer Paragon 1000 FT-IR spectrometer, and saved to disc for later display and output using software developed by the author.

Stable compounds of sufficient vapour pressure were studied in a standard 10 cm gas cell fitted with caesium iodide windows, while solids were ground with dried potassium bromide, compressed, and studied as a translucent disc.

Low temperature spectra of volatile materials were recorded using the 'cold cell' shown in Figure 2.3. Sample vapours were condensed from the inlet system onto the cooled caesium iodide window, which was then rotated about the ground glass joint to the position shown in the figure. Spectra were recorded through salt windows attached to the vacuum jacket using 'black wax', above and below the cooled window.

Chemical reactions could be performed *in situ* by condensing more than one species from the inlet system onto the cooled window. By varying the temperature of the coolant, the temperature of the window could also be raised, and then subsequently lowered, allowing the formation and study of thermally fragile species by infra-red spectroscopy.

2.2.2 Ultra-violet/Visible Spectroscopy

Ultra-violet/visible spectra were recorded on a Unicam UV2 spectrometer, controlled by a neighbouring personal computer. The data collected were saved to disk for later plotting using Microsoft Excel.

Low temperature spectra were recorded using the cell shown in Figure 2.4. Samples were either condensed, or syringed into the central chamber, around which a stream of cooled nitrogen flowed allowing the sample temperature to be varied. The cryogenic assembly was surrounded by an evacuated jacket providing thermal insulation, and eliminating problems of frosting on the cell walls. Spectra were recorded through quartz windows mounted in the outer jacket which are not shown in the figure.

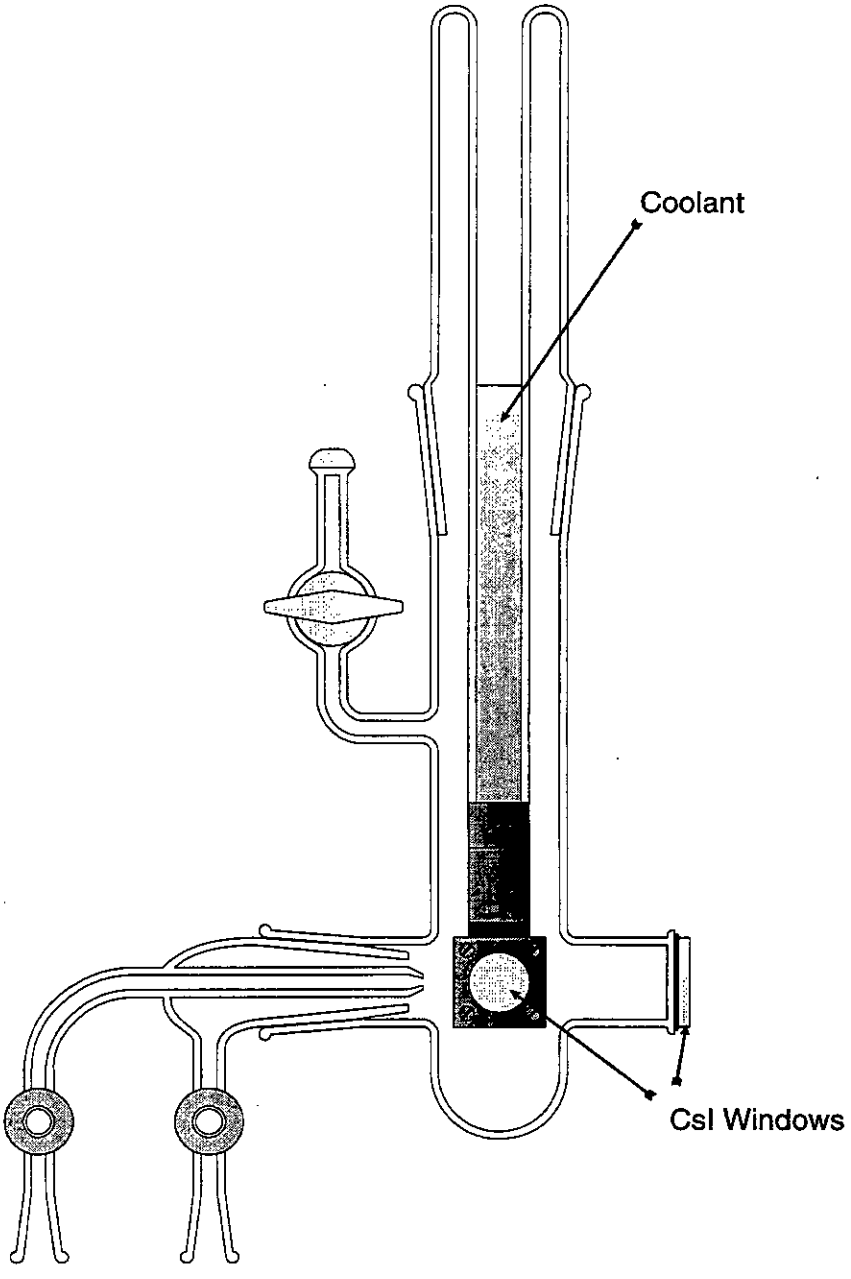

Figure 2.3. A cell for low temperature infra-red spectroscopy. Samples are condensed from the inlet nozzle onto the cold window, which is then rotated through 90° about the ground glass joint to the position shown. Spectra are recorded through salt windows built into the outer jacket (not shown).

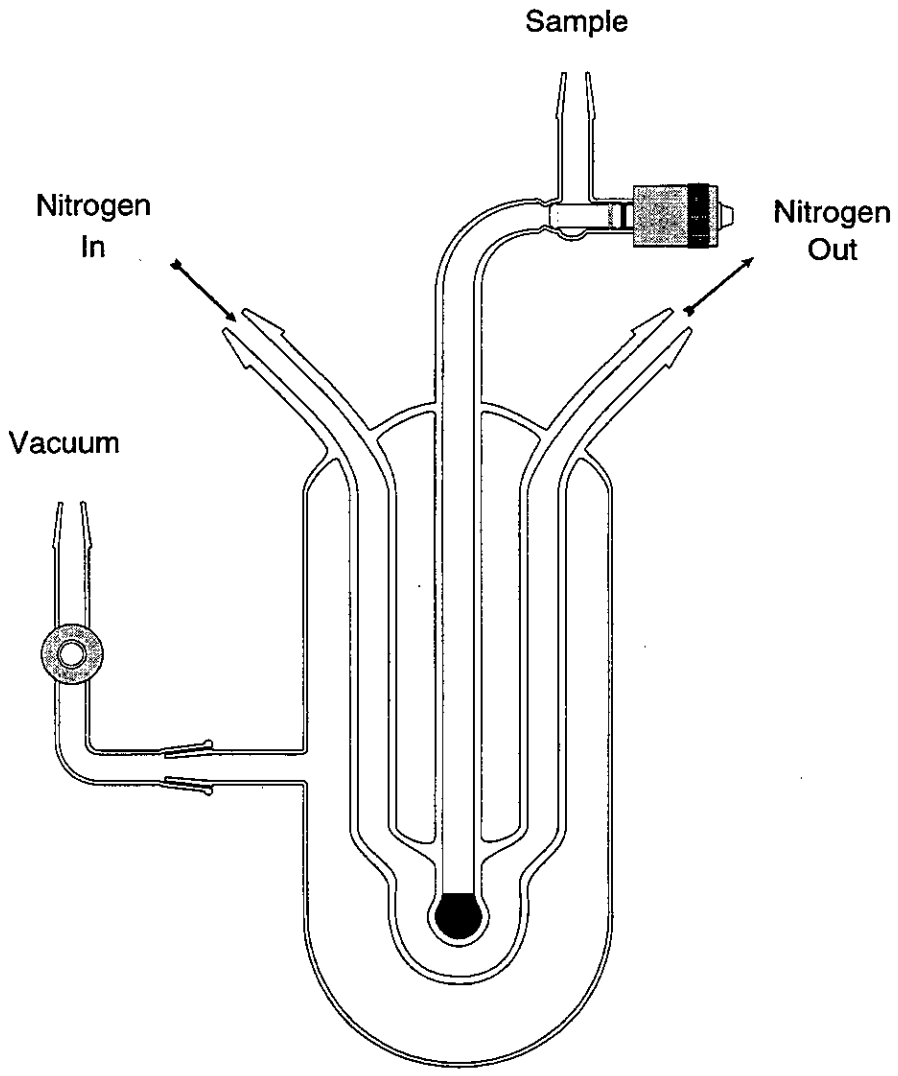

Figure 2.4. Cross Section through a Cell designed for Low Temperature Ultra-Violet/Visible Spectroscopy. The Central Sample Chamber is Viewed through Quartz Windows in the Outer Vacuum Jacket.

2.2.3 Nuclear Magnetic Resonance Measurements

NMR spectra were recorded on Bruker AC250, and WP250 FT spectrometers by the departmental service. Samples were made up within, or poured into an evacuated Pyrex 5mm glass NMR tube before sealing off under vacuum.

2.2.4 Mass Spectrometry

Mass spectra were recorded on a Hiden Analytical quadrupole mass spectrometer, with a range of 1–300 mass units. The sample ampoule was attached *via* a glass inlet and allowed to expand directly into the stainless steel spectrometer chamber. The data collected were saved to disc for later display and output using software developed by the author.

2.2.5 Theoretical Calculations

The calculations described in this work were performed using the Gaussian 94 package[42] running on a Digital AlphaServer 1000 4/200 under Digital Unix V3.2. Two styles of basis set were used to ensure that the results of calculations were obtained with the maximum computational efficiency. In the general case, pseudopotentials were introduced on heavy atoms, reducing the time required for the calculation to complete, and also improving the degree to which relativistic effects could be taken into account. In some cases, all electron calculations were also performed using basis sets of double-ζ and triple-ζ quality, to enable a critical evaluation of the results derived using pseudopotentials. The basis sets for both these types of calculations are described below.

Pseudopotential Calculations

The (valence) double-ζ pseudopotential basis sets of Hay and Wadt[43–45] supplemented with a single set of d-type polarisation functions were used for tin, lead, and chlorine (using exponents d(ζ) of 0.180, 0.172, and 0.640 respectively) while the double-ζ all-electron basis sets of Dunning[46] were used for carbon and hydrogen. This basis set is referred to hereafter as 'DZ(P)'.

All-Electron Calculations

All-electron calculations of double-ζ quality used basis sets due to Dunning taken from Ref. 46 (C, Cl, and H) and Ref. 47 (Sn), and were supplemented by a single set of d-type polarisation functions for tin and chlorine (d(ζ) = 0.18, and 0.60 respectively), and p-type polarisation functions for hydrogen (p(ζ) = 0.10). This basis set is referred to hereafter as "A-DZP".

Triple-ζ all-electron calculations were performed using a basis set for tin due to Sadlej,[48] for chlorine due to McLean and Chandler,[49] and for hydrogen due to Dunning[50] and Huzinaga.[51] These were supplemented with a single set of f-type polarisation functions for tin (f(ζ) = 0.20), d-type polarisation functions for chlorine (d(ζ) = 0.75), and p-type polarisation functions for hydrogen (p(ζ) = 0.75). This basis set is referred to hereafter as "A-TZP".

2.3 The Preparation and Purification of Essential Reagents and Solvents

The materials synthesised and studied in the course of this investigation had as precursors compounds which were not themselves readily available. These precursors were prepared from commercially available laboratory chemicals which often required purification prior to use. The solvents used throughout this work were also subject to rigorous drying procedures.

Tables 2.2 and 2.3 describe the procedures undertaken for the purification of readily available reagents and solvents. The preparation of essential reagents according to literature methods is described in Table 2.4.

Solvent	Source	Purification Procedure
Hexane	Rathburn	
Diethyl ether	Prolabo	Refluxed over CaH_2 followed
Dibutyl ether	Prolabo	by distillation, and storage
Tetrahydrofuran	Prolabo	over molecular sieves.
n-Pentane	BDH	
Toluene	Prolabo	Refluxed over Na/K, then as above.
Toluene-d_8		Trap to trap distillation
Tetrahydrofuran-d_8	Aldrich	*in vacuo* followed by storage
Benzene-d_6		over molecular sieves.
Dimethyl ether	Aldrich	Used as supplied.
D_2O	Acros	

Table 2.2. The Purification of Solvents

Compound	Source	Purification Procedure
$LiAlH_4$	Aldrich	Recrystallisation from dry diethyl ether.
TMEDA	BDH	Refluxed over CaH_2 followed by distillation and storage over molecular sieves.
N_2	BOC	Boil off from a Statebourne Cryogenics liquid N_2 dewar, dried by passage through molecular sieves.
NH_3	BOC	Condensed on sodium followed by trap to trap distillation.
Me_3SiCl	Aldrich	Trap to trap distillation followed by storage over
MeI	Aldrich	molecular sieves.
H_2	BOC	Used as supplied.
HCl	Argo	Used as supplied.
$LiAlD_4$		
CaH_2		
$P(OPh)_3$		
$Ph_3PMe^+ Br^-$		
NaO^tBu		
MeBr	Aldrich	Used as supplied.
MeI		
$SnCl_4$		
$MeSnCl_3$		
Me_2SnCl_2		
Me_3SnCl		
BuLi	Aldrich	Used as supplied (1.6 M solution in hexanes).
MeLi	Aldrich	Used as supplied (1.4 M solution in Et_2O).

Table 2.3. The Purification of Essential Reagents and Solvents

Compound	Synthetic Route	References
KH	$2\ K + H_2 \longrightarrow 2\ KH$ Courtesy of Dr. R. J. Pulham (University of Nottingham).	
NaH	$NaO^tBu + BuLi + TMEDA \xrightarrow{H_2} NaH + \ldots$ Vigorously stir reactants in hexane under hydrogen, then filter, wash with hexane/TMEDA, and warm *in vacuo*.	52
$NaNH_2$	$Na + NH_3 \xrightarrow{\text{liq. } NH_3,\ Fe_3O_4 \text{ cat.}} NaNH_2 + 1/2\ H_2$ Add catalyst to liquid ammonia, followed by sodium metal. Isolate product *in vacuo*.	53
Me_3P	$P(OPh)_3 + MeMgI \xrightarrow{Bu_2O} PMe_3 + \ldots$ Reflux in Bu_2O, separate by fractional distillation, and purify by trap to trap distillation.	54
Me_4PBr	$Me_3P + MeBr \longrightarrow Me_4PBr$ Reflux in thf on dry ice/acetone condenser, then isolate product *in vacuo*.	55
Me_3PCH_2	$Me_4PBr + KH \xrightarrow{thf} Me_3PCH_2 + KBr$ Reflux in thf, remove solvent by fractional distillation, and purify by trap to trap distillation.	55, 56, 57
Ph_3PCH_2	$[Ph_3PMe]^+Br^- + NaNH_2 \xrightarrow{thf} Ph_3PCH_2 + NaBr + NH_3$ Stir for 24 hours at room temperature. Filter, isolate product *in vacuo* then recrystallise from 40–60 Petroleum ether	58

Table 2.4. The Preparation and Purification of Essential Reagents not Commercially Available

Compound	Synthetic Route	References
SnH_4	$SnCl_4 + LiAlH_4 \xrightarrow{Et_2O} SnH_4 + \ldots$ Add ethereal solution of $LiAlH_4$ to ethereal slurry of $SnCl_4$ at -78°C, and then warm slowly to room temperature, pumping off evolved SnH_4 into liquid nitrogen traps. Purify by trap to trap distillation.	7
Me_xSnH_{4-x}	$Me_xSnCl_{4-x} + LiAlH_4 \xrightarrow{Bu_2O} Me_xSnH_{4-x}$ As SnH_4 but with Bu_2O as solvent.	7, 59, 31
Me_4Pb	$PbI_2 + MeI + MeLi \xrightarrow{Et_2O} PbMe_4 + \ldots$ Add MeLi to a vigorously stirred suspension of PbI_2 in an ethereal solution of MeI, then reflux. Remove solvent by fractional distillation, then purify by trap to trap distillation.	60, 61
Me_3PbBr	$PbMe_4 + Br_2 \xrightarrow{Et_2O} Me_3PbBr + MeBr$ Add Br_2 to $PbMe_4$ in ethereal solution, then pump off solvent, and warm *in vacuo*.	62, 63

Chapter 3

The Synthesis and Characterisation of Organostannyl Anions

3.1 Introduction

Organostannyl anions were first synthesised in 1922 and have since been much used in the preparation of organotin hydrides, mixed tetraalkyltin compounds, and tin–transition metal complexes by reaction of R_3Sn^- with the appropriate electrophile.[26,27,30,64,65]

Organostannyl anions have been prepared by a number of methods, of which the most common was the reaction between R_6Sn_2,[26] R_3SnCl,[27,30] or R_3SnH[28,66,67] and sodium in liquid ammonia. More recently tetrahydrofuran has become the solvent of choice.[65,68,69]

Evidence for the formation of R_3Sn^- in solution has been derived conductometrically,[28,67] from NMR studies, and from trapping reactions. The SnH_3^- anion has been characterised by both ^1H and ^{119}Sn NMR,[70,71] while ^1H NMR and Mössbauer spectra[72] of many other methyl-, and phenyltin anions provide convincing evidence for their formation.

Trapping reactions have generally exploited the highly nucleophilic nature of R_3Sn^- (Me_3Sn^-, for example, being one of the most powerful simple nucleophiles

available[6]), through the addition of electrophiles such as R_3SiCl.[68,69] This style of reaction has been exploited as a straightforward method for the formation of bonds from tin to germanium and silicon,[73] for example.

$$Me_3Sn^- + Me_3SiCl \xrightarrow{\text{thf, 0°C}} Me_3SnSiMe_3 + Cl^- \qquad (1)$$

Solutions containing R_3Sn^- tend to be colourless or pale yellow, and decompose on warming at a temperature dependent upon the nature of the R group. Me_3SnLi, for example, decomposes slowly in tetrahydrofuran solution at room temperature,[36] while solutions of Ph_3SnLi, olive green in colour, may be refluxed for 24 hours without noticeable degradation.[68]

One of the potential strategies for the preparation of Sn_2H_6 (see Chapter 4) was the reaction between SnH_3Cl and a source of SnH_3^-.

$$SnH_3Cl + SnH_3^- \longrightarrow Sn_2H_6 + Cl^- \qquad (2)$$

Although $NaSnH_3$ has been reported in the reaction between Na and SnH_4 in liquid ammonia,[67] decomposition occurs at -63°C on removal of the solvent. Hence it was desirable to develop a source of SnH_3^- which had increased thermal stability, ideally being stable at or near ambient temperatures. A further drawback of the use of ammonia as solvent is the observation by Cormack[74] that SnH_3Cl reacts rapidly with NH_3 even at low temperatures.

At the outset of this investigation, the thermal stability of SnH_3^-, was expected to depend upon a variety of factors. It seemed reasonable that stannyl salts containing large cations would probably be more thermally robust than those containing smaller cations, in a manner analogous to the increase in stability of the superoxides of the alkali metals with increasing cation size. The choice of a polar solvent over a less polar one was also expected to increase the thermodynamic stability of SnH_3^- in solution as a result of an increase in the enthalpy of solvation of the stannyl salt.

An investigation was therefore undertaken of the thermal stability of SnH_3^- with a variety of counterions, with the initial aim of producing a solution containing SnH_3^- of sufficient thermal stability to enable its use in the synthesis of distannane, but with the parallel intention of developing the chemistry of the

more thermally fragile stannyl anions to explore their synthetic utility, and to characterise them in more detail.

As liquid ammonia reacts vigorously with SnH_3Cl,[74] an approach to the formation of distannane using solutions of alkali metals could not be employed. Instead, acid–base reactions were explored of the form,

$$SnH_4 + B \longrightarrow [BH]^+ SnH_3^- \qquad (3)$$

analogous to the deprotonation of stannane in liquid ammonia solution observed by Birchall,[72]

$$SnH_4 + NH_3 \xrightarrow{\text{liq. } NH_3} NH_4^+ SnH_3^- \qquad (4)$$

A number of bases were studied, including ammonia, the alkali metal hydrides, alkyl lithium reagents, and the basic phosphorus ylids Me_3PCH_2, and Ph_3PCH_2.

These investigations, and the conclusions drawn from them make up the remainder of this chapter.

3.2 The Reaction between Stannane and NH_3

3.2.1 Experimental

Stannane and ammonia (1 mmol each) and toluene (2–3 ml) were condensed at -196°C into a Young's tap ampoule (see Figure 2.2) and then warmed to -63°C. No obvious reaction was observed, and so the ampoule was removed from the 'slush' bath and allowed to warm further, during which time the initially colourless solution turned orange, producing a brown precipitate which eventually turned black, accompanied by the evolution of a steady stream of non-condensable gas.

In a similar experiment, 0.1 mmol of stannane and trimethylphosphine were condensed into ampoules containing either hexane, tetrahydrofuran, or no solvent at all, and allowed to warm to room temperature. No reaction was observed in hexane solution after one hour, while in the presence of tetrahydrofuran effervescence was noticed in solution after 15 minutes, and decomposition to a tin mirror was complete after 40 minutes. At no time were the colours characteristic of the decomposition of stannane in the presence of ammonia observed.

In the absence of solvent, the formation of a tin mirror began after about 10–15 minutes at room temperature and was complete within a few seconds.

3.2.2 Interpretation

The reaction between stannane and liquid ammonia has been interpreted by Birchall[72] in terms of the formation of NH_4^+ SnH_3^- by an acid–base reaction. In toluene solution a similar process would appear to occur, the stannyl anion decomposing on warming most probably *via* the highly coloured polymeric $(SnH_2)_x$ to tin metal, and hydrogen gas,

$$NH_4^+ \, SnH_3^- \xrightarrow{\text{toluene, } \Delta} NH_3 + Sn + 2\,H_2 \qquad (5)$$

The absence of a similar sequence of colour changes during the decomposition of stannane in the presence of trimethylphosphine suggests that the phosphine is not sufficiently basic to deprotonate stannane. The tin mirrors observed indicate that the usual autocatalytic thermal decomposition of stannane occurred instead.

3.3 The Reaction between Stannane and the Alkali Metal Hydrides.

3.3.1 Stannane and Sodium Hydride.

Experimental

0.1 mmol stannane was condensed onto 10 mg NaH in a Young's tap ampoule and allowed to warm to room temperature in the absence of solvent. During warming a violent reaction was observed at the surface of the hydride which rapidly changed colour, turning yellow, then brown, and ultimately black, while a mirror formed on the sides of the ampoule.

The experiment was repeated using similar quantities of reactants, but with tetrahydrofuran as solvent and at -63°C. The white sodium hydride dissolved with a small amount of effervescence, a faint yellow colour appearing in the ampoule. After addition of one equivalent of iodomethane, the contents of the ampoule were

analysed by mass spectrometry. Multiplets centered at m/z = 117, and m/z = 135 were observed, corresponding to the fragmentation pattern of $MeSnH_3$.

Finally, an ampoule was prepared containing stannane (1 mmol) and sodium hydride (0.5 mmol) with tetrahydrofuran as solvent, and was warmed to -63°C until the effervescence around the hydride had subsided giving a colourless solution, and then slowly to room temperature.

At around -20°C to -10°C, a yellow colouration was observed on the traces of remaining solid in the ampoule, which slowly deepened on further warming, eventually turning black while a colourless, non-condensable gas was released.

Interpretation

The reactions between sodium hydride and stannane can be interpreted in a similar manner to those of ammonia with stannane. Hydride anion deprotonates stannane to give sodium stannyl, either as the solid, or in solution, with accompanying evolution of hydrogen gas.

$$SnH_4 + NaH \longrightarrow NaSnH_3 + H_2 \qquad (6)$$

Treatment of sodium stannyl with iodomethane liberates methylstannane (m/z $Me^{120}SnH_3^+ = 138$).

$$SnH_3^- + MeI \longrightarrow MeSnH_3 + I^- \qquad (7)$$

3.3.2 Stannane and Potassium Hydride.

Experimental

An ampoule containing stannane (0.1 mmol), potassium hydride (0.1 mmol), and tetrahydrofuran (2–3 ml) was warmed to -63°C, at which point effervescence was observed and the hydride dissolved. On further warming no change was noticed until the ampoule reached *ca.* 0°C, when a mirror began to form above the level of the liquid in the ampoule, and a colourless non-condensable gas was evolved.

A similar experiment was performed using identical amounts of reagents, reaction proceeding at -63°C for one hour after which one equivalent of iodomethane was added, and the ampoule left at -63°C for a further hour. Subsequent analysis

of the contents by mass spectrometry yielded peaks centered at m/z = 120, and 135.

Finally, 0.1 mmol of potassium hydride, [2,2,2-crypt], and stannane were condensed in an ampoule with tetrahydrofuran, warmed to -63°C until effervescence had ceased, and then slowly to room temperature. A pale yellow solution was formed, which effervesced slightly from residual base at the bottom of the ampoule.

With the very bottom of the ampoule cooled in liquid nitrogen, thereby immobilising the residual base in a small quantity of solid solvent, the remaining liquid solvent was removed under vacuum. A yellow solid precipitated which was stable at room temperature for 5–10 minutes before slowly turning orange

To determine the effect of [2,2,2-crypt] on stannane, 0.1 mmol SnH_4 was condensed into an ampoule containing an excess of [2,2,2-crypt] dissolved in tetrahydrofuran. The resultant solution was warmed to -63°C, and then to around 0°C, at which point effervescence was observed accompanied by the formation of a brown precipitate that subsequently turned grey.

Interpretation

The reaction between stannane and potassium hydride can be interpreted in a similar manner to that between stannane and sodium hydride, except that instead of decomposing at around -20°C to -10°C, the stannyl salts begin to decompose at around 0°C, and in the presence of [2,2,2-crypt], slowly at room temperature.

$$KH + SnH_4 \xrightarrow{\text{thf, -63°C}} KSnH_3 + H_2 \quad (8)$$

$$KH + SnH_4 + [2,2,2\text{-crypt}] \xrightarrow{\text{thf, -63°C}} K[2,2,2\text{-crypt}]^+ SnH_3^- \quad (9)$$

Thus it appears that the increase in cation size from Na^+ to K^+, and from K^+ to $K[2,2,2\text{-crypt}]^+$ has a significant effect on the stability of the stannyl anion.

The reaction between the cryptand and stannane alone suggests that the ligand is sufficiently basic to deprotonate stannane, but that the resultant salt has little thermal stability, decomposing rapidly to tin metal, and hydrogen gas. The absence of this reaction in the presence of K^+ suggests that the ligand is indeed coordinating to potassium, and that the yellow solid produced on removal

of solvent at room temperature does contain K[2,2,2-crypt]$^+$ SnH_3^-, and not simply $KSnH_3$.

3.4 The Reaction between Stannanes and Alkyl Lithium Reagents.

3.4.1 Introduction

The reactions between stannane and alkali metal hydrides were complicated by difficulties encountered in manipulating the hydrides. These were transferred in the dry box to the ampoules used for reaction, careful addition ensuring that the vast majority of the hydride added settled to the bottoms of the ampoules. However, it proved impossible to avoid completely contamination of the sides of the ampoules with the bases. On subsequent addition of solvent and stannane on the high vacuum line, it was found that small quantities of bases inevitably remained above the level of the solvent and the 'slush' bath. These traces of base then acted as catalytic centres for stannane decomposition, producing quantities of tin metal over which solutions of SnH_3^- could not be transferred without substantial decomposition of the stannyl salt.

To avoid this problem, bases were sought that could be handled in a more quantitative fashion, and ideally in solution or in the gas phase. Solutions of alkyl lithium reagents were considered as they could be easily manipulated on the Schlenk line, were free of dissolved basic impurities, and were expected to react cleanly by evolution of an alkane,

$$RLi + SnH_4 \longrightarrow RH + Li^+ SnH_3^- \qquad (10)$$

In the following sections we describe the reactions of alkyl lithium reagents with the stannanes Me_xSnH_{4-x} (x = 1-3).

3.4.2 The Reactions between Me_2SnH_2 or Me_3SnH and Alkyl Lithium Reagents

Experimental

MeLi + Me_3SnH in Et_2O Methyl lithium (1 mmol) was syringed into a Schlenk tube containing an equivalent amount of trimethylstannane dissolved in diethyl ether. The resulting solution was stirred at -78°C for 90 minutes during which time a white precipitate formed. An equivalent of trimethylsilyl chloride was then condensed into the ampoule and the mixture stirred at -78°C for a further 150 minutes.

The contents of the ampoule were then warmed to room temperature and distilled through traps cooled to -78°C, and -196°C to the high vacuum line. The small quantity of colourless liquid that condensed in the -78°C trap was dissolved in toluene-d^8 for NMR analysis, giving a ^1H spectrum that by comparison with literature data[59,75] indicated the presence of diethyl ether, and tetramethylstannane only. (^1H: $\delta = 0.98$ (t, $^3J_{H-H} = 7.0$ Hz), $\delta = 3.16$ (q, $^3J_{H-H} = 7.0$ Hz), $\delta =$ -0.05 ($^2J_{^{119}Sn-H} = 54.1$ Hz))

The white solid remaining in the ampoule dissolved in water with violent effervescence producing a highly alkaline solution that gave a red flame test.

BuLi + Me_3SnH in Et_2O A similar experiment was carried in which butyl lithium (1 mmol) and an equivalent of trimethylstannane were stirred at room temperature in hexane solution. A white precipitate was again observed, and after 3 hours of stirring at room temperature, one equivalent of trimethylsilyl chloride was added and the mixture stirred for a further 90 minutes.

Distillation through traps at -31°C, -78°C, and -196°C yielded a small quantity of liquid in the -31°C trap, which was dissolved in benzene-d^6 and analysed by NMR spectroscopy, giving ^1H, and ^{13}C spectra which by comparison with the literature[75] indicated the presence of $BuSnMe_3$ only (see Table 3.1).

MeLi + Me_2SnH_2 in Et_2O Dimethylstannane (2.6 mmol) and an equivalent of methyl lithium were warmed from -78°C to room temperature in diethyl ether

	Observed (C_6D_6)
^{1}H:	δ = 0.08 (s, $^2J_{^{119}Sn-H}$ = 52.3 Hz), δ = 0.79 (t, $^3J_{H-H}$ = 7.7 Hz), δ = 1.24–1.36 (m), 1.38–1.51 (m), δ = 0.90 (t, $^3J_{H-H}$ = 7.0 Hz)
^{13}C:	δ = -10.4 ($^1J_{^{119}Sn-C}$ = 317.0 Hz), δ = 10.9 ($^1J_{^{119}Sn-C}$ = 358.8 Hz), δ = 29.3 ($^2J_{Sn-C}$ = 20.6 Hz), δ = 27.3 ($^3J_{Sn-C}$ = 55.1 Hz), δ = 13.9 (no resolved Sn-C coupling)
	Ref. 75 (Neat liq.)
^{13}C:	δ = -10.5 ($^1J_{Sn-C}$ = 319.0 Hz), δ = 11.1 ($^1J_{Sn-C}$ = 368.0 Hz), δ = 29.2 ($^2J_{Sn-C}$ = 21.0 Hz), δ = 27.3 ($^3J_{Sn-C}$ = 53.0 Hz), δ = 13.8 (no resolved Sn-C coupling)

Table 3.1. Observed and Literature NMR Data for $BuSnMe_3$

solution. A white precipitate rapidly formed that remained unchanged on standing for several minutes. One equivalent of trimethylsilyl chloride was condensed into the reaction mixture which was then left at -20°C overnight.

The contents of the reaction vessel were not visibly different and contained a colourless solution and a white precipitate as before. The solution was distilled through traps held at -78°C and -196°C to the high vacuum line and a small quantity of a colourless liquid condensed in the -78°C trap. The IR spectrum of this vapour displayed an absorption at 1844cm^{-1}, corresponding to the Sn–H stretching frequency of trimethylstannane.

Interpretation

The reactions between Me_3SnH or Me_2SnH_2 and RLi can be interpreted in terms of a nucleophilic substitution of hydride by the alkyl anion at tin,

$$R_3SnH + R'Li \longrightarrow R_3SnR' + LiH \qquad (11)$$

Thus, trimethylstannane reacts with methyl lithium to produce tetramethylstannane, and with butyl lithium to produce $BuSnMe_3$. Dimethylstannane reacts with methyl lithium to produce trimethylstannane,

$$Me_3SnH + MeLi \xrightarrow{Et_2O} Me_4Sn + LiH \qquad (12)$$

$$Me_3SnH + BuLi \xrightarrow{\text{hexanes}} BuSnMe_3 + LiH \quad (13)$$

$$Me_2SnH_2 + MeLi \xrightarrow{Et_2O} Me_3SnH + LiH \quad (14)$$

In all three cases, addition of Me_3SiCl did not result in the formation of any $Me_3SiSnMe_3$, suggesting that no Me_3Sn^- was present at all. In the case of dimethylstannane this was unexpected as it was anticipated that the trimethylstannane would react further with the resulting lithium hydride, thereby generating Me_3Sn^- Li^+. This did not happen, indicating that trimethylstannane is either not sufficiently acidic to be deprotonated by lithium hydride or that the reaction happens extremely slowly at room temperature.

3.4.3 The Reaction between Methylstannane and Alkyl Lithium Reagents

Experimental

MeLi + $MeSnH_3$ in Et_2O Methylstannane (1.23 mmol) and an equivalent of methyl lithium were dissolved in diethyl ether, and warmed from -83°C to room temperature. A bright yellow precipitate formed that persisted until the temperature of the solution reached around -10°C, at which point it began to change colour, turning first orange, then red and ultimately black at room temperature with slow effervescence of a colourless gas.

MeLi + $MeSnH_3$ in THF Methylstannane (1.74 mmol) and an equivalent of methyl lithium were dissolved in tetrahydrofuran and warmed from -83°C to room temperature. A white precipitate formed as the reagents mixed that turned pale yellow on warming. The solution also slowly turned yellow on warming with slow effervescence of a colourless gas, until at room temperature both precipitate and solution were canary yellow in colour.

The resulting mixture was left to stand for a number of days, during which the colour of the solution and precipitate became more intense, until after 7 days, a deep red solution over a brown precipitate remained.

Interpretation

The reaction between methylstannane and methyl lithium can be interpreted by comparison with the reactions of stannane with the alkali metal hydrides, and the reaction of dimethylstannane with methyl lithium.

An acid-base reaction would be expected to produce $MeSnH_2^-$, decomposing on warming in a manner similar to the decomposition of SnH_3^-,

$$MeSnH_3 + MeLi \longrightarrow Li^+ MeSnH_2^- + MeH \quad (15)$$

A substitution reaction would be expected to produce Me_2SnH_2,

$$MeSnH_3 + MeLi \longrightarrow Me_2SnH_2 + LiH \quad (16)$$

In tetrahydrofuran solution, a yellow product appears that persists at room temperature for several hours before very slowly deepening in colour. This suggests the presence of polymeric dimethyltin, produced through the formation, deprotonation, and decomposition of dimethylstannane,

$$Me_2SnH_2 + LiH \longrightarrow Li^+ Me_2SnH^- + H_2 \quad (17)$$

$$Li^+ Me_2SnH^- \longrightarrow (Me_2Sn)_x + LiH \quad (18)$$

The marked thermal stability of this product at room temperature contrasts highly with that of the product of the reaction when performed in diethyl ether. Here, a yellow precipitate forms that deepens in colour on warming, becoming black at room temperature. These observations are consistent with the formation of $Li^+ MeSnH_2^-$, followed by its rapid decomposition, perhaps *via* $(MeSnH)_x$, which would be expected to have properties similar to $(Me_2Sn)_x$, and $(SnH_2)_x$.

3.4.4 The Reaction between Stannane and Alkyl Lithium Reagents

Experimental

MeLi + SnH_4 in Et_2O Stannane (3.63 mmol) and one equivalent of methyl lithium were dissolved in diethyl ether and warmed from -78°C to room temperature. On mixing the reactants, a white precipitate formed which turned

bright orange on warming, accompanied by evolution of a colourless gas. At around -10°C, the precipitate began to turn brown, then black, while more gas was evolved.

MeLi + SnH_4 in THF Stannane (0.97 mmol) and one equivalent of methyl lithium were dissolved in tetrahydrofuran and warmed from -78°C to room temperature. A white precipitate formed with evolution of a colourless gas as the reactants were mixed. On warming to around -10°C, the precipitate slowly turned yellow, accompanied by more effervescence, becoming brown at room temperature.

BuLi + SnH_4 Stannane (0.1 mmol) and one equivalent of butyl lithium were dissolved in hexane and warmed to -78°C. No obvious reaction was observed, and so the ampoule was warmed further, during which time the solution turned yellow, and a yellow precipitate formed. Both solution and precipitate darkened in colour on subsequent warming, turning first red, then brown, until at room temperature both turned dark brown, while a colourless gas was evolved.

Interpretation

The reactions between stananne and alkyl lithium reagents resemble to some degree those between stannane and the alkali metal hydrides. However, the range of possible products formed when RLi and SnH_4 react is greater, as the possibility of nucleophilic substitution at tin must be recognised. The tin-containing species present in the product mixture may therefore include Li^+ SnH_3^-, Li^+ $MeSnH_2^-$, $(SnH_2)_x$, $(Me_2Sn)_x$, and $(MeSnH)_x$. Further characterisation is required before the actual course of these reactions can be stated with any degree of certainty.

3.5 The Reaction between Stannanes and Phosphorus Ylids

3.5.1 Introduction

The reactions between alkyl lithium reagents and stannanes did not provide the simple, straightforward route to organostannyl anions that was expected. Alternative bases were therefore sought that fulfilled the original criterion of ease of manipulation, but were also non-nucleophilic in character.

The phosphorus ylid Me_3PCH_2 is one such base. It is a liquid at room temperature, with sufficient vapour pressure to allow its manipulation on the vacuum line. It reacts with acids to give tetramethylphosphonium salts,

$$Me_3PCH_2 + HA \longrightarrow Me_4P^+ A^- \qquad (19)$$

The reactions between the stannanes Me_xSnH_{4-x} (x = 0–3) and Me_3PCH_2 are described in the following sections. The volatility of the ylid also enabled these reactions to be studied at low temperature by infra-red spectroscopy. The results of this study follow on from this introduction.

The preparation of Me_3PCH_2 as outlined in Chapter 2 is time consuming and experimentally demanding, however, and although it may be handled on a high vacuum line, the reactivity of the ylid to air and moisture is such that it is not an ideal reagent for work on a preparative scale. Triphenylphosphonium methylid, however, may be prepared as a bright yellow solid in high yield from readily available starting materials, and may be handled with relative ease in a dry box. Its solubility in tetrahydrofuran and diethyl ether also allows the experimental problems associated with the use of alkali metal hydrides to be minimised. The reactions between Ph_3PCH_2 and the stannanes are described in the final sections of this chapter.

3.5.2 Low Temperature Infra-red Studies

Experimental

Trimethylphosphonium methylid (0.035 mmol) was condensed onto on a caesium iodide window cooled to -196°C in an infra-red cold cell (see Figure 2.3). The stannane to be studied (0.058 mmol) was then condensed on top of the solid ylid, an infra-red spectrum recorded, and the cold window warmed to -78°C while reaction took place. The cold cell was then attached to the high vacuum line and any volatile contents pumped away before the cold window was cooled back to -196°C, and a final infra-red spectrum recorded.

Spectra were recorded for the reaction between trimethylphosphine methylid and SnH_4, SnD_4, $MeSnH_3$, Me_2SnH_2, and Me_3SnH, and are shown in Figures 3.2, 3.3, 3.4, 3.5, and 3.6 respectively. The infra-red spectra of Me_4PBr as a KBr disc, and Me_3PCH_2 as a solid at -196°C are also shown for comparison in Figure 3.1.

Stannane and Me_3PCH_2

The reaction between stannane and Me_3PCH_2 at -78°C on a CsI window may be observed by infra-red spectroscopy by the disappearance of bands present in the spectrum taken before reaction, and the appearance of new bands in the spectrum recorded after reaction had taken place. The progress of the reaction may therefore be followed by observing the decline in intensity of the band due to the asymmetric Sn–H stretching mode of stannane, and through the increase in intensity of new bands in other parts of the spectrum.

The formation of Me_4P^+ is indicated by the appearance of bands at 1291cm^{-1}, 992cm^{-1}, and 774cm^{-1}, due to the symmetric bending and rocking modes of the methyl groups, and the asymmetric stretching mode of the PC_4 skeleton.

The formation of SnH_3^- can be inferred from the appearance of a very strong and broad absorption at roughly 80% of the frequency of the asymmetric stretching mode of SnH_4. This, coupled with the formation of two further bands of high intensity at slightly higher energies than the asymmetric bending mode of SnH_4 suggests that the peaks at 1557cm^{-1}, 752cm^{-1}, and 720cm^{-1}be assigned to the unresolved stretching modes, and the asymmetric, and symmetric bending modes of SnH_3^-.

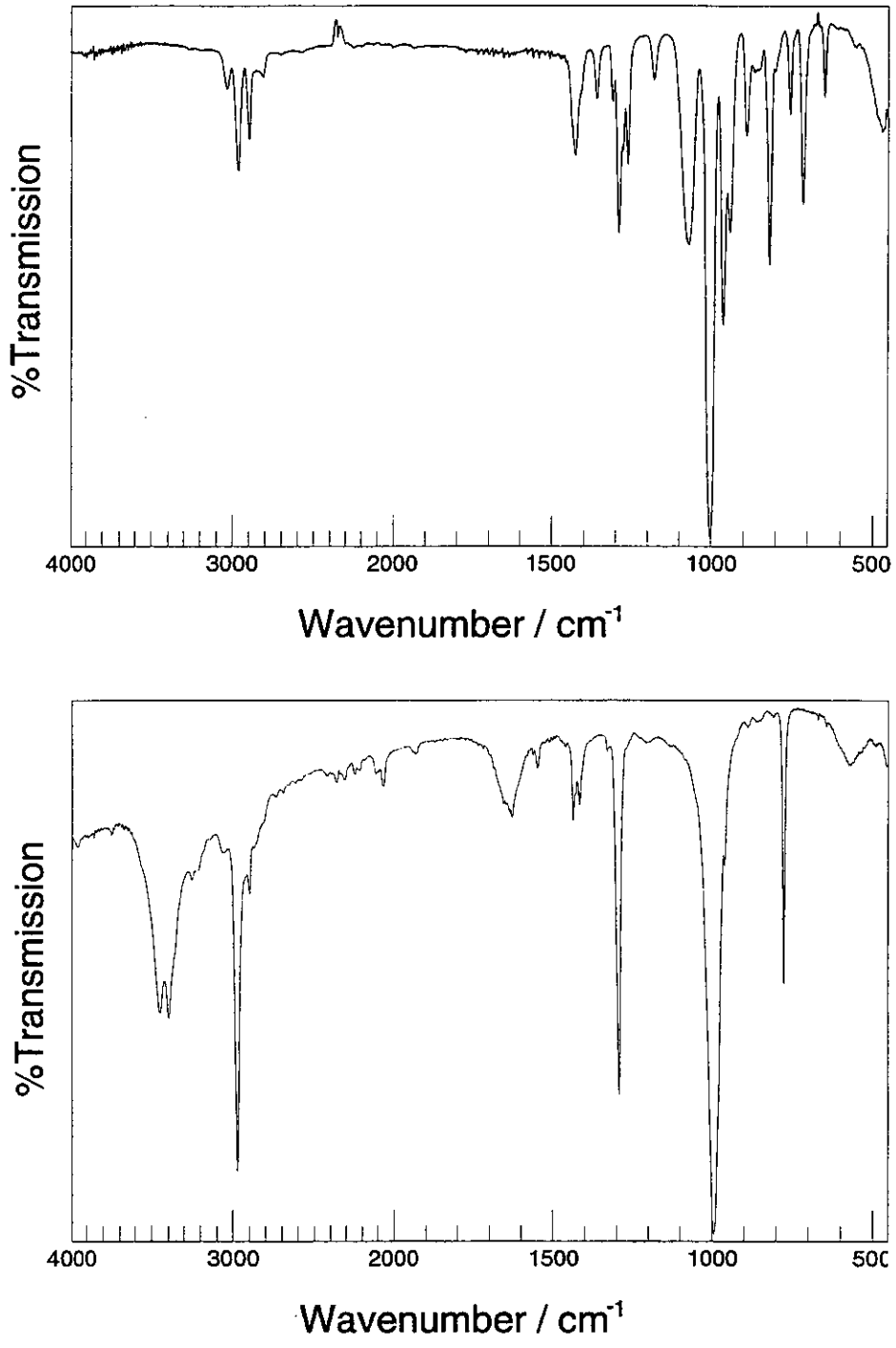

Figure 3.1. Infra-red Spectra of Me_3PCH_2 at -196°C (top), and Me_4PBr (bottom, dispersed in a KBr disc).

Me_3PCH_2		Assignment	Me_4PBr		Assignment
3032	w		2972	vs	$\nu_{as}(CH_3)$
2963	m	$\nu_{as}(CH_3)$	2899	vw	$\nu_s(CH_3)$
2895	w	$\nu_s(CH_3)$	1434	w	$\delta_{as}(CH_3)$
1424	m	$\delta_{as}(CH_3)$	1414	w	$\delta_{as}(CH_3)$
1358	w	$\delta(CH_2)$	1291	vs	$\delta_s(CH_3)$
1304	sh		992	vs	$\rho(CH_3)$
1288	m	$\delta_s(CH_3)$	774	m	ν_{as}(P–C)
1277	sh				
1260	w	Me_3PO			
1174	vw	Me_3PO			
1065	m				
1010	vs	ν(P–C)			
960	s	$\rho(CH_3)$			
942	m	Me_3PO			
885	m	$\rho(CH_3)$			
854	w	Me_3PO			
815	m	Me_3PO			
753	w	ν_{as}(P–C)			
715	m	ν_{as}(P–C)			
646	w	ν_s(P–C)			

Table 3.2. Infra-red Peak Listings for Me_3PCH_2 and Me_4PBr. Frequencies are in wavenumbers. Assignments were made by comparison with those proposed for Me_3PCH_2 liquid by Sawodny[56]

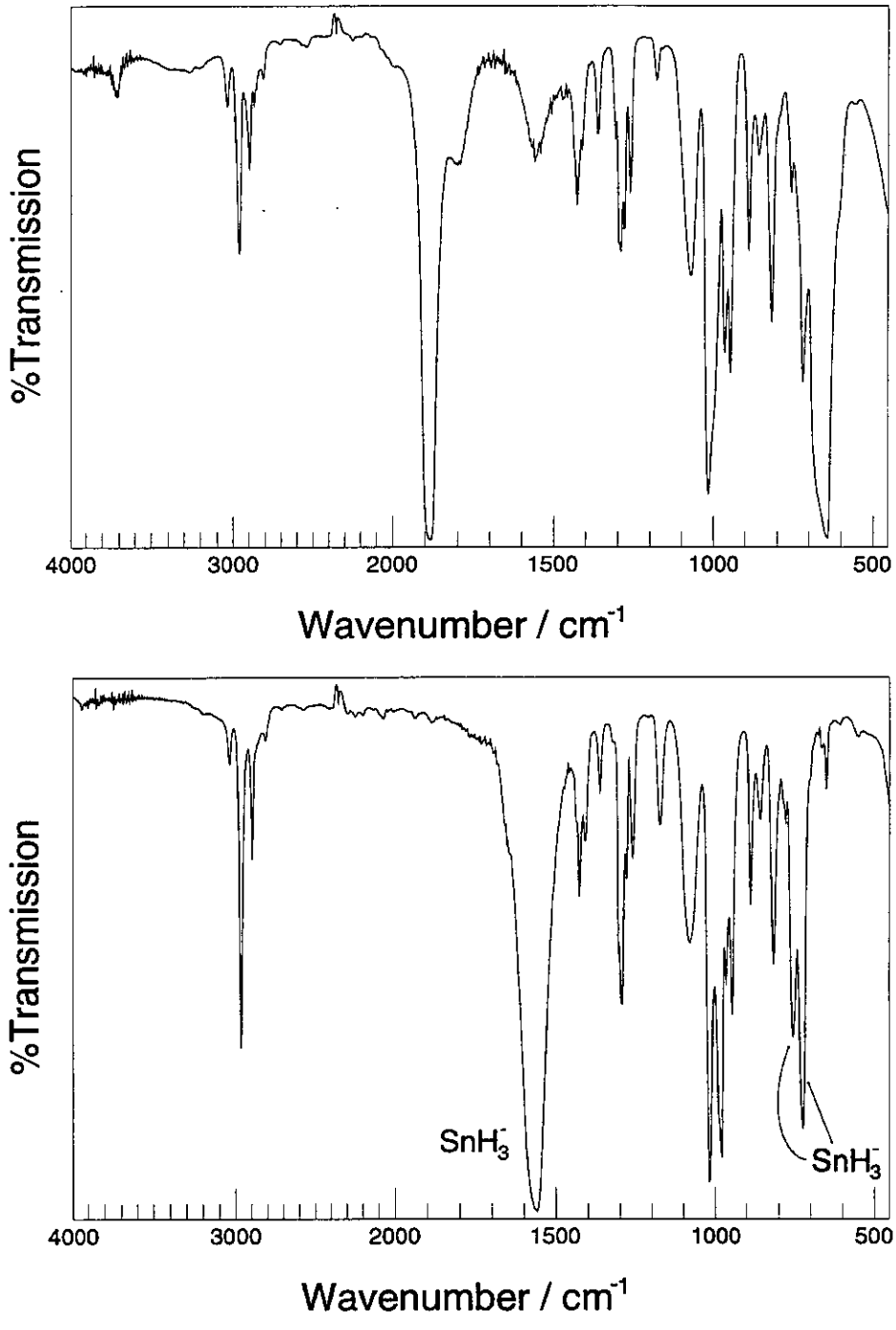

Figure 3.2. Infra-red Spectra of SnH_4 and trimethylphosphonium methylid on a CsI window at -196°C before warming (top), and after reaction (bottom).

Peak/cm^{-1}		Species	Type
3032	w	Me_3PCH_2	
2962	s	Me_3PCH_2, $[Me_4P]^+$	$\nu_{as}(CH_3)$
2892	m	Me_3PCH_2, $[Me_4P]^+$	$\nu_s(CH_3)$
1557	vs	SnH_3^-	ν(Sn–H)
1423	m	Me_3PCH_2	
1407	w	$[Me_4P]^+$	$\delta_{as}(CH_3)$
1360	w	Me_3PCH_2	
1291	m	$[Me_4P]^+$, Me_3PCH_2	$\delta_s(CH_3)$
1278	vw	Me_3PCH_2	$\delta_s(CH_3)$
1259	m	Me_3PO	
1170	m	Me_3PO	
1077	m	Me_3PO	
1013	s	Me_3PCH_2	ν(P–C)
976	s	$[Me_4P]^+$	$\rho(CH_3)$
962	w	Me_3PCH_2	
942	m	Me_3PO	
885	m	Me_3PCH_2	
854	w	Me_3PO	
813	m	Me_3PO	
774	vw	$[Me_4P]^+$	ν_{as}(P–C)
752	s	SnH_3^-	$\delta_{as}(SnH_3)$
720	s	SnH_3^-	$\delta_s(SnH_3)$
647	w	Me_3PCH_2	

Table 3.3. Infra-red Peak Listings for the Reaction between SnH_4 and Me_3PCH_2

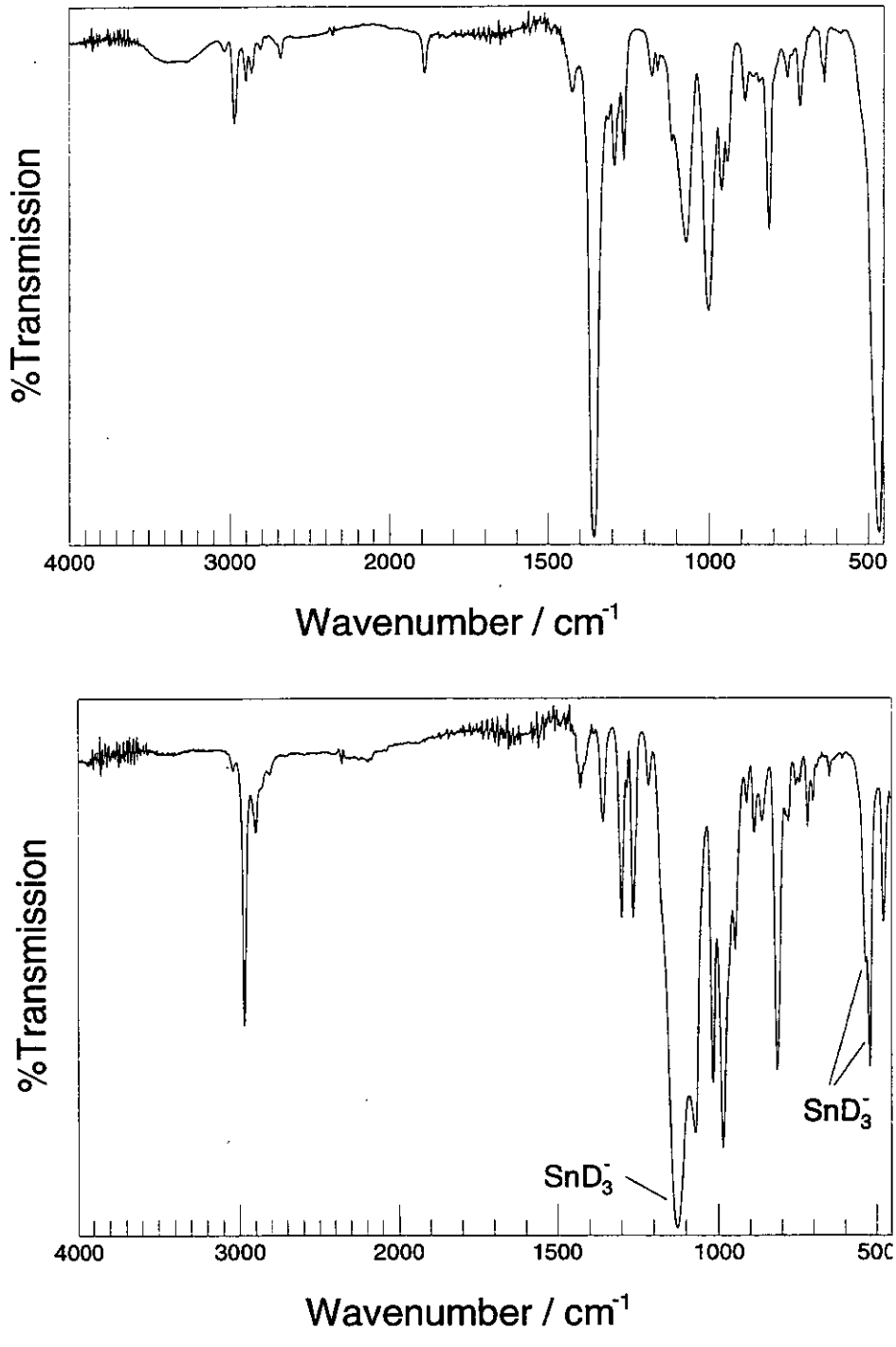

Figure 3.3. Infra-red spectra of SnD_4 and trimethylphosphonium methylid on a CsI window at -196°C before warming (top), and after reaction (bottom).

Peak/cm^{-1}		Species	Type
2964	m	Me_3PCH_2, $[Me_4P]^+$	$\nu_{as}(CH_3)$
2895	w	Me_3PCH_2, $[Me_4P]^+$	$\nu_s(CH_3)$
1424	w	Me_3PCH_2, $[Me_4P]^+$	$\delta_{as}(CH_3)$
1354	w	SnD_4	ν(Sn–D)
1294	m	$[Me_4P]^+$	$\delta_s(CH_3)$
1260	m	Me_3PO	
1125	vs	SnD_3^-	ν(Sn–D)
1067	w	Me_3PCH_2	
1011	s	Me_3PCH_2	
982	s	$[Me_4P]^+$	$\rho(CH_3)$
942	w	Me_3PO	
885	w	Me_3PCH_2	
811	s	Me_3PO	
776	vw	$[Me_4P]^+$	ν_{as}(P–C)
753	vw	Me_3PCH_2	
716	w	Me_3PCH_2	
646	vw	Me_3PCH_2	
530	sh	SnD_3^-	$\delta_{as}(SnD_3)$
517	s	SnD_3^-	$\delta_s(SnD_3)$
475	m	SnD_4	$\delta(SnD_4)$

Table 3.4. Infra-red Peak Listings for the Reaction between SnD_4 and Me_3PCH_2

Examination of the spectra of the reaction between SnD_4 and Me_3PCH_2 reveals strong corroborative evidence for this assignment. Peaks at 1125cm^{-1}, 530cm^{-1}, and 517cm^{-1}appear in positions relative to those of SnD_4 in a manner entirely analogous to those observed for the reaction with SnH_4. Moreover, the ratios of the frequencies of these peaks to those assigned to SnH_3^- are $[SnH_3^- : SnD_3^-] = 1.38, 1.42, 1.39$ respectively. A harmonic model predicts that the vibrational frequency of an object attached by a spring to an infinite mass should increase by a factor of $\sqrt{2} = 1.414$ if the mass of the body is doubled. Here, the tin atom is some 60 times heavier than a deuterium atom, suggesting that this approximation is a good one, and therefore provides convincing evidence for the assignment of these modes of vibration to SnH_3^-, and SnD_3^-.

To investigate further the validity of these assignments, *ab initio* calculations were performed to determine the vibrational frequencies of isolated pyramidal SnH_3^- and SnD_3^- anions in the gas phase. The results of these calculations are shown in Table 3.5.

SnH_3^-		SnD_3^-	
Observed	DZ(P)/MP2	Observed	DZ(P)/MP2
1557	1642.5, 1636.4	1125	1165.7, 1162.7
752	796.8	530	565.0
720	767.6	517	548.0

Table 3.5. Observed and Predicted Vibrational Frequencies (cm^{-1}) for SnH_3^- and SnD_3^-.

It is usual for vibrational frequencies calculated at the MP2 level for gas phase species to be overestimated by *ca.* 5%.[76] When this is taken into account, the agreement between theory and experiment is remarkable, especially considering that the experimental results are for a species in the solid state in a presumably ionic salt.

A similar *ab initio* calculation was performed for planar SnH_3^-, to determine the likelihood of the presence of planar SnH_3^- anions in the solid state. The calculations predicted Sn–H stretching frequencies of a similar magnitude to those of SnH_4, and also one vibrational frequency of negative sign, indicating that the

structure of a transition state had been calculated. On this basis, and in the light of the excellent agreement between experimental and calculated vibrational frequencies for a pyramidal structure, it would seem almost certain that SnH_3^- is indeed pyramidal in the solid state.

The infra red spectra of the reaction between Me_3PCH_2 and SnH_4 at low temperature therefore provide convincing evidence for the formation of an ionic tetramethylphosphonium salt containing the pyramidal anion, SnH_3^-.

$$Me_3PCH_2 + SnH_4 \longrightarrow Me_4P^+ SnH_3^- \qquad (20)$$

$MeSnH_3$ and Me_3PCH_2

The reaction between $MeSnH_3$ and Me_3PCH_2 at low temperature as observed by infra-red spectroscopy bears a strong resemblance to that described above between stannane and Me_3PCH_2.

Reaction is indicated by the disappearance of the intense band due to ν(Sn–H) in $MeSnH_3$ and by the formation of bands assignable to vibrational modes of the tetramethylphosphonium cation, at 1294cm^{-1}, 981cm^{-1}, and 780cm^{-1}. The appearance of an intense absorption at 1538cm^{-1}, again roughly 80% of the energy of the Sn–H stretch in the parent stannane, strongly suggests the presence of the organostannyl anion, $MeSnH_2^-$. This is corroborated by the observation of new bands assignable to the anion, at 1171cm^{-1}, 742cm^{-1}, 717cm^{-1}, 519cm^{-1}, and 450cm^{-1}, as shown in Table 3.6. The number of bands observed here is substantially greater than for the SnH_3^- as a result of the substitution of one hydride by -CH_3. Absorptions due to the symmetric stretching mode of the methyl group, the asymmetric and symmetric bending modes of the H_2SnC skeleton, and the stretching vibrations of the Sn–C bond are observed. The asymmetric CH_3 stretching mode is expected to appear at around 1400cm^{-1}, in a similar region to the asymmetric CH_3 stretching modes of the methyl groups of Me_4P^+, and residual Me_3PCH_2, and is therefore not resolved.

Again, *ab initio* calculations were performed to investigate the likelihood of these assignments, and the results of these are shown in Table 3.7,

The general agreement between predicted and observed frequencies is good, except in the Sn–C stretching region. The results of calculations performed on

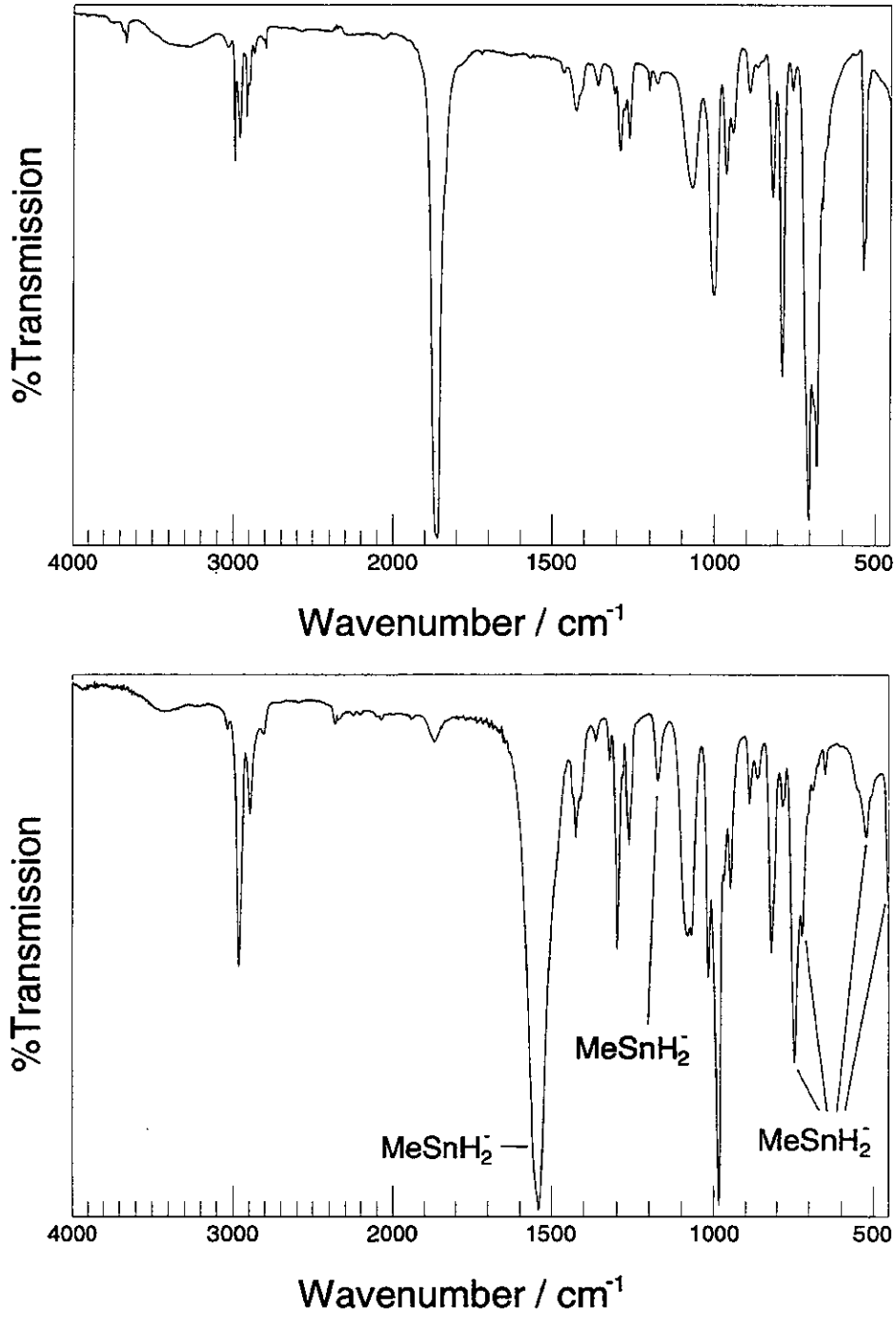

Figure 3.4. Infra-red spectra of $MeSnH_3$ and trimethylphosphonium methylid on a CsI window at -196°C before warming (top), and after reaction (bottom).

Peak/cm^{-1}		Species	Type
2960	m	Me_3PCH_2, $[MeSnH_2^-]$	$\nu_{as}(CH_3)$
2889	w	$[MeSnH_2^-]$, $[Me_4P]^+$	$\nu_s(CH_3)$
1866	vw	$MeSnH_3$	ν(Sn–H)
1538	vs	$[MeSnH_2^-]$	ν(Sn–H)
1422	w		$\delta_{as}(CH_3)$
1360	vw	Me_3PCH_2	
1294	m	Me_3PCH_2, $[Me_4P]^+$	$\delta_s(PCH_3)$
1258	w	Me_3PO	
1171	w	$[MeSnH_2^-]$	$\delta_s(CH_3)$
1078	m	Me_3PCH_2	ν(P–C)
1013	m	Me_3PCH_2	
981	s	$[Me_4P]^+$	$\rho(CH_3)$
942	w	Me_3PO	
884	w	Me_3PCH_2	
859	vw	Me_3PO	
813	m	Me_3PO	
780	w	$[Me_4P]^+$	ν_{as}(P–C)
742	s	$[MeSnH_2^-]$	$\delta_{as}(H_2SnC)$
717	w	$[MeSnH_2^-]$	$\delta_s(H_2SnC)$
647	vw	Me_3PCH_2	
519	w	$[MeSnH_2^-]$	ν(Sn–C)
450	m	$[MeSnH_2^-]$	ν(Sn–C)

Table 3.6. Infra-red Peak Listings for the Reaction between $MeSnH_3$ and Me_3PCH_2

Observed	DZ(P)/MP2
1538	1623.6, 1620.1
1171	1202.4
742	793.9
717	771.0, 756.6
519	492.3
450	427.4

Table 3.7. Observed and Predicted Vibrational Stretching Frequencies (cm^{-1}) for $MeSnH_2^-$

methylstannane also agree less well in this region with observed vibrational frequencies both in the solid and gas phases. It is possible, therefore, that the prediction of vibrational frequencies involving the Sn–C skeleton is not something that can be done with great accuracy using this style of calculation, though it must be acknowledged that the quality of the spectra recorded limits significantly the certainty with which spectral assignments can be made.

In summary, the spectra described above provide good evidence for the reaction of Me_3PCH_2 with $MeSnH_3$ to form Me_4P^+ $MeSnH_2^-$,

$$Me_3PCH_2 + MeSnH_3 \longrightarrow Me_4P^+ \; MeSnH_2^- \qquad (21)$$

Me_2SnH_2 + Me_3PCH_2

The spectra recorded for the reaction between Me_2SnH_2 and Me_3PCH_2 at -78°C can be interpreted in a similar manner to those discussed previously. The disappearance of the band due to the Sn–H stretching mode in Me_2SnH_2, and the appearance of a similarly intense absorption at around 80% of its frequency is consistent with the general pattern reported, and the appearance of bands at 1296cm^{-1}, 980cm^{-1}, and 779cm^{-1} is indicative of the formation of Me_4P^+.

The infra-red spectrum of Me_2SnH^- would be expected to contain bands due to the Sn–H stretching mode, the symmetric and asymmetric bending modes of the methyl groups, the bending modes of the $HSnC_2$ skeleton, and the Sn–C stretching modes. All may be assigned in the spectrum recorded, except $\nu_{as}(CH_3)$, which probably cannot be resolved from the cluster of absorptions at around 1400cm^{-1} and the Sn–H stretching mode of the anion at 1496cm^{-1}.

The agreement between the vibrational frequencies thereby assigned (shown in Table 3.8) and those calculated *ab initio* (see Table 3.9) is good, with acknowledgment of the caveats described previously.

The spectra recorded therefore provide good evidence for the formation of Me_2SnH^- by reaction of Me_3PCH_2 and Me_2SnH_2,

$$Me_3PCH_2 + Me_2SnH_2 \longrightarrow Me_4P^+ \; Me_2SnH^- \qquad (22)$$

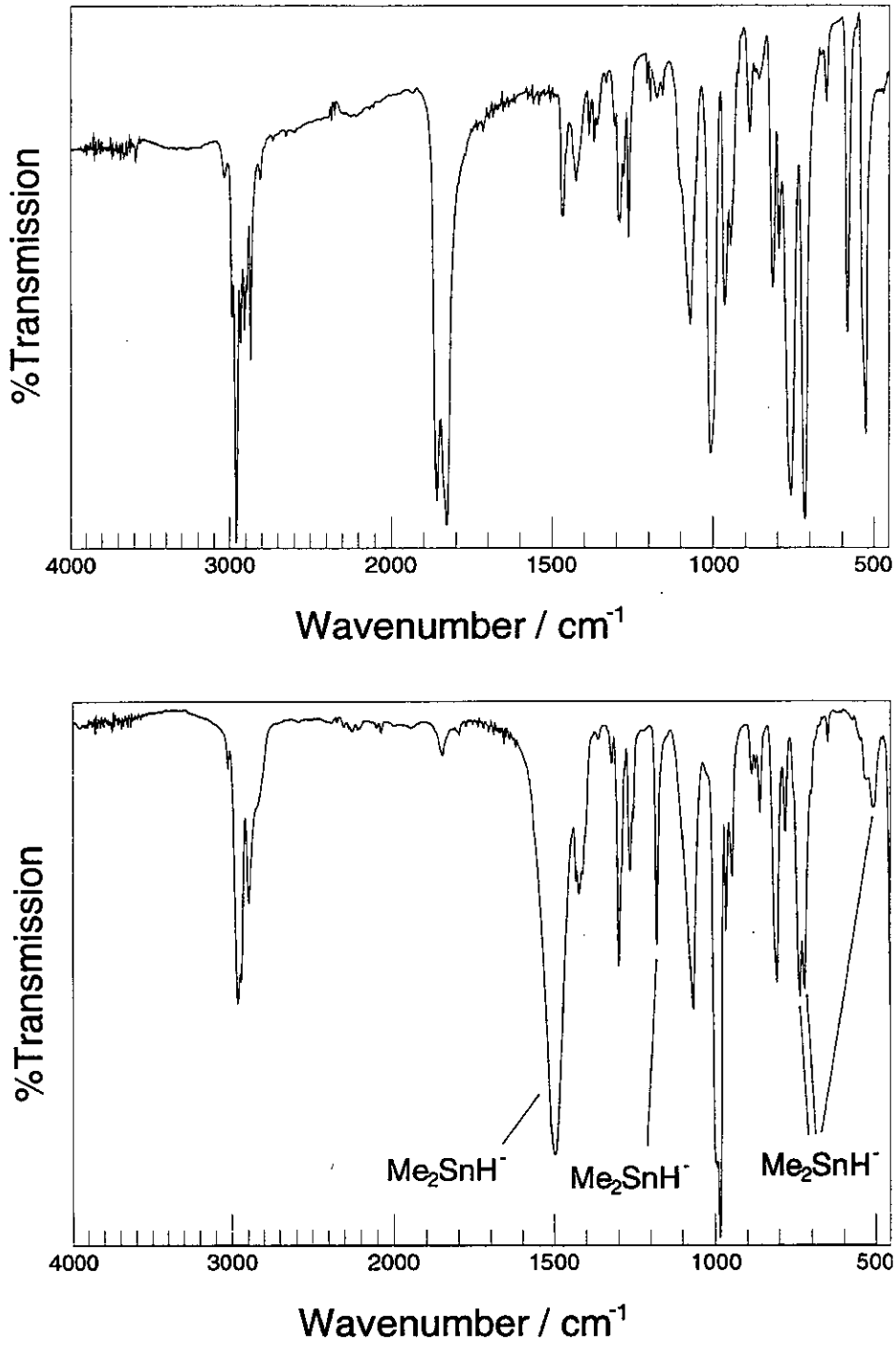

Figure 3.5. Infra-red spectra of Me_2SnH_2 and trimethylphosphonium methylid on a CsI window at -196°C before warming (top), and after reaction (bottom).

Peak/cm^{-1}		Species	Type
2959	m		ν_{as}(C–H)
2892	m		ν_{s}(C–H)
1846	vw	Me_2SnH_2	ν(Sn–H)
1496	vs	$[Me_2SnH^-]$	ν(Sn–H)
1420	m	Me_3PCH_2, $[Me_2SnH^-]$	$\delta_{as}(CH_3)$
1319	vw	Me_3PCH_2	
1296	m	$[Me_4P]^+$	$\delta_{s}(CH_3)$
1259	w	Me_3PO	
1178	m	$[Me_2SnH^-]$	$\delta_{s}(CH_3)$
1065	m	Me_3PCH_2	
980	vs	$[Me_4P]^+$	$\rho(CH_3)$
961	m	Me_3PCH_2	
943	w	Me_3PO	
858	w	Me_3PO	
803	m	Me_3PCH_2	
779	w	$[Me_4P]^+$	ν_{as}(P–C)
734	m	$[Me_2SnH^-]$	$\delta_{as}(HSnC_2)$
718	m	$[Me_2SnH^-]$	$\delta_{s}(HSnC_2)$
646	vw	Me_3PCH_2	
503	w	$[Me_2SnH^-]$	ν(Sn-C)

Table 3.8. Infra-red Peak Listings for the Reaction between Me_2SnH_2 and Me_3PCH_2

Observed	DZ(P)/MP2
1496	1605.2
1178	1208, 1199
734	777.2
718	751.4, 742.6
503	497.3, 472.6

Table 3.9. Observed and Predicted Vibrational Frequencies (cm^{-1}) for Me_2SnH^-

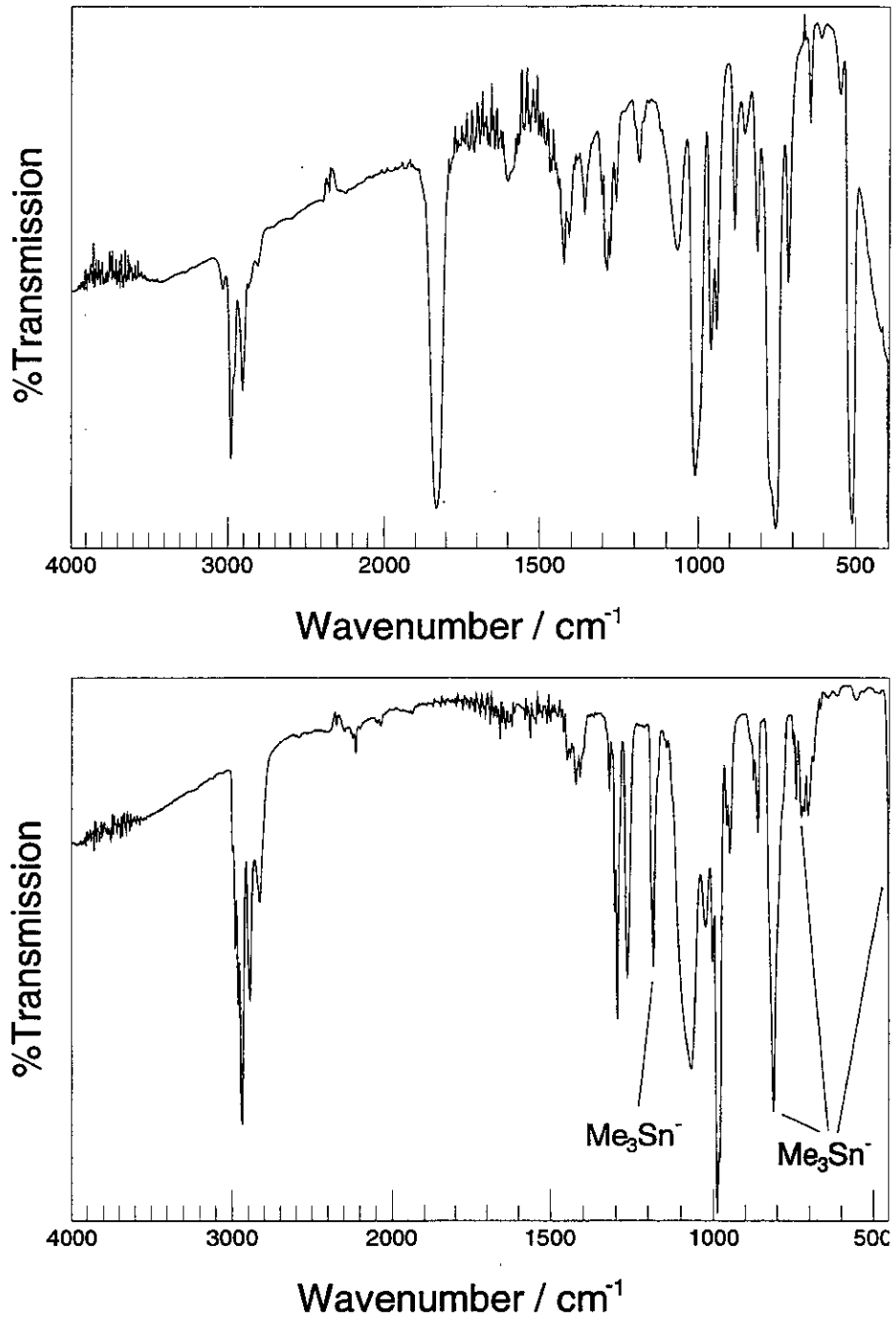

Figure 3.6. Infra-red spectra of Me_3SnH and trimethylphosphonium methylid on a CsI window at -196°C before warming (top), and after reaction (bottom).

Peak/cm^{-1}		Species	Type
2972	m		
2958	m		
2936	s		ν(C–H)
2886	m		
2825	m		
1428	w	Me_3PCH_2, $[Me_4P]^+$	$\delta_{as}(CH_3)$
1407	w	Me_3PCH_2, $[Me_3Sn^-]$	$\delta_{as}(CH_3)$
1299	m	$[Me_4P]^+$	$\delta_s(CH_3)$
1292	w	Me_3PCH_2	
1260	m	Me_3PO	
1186	m	Me_3PO	
1178	m	$[Me_3Sn^-]$	$\delta_s(CH_3)$
1065	s	Me_3PCH_2	
1020	w	Me_3PCH_2	
984	vs	$[Me_4P]^+$	$\rho(CH_3)$
944	w	Me_3PO	
858	w	Me_3PO	
808	s	$[Me_3Sn^-]$, $[Me_4P]^+$	$\rho(CH_3)$, ν_{as}(P–C)
740	w		
722	w	Me_3PCH_2, $[Me_3Sn^-]$	ν_{as}(P–C), $\rho(CH_3)$?
702	w		
440	s	$[Me_3Sn^-]$	ν_{as}(Sn–C)

Table 3.10. Infra-red Peak Listings for the Reaction between Me_3SnH and Me_3PCH_2

$Me_3SnH + Me_3PCH_2$

The interpretation of the reaction between Me_3SnH and Me_3PCH_2 at low temperature is slightly less certain than those described previously due to the complete absence of a Sn–H stretching vibration in the spectrum of the product. This is to be expected if the reaction proceeds in the pattern described above, but as the shift in the frequency of this mode to low energy provides one of the more convincing pieces of evidence for reaction as described, its absence places more emphasis on the less concrete assignments made of other peaks in the spectrum.

The presence of Me_4P^+ is indicated, however, suggesting that reaction does indeed proceed as expected. The bands at 1299cm^{-1}, 984cm^{-1}, and *ca.* 808cm^{-1} (as a shoulder to the more intense absorption there) may be assigned to the cation in the usual manner. The infra-red spectrum of the Me_3Sn^- anion would be expected to be of a similar pattern to those vibrations assigned by Schumann and Ronecker[73] to the $SnMe_3$ fragment in $Me_3SnSiMe_3$. They reported a band at 1180cm^{-1} due to $\delta_s(CH_3)$, which corresponds closely to that observed here at 1178cm^{-1}. Similarly, they report the methyl rocking mode, $\rho(CH_3)$ to occur at 762cm^{-1}: here we observe a strong absorption at 808cm^{-1}. The SnC_3 stretching vibrations for $Me_3SiSnMe_3$ are reported at 512cm^{-1} and 505cm^{-1}. It is not unreasonable to assign the band at 440cm^{-1} to the asymmetric SnC_3 stretch of $SnMe_3^-$, the symmetric stretch occurring beyond the frequency range of the spectrometer used.

Again, *ab initio* calculations were performed on $SnMe_3^-$ to determine the plausibility of these assignments, and are shown in Table 3.11.

Observed	DZ(P)/MP2
1178	1215.1, 1201.7
808, 722 ?	751.7, 734.6
440	440.9, 431.9

Table 3.11. Observed and Predicted Vibrational Frequencies (cm^{-1}) for Me_3Sn^-

The assignment of the bands around 722cm^{-1} to ν_{as}(P–C) of Me_4P^+, and a rocking mode of the methyl groups of $SnMe_3^-$ is somewhat tenuous as the

resolution of the spectrum is insufficient to distinguish the number of absorptions present in that region.

Evidence for the formation of Me_3Sn^- by reaction between Me_3PCH_2 and Me_3SnH stems from the absence of the Sn–H stretch in the product spectrum, the presence of peaks assignable to Me_4P^+, and the presence of peaks that may be assigned to an $SnMe_3$ species, but not to Me_3SnH. On this evidence, and in the light of the spectra described in previous sections, it seems reasonable to suggest that reaction does indeed proceed as expected, giving Me_4P^+ $SnMe_3^-$,

$$Me_3PCH_2 + Me_3SnH \longrightarrow Me_4P^+ \; SnMe_3^- \qquad (23)$$

The Geometries of Organostannyl Anions by *Ab initio* Calculation

In the previous sections we have described vibrational frequencies calculated *ab initio* for the organostannyl anions Me_xSnH_{3-x} (x = 0–3) and used these results to aid in the interpretation of infra-red spectra derived from the reaction between Me_3PCH_2 and their parent stannanes. The geometries of the organostannyl anions were calculated as a precursor to their vibrational frequencies, as were the geometries and vibrational frequencies of the corresponding stannanes for comparison purposes. These are shown in Table 3.12.

The effects of deprotonation on the geometries calculated are similar for each stannane studied. The angles between atoms bound directly to tin fall substantially, and their bond lengths increase throughout. The frequencies of the Sn–H stretches in the anions are some 20% less than those in the corresponding stannanes also, indicative of the weakening of the remaining Sn–H bonds on deprotonation. A similar drop in frequency has been observed on the addition of hydride anion to digallane, for example.[77] (ν_1(Ga–H_t) in Ga_2H_6 is 1993cm^{-1}, and ν_3(Ga–H) in $NaGaH_4$ is 1760cm^{-1}.) This suggests that the source of the decrease in vibrational frequency lies in the increase in negative charge on the central atom in all these species. SnH_3^- can be formally regarded as containing Sn(II), surrounded by three hydride anions. The decreased effective nuclear charge on the tin centre results in valence orbitals of increased size, and therefore increased Sn–H bond lengths. The force constant of the Sn–H bond is decreased

Parameter	SnH_4	$MeSnH_3$	Me_2SnH_2	Me_3SnH
Sn–H/Å	1.7191	1.7232	1.7269	1.7310
Sn–C/Å		2.1455	2.1468	2.1480
C–H/Å		1.0970	1.0975	1.0980
H–Sn–H(°)	109.47	108.59	107.84	
H–Sn–C(°)		110.34	109.76	109.16
C–Sn–C(°)			109.91	109.78

Parameter	SnH_3^-	$MeSnH_2^-$	Me_2SnH^-	Me_3Sn^-
Sn–H/Å	1.8025	1.8068	1.8111	
Sn–C/Å		2.2672	2.2609	2.2541
C–H/Å		1.0992	1.1024	1.1032
H–Sn–H(°)	93.13	92.65		
H–Sn–C(°)		94.14	93.63	
C–Sn–C(°)			92.73	92.41

Table 3.12. The Geometries of the Stannanes and their Anions by *ab initio* calculation (DZ(P)/MP2).

in consequence, and so the Sn–H stretching frequency in SnH_3^- is expected to be smaller than that in SnH_4.

The increase in bond length on deprotonation may also be viewed as a consequence of a change in hybridisation state at the tin centre. The decrease in bond angles around tin from roughly 109° to almost 90° strongly suggests a change in hybridisation from sp^3 to p^3, the tin 5s orbital being substantially lower in energy than the 5p orbitals in the anions, and so taking little part in bonding.

3.5.3 The Reaction between Stannanes and Me_3PCH_2 in Solution

The Reaction between Me_3SnH and Me_3PCH_2

Trimethylphosphonium methylid (0.06 mmol) and a slight excess of trimethylstannane were condensed in an ampoule containing tetrahydrofuran (2–3 ml) and warmed to -78°C, and then to room temperature, giving a pale yellow solution the colour of which faded on cooling to -78°C, but returned on re-warming

to room temperature.

In a similar experiment, trimethylstannane (1.28 mmol) and trimethylphosphonium methylid (1.11 mmol) were dissolved in diethyl ether and warmed to -78°C for 30 minutes, during which time a white precipitate slowly formed. Trimethylsilyl chloride (1.33 mmol) was then added, and the resulting mixture warmed to -40°C to allow the reactant to melt and dissolve, and stirred at -78°C for a further 30 minutes before being left to stand at room temperature.

The volatile products of the reaction were distilled through traps at -78°C, and -196°C, leaving behind a white solid with an infra-red spectrum (as a KBr pellet), and ^{1}H, ^{13}C, and ^{31}P NMR spectra corresponding to that of Me_4PCl.

The small quantity of colourless liquid present in the -78°C trap was warmed to room temperature, and distilled through a trap held at -63°C into one at -196°C. A small quantity of a white solid was found in the -63°C trap that melted on warming to around -30°C. A subsequent infra-red spectrum of the vapour corresponded to that reported by Schumann[73] in 1967 for $Me_3SiSnMe_3$, and ^{1}H and ^{13}C NMR spectra also agreed well with previously published results (see Table 3.13).

	Observed (C_6D_6)
^{1}H:	δ = 0.19 (s, $^{2}J_{^{119}Sn-H}$ = 46.6 Hz, $^{3}J_{^{29}Si-H}$ = 1.5 Hz),
	δ = 0.17 (s, $^{3}J_{^{119}Sn-H}$ = 31.4 Hz, $^{2}J_{^{29}Si-H}$ = 2.5 Hz)
^{13}C:	δ = -12.13, 0.42 ($^{2}J_{Sn-C}$ = 59.2 Hz)
	Ref. 78 (Neat liquid)
^{1}H:	$^{2}J_{^{119}Sn-H}$ = 46.8 Hz, $^{3}J_{^{119}Sn-H}$ = 31.2 Hz
^{13}C:	δ = -11.52 ($SnMe_3$), 1.13 ($SiMe_3$)
	Ref. 79 (Neat liquid)
^{13}C:	δ = -12.21 ($SnMe_3$), 0.48 ($SiMe_3$, $^{3}J_{^{119}Sn-H}$ = 54.4 Hz)

Table 3.13. Observed and Literature NMR Data for $Me_3SiSnMe_3$

The formation of $Me_3SiSnMe_3$ is indicative of the presence of Me_3Sn^-, reacting by nucleophilic substitution at silicon, and producing $Me_3SiSnMe_3$ and Me_4P^+ Cl^- as observed.

$$Me_3PCH_2 + Me_3SnH \xrightarrow{\text{thf, -78°C}} Me_4P^+ SnMe_3^- \quad (24)$$

$$Me_4P^+ SnMe_3^- + Me_3SiCl \xrightarrow{\text{thf, -78°C}} Me_3SiSnMe_3 + Me_4P^+ Cl^- \quad (25)$$

In an attempt to derive direct evidence for the presence of Me_3Sn^- in solution, the reaction between trimethylphosphonium methylid and Me_3SnH was investigated by NMR spectroscopy. Me_3PCH_2 (0.35 mmol) was condensed into an NMR tube followed by d^8-tetrahydrofuran, and allowed to dissolve. Me_3SnH (one equivalent) was then added, and the NMR tube sealed off with a hand torch and warmed to room temperature. A yellow, thermochromic solution formed (becoming colourless at -78°C), which was stored at -20°C until room temperature ^1H, ^{13}C, and ^{31}P NMR spectra were recorded. These spectra are shown in Figures 3.7, 3.8, and 3.9.

The ^1H NMR spectrum of the products of the reaction between Me_3SnH and Me_3PCH_2 contains a number of small sharp peaks, and two substantially more intense features. Me_3PO, produced by the reaction of Me_3PCH_2 with traces of air and moisture, may be assigned to the peak at $\delta = 1.60$ ($^2J_{P-H} = 12.9$ Hz) by comparison with a report by Hendrickson *et al.*[80] of the oxide dissolved in D_2O ($\delta = 1.93$, $^2J_{P-H} = 13.6$ Hz). Traces of silicone grease are most probably responsible for the small peak at $\delta = 0.24$, present as a result of the ease with which the ylid dissolves in, and possibly reacts with the grease used during this investigation.

This leaves two features unaccounted for in the ^1H spectrum - the broad signal centered at $\delta = 2.0$, and the relatively sharp singlet at $\delta = 0.11$. The ^{31}P and ^{13}C NMR spectra also show broad features, centered at $\delta = 21.2$, and 13.2 respectively which, in conjunction with the broad feature in the ^1H spectrum, correspond well with spectra recorded for a sample of Me_4PBr in D_2O prepared as described in Chapter 2 (^1H: $\delta = 1.91$ ($^2J_{P-H} = 14.7$ Hz), ^{13}C: $\delta = 9.1$ ($^1J_{P-C} = 56.5$ Hz), ^{31}P: $\delta = 23.7$ ($^1J_{P-C} = 56.4$ Hz)). Additionally, Me_3PCH_2 has been reported to undergo rapid inter-, and intra-molecular proton exchange.[81,82] The resonances observed here may therefore have been broadened due to the presence of a small excess of the ylid in the NMR tube.

The remaining feature in the ^1H spectrum, at $\delta = 0.11$, shows couplings of $^2J_{Sn-H} = 19.4$ Hz, and $^1J_{C-H} = 125.5$ Hz. The Sn–H coupling is of a magnitude

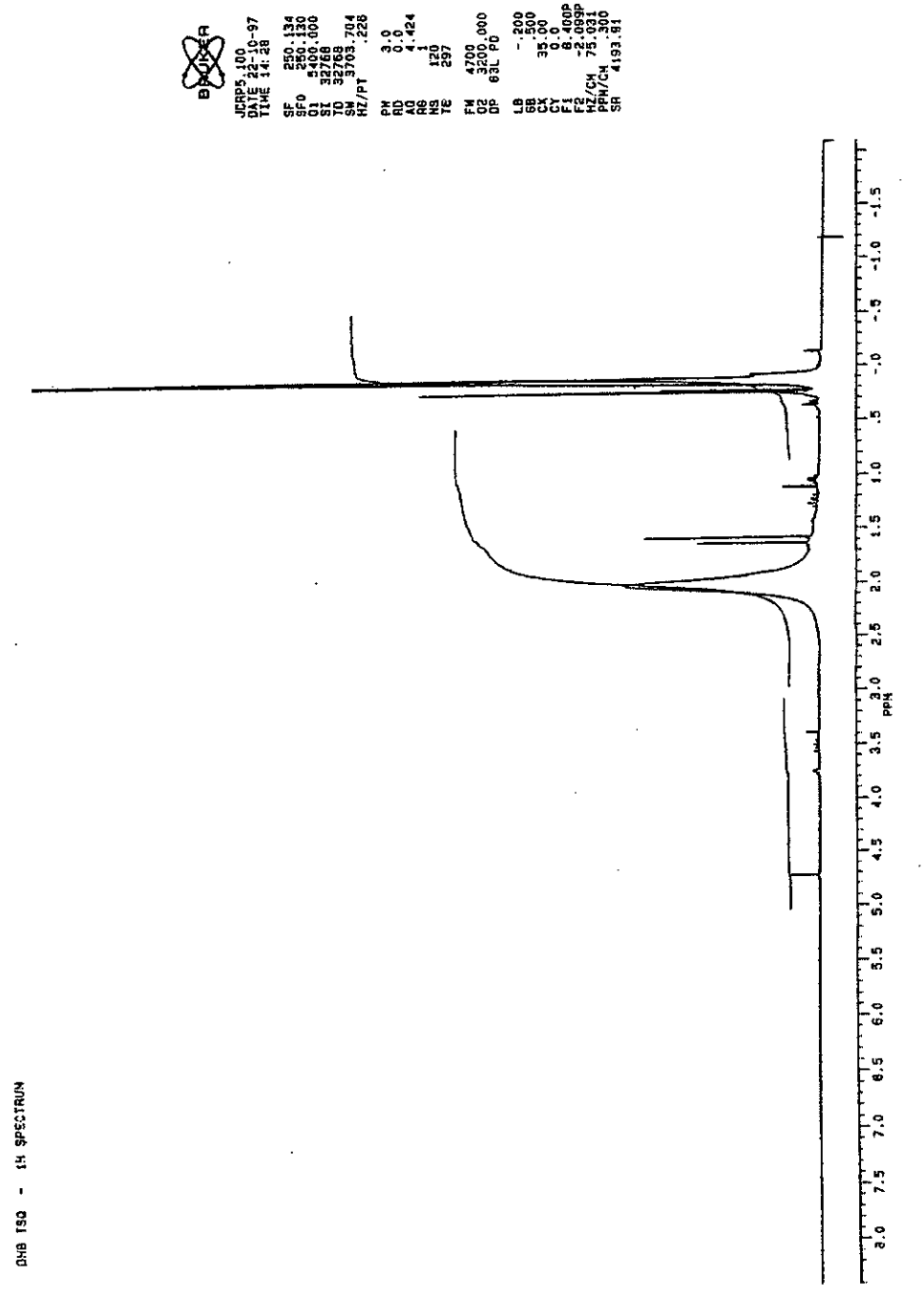

Figure 3.7. The ^{1}H NMR Spectrum of a Solution of Me_3PCH_2 and Me_3SnH in d^8-tetrahydrofuran at room temperature.

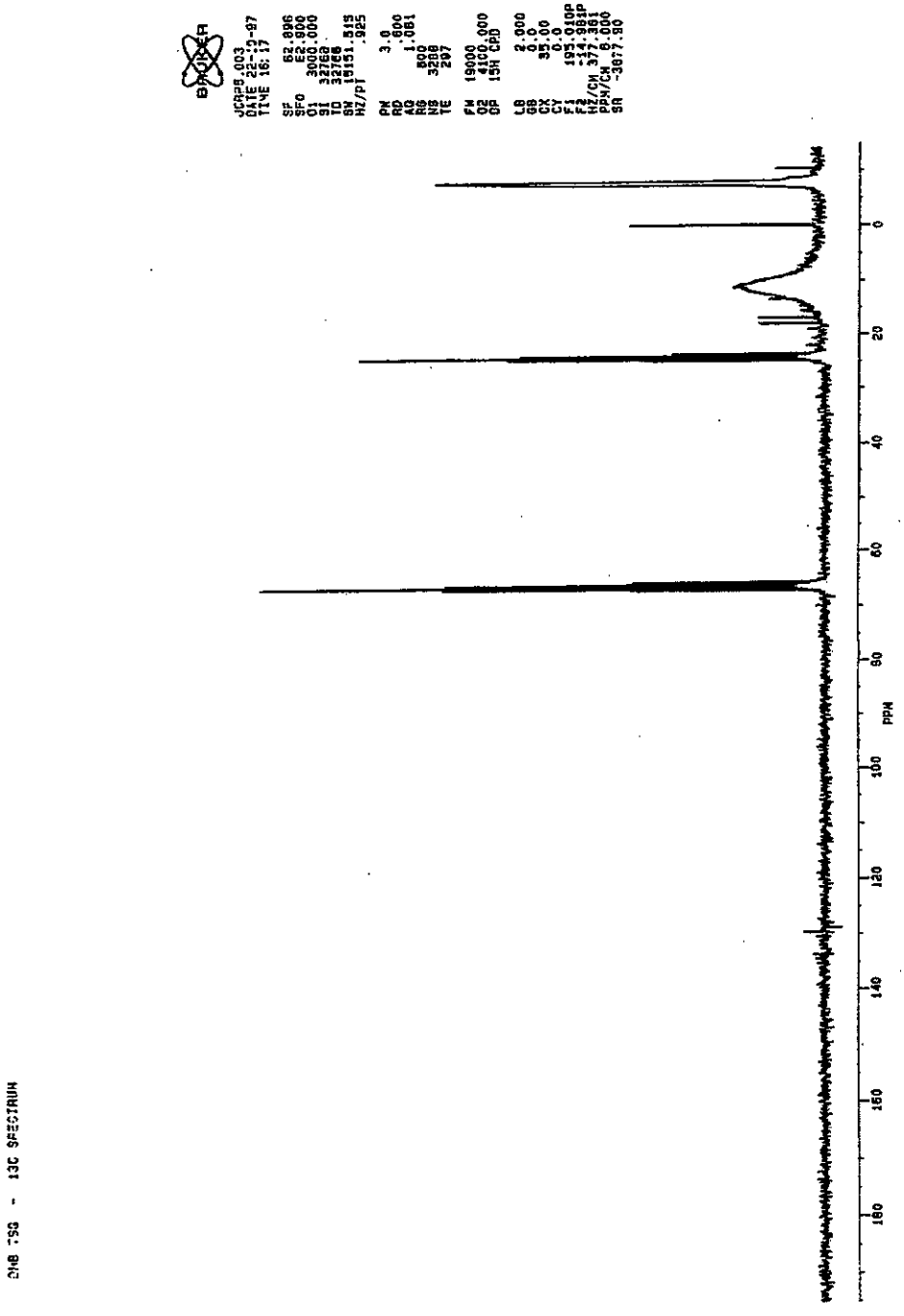

Figure 3.8. The ^{13}C NMR Spectrum of a Solution of Me_3PCH_2 and Me_3SnH in d^8-tetrahydrofuran at room temperature.

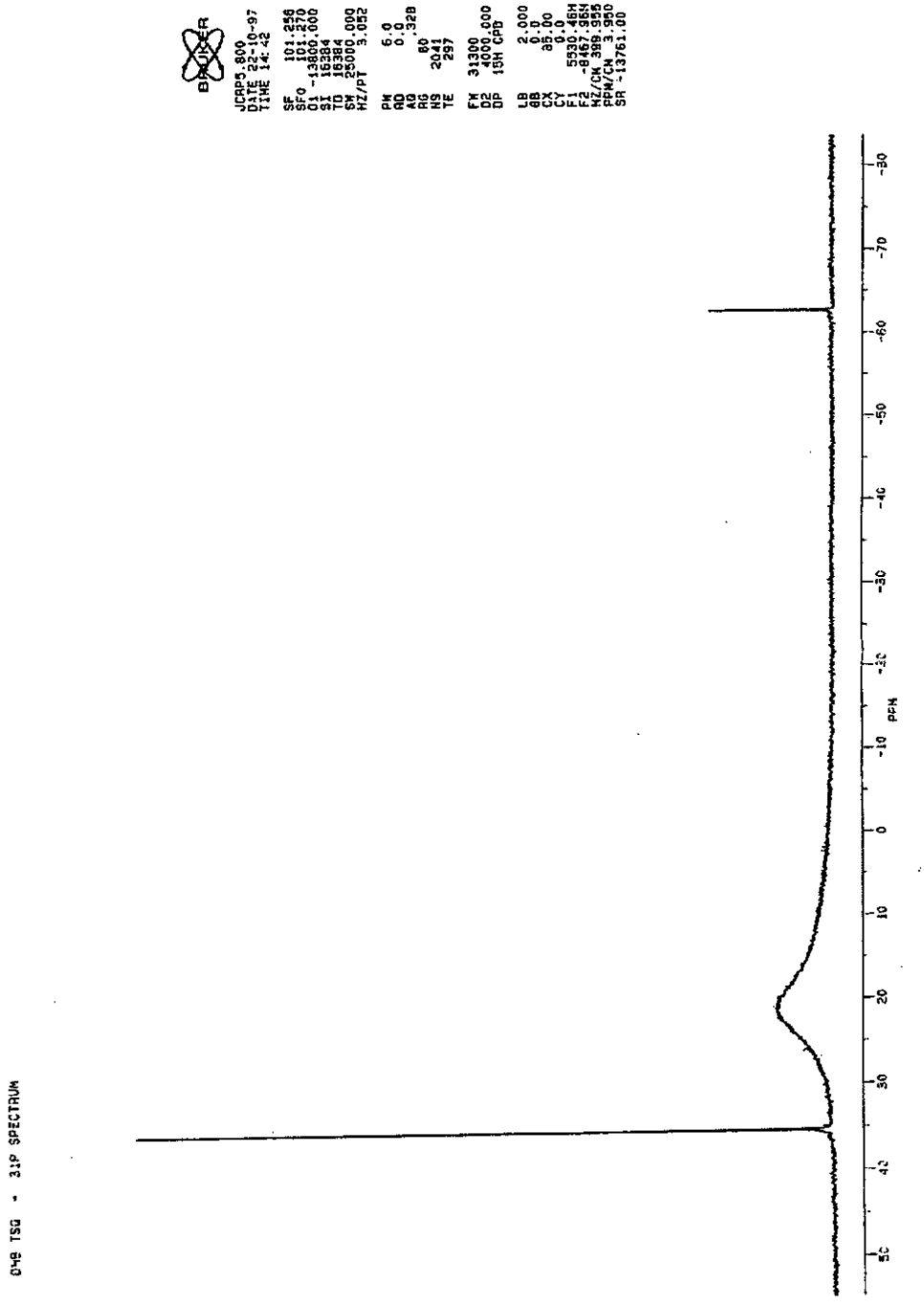

Figure 3.9. The ^{31}P NMR Spectrum of a Solution of Me_3PCH_2 and Me_3SnH in d^8-tetrahydrofuran at room temperature.

observed by Birchall[72] for Me_3Sn^-. They recorded the ^1H NMR spectrum of $NaSnMe_3$ at -60°C in liquid ammonia, quoting δ = -0.57, $^2J_{Sn-H}$ = 14.2 Hz. Our observation of a resonance at δ = 0.11, $^2J_{Sn-H}$ = 19.4 Hz, in tetrahydrofuran at room temperature corresponds well with this. The observation in the ^{13}C spectrum of a resonance (δ = -8.1) of comparable intensity to that assigned to Me_4P^+ and the absence of a corresponding resonance in the ^{31}P spectrum is also in agreement, suggesting that the species responsible contains hydrogen, carbon, and tin only.

This NMR investigation therefore provides substantial evidence for the formation of Me_4P^+ $SnMe_3^-$ as a product of the reaction between Me_3PCH_2 and Me_3SnH.

The Reaction between SnH_4 and Me_3PCH_2

Trimethylphosphonium methylid (0.06 mmol) and a slight excess of stannane were condensed from the high vacuum line into a Young's tap ampoule containing diethyl ether, and warmed to -78°C. A white precipitate was formed that turned a pale yellow colour on warming to room temperature, and decomposed on standing over night. The volatile contents of the ampoule were analysed by mass spectrometry (see Figure 3.10) and found to be trimethylphosphine (m/z = 76), methane (m/z = 16), and hydrogen gas, with metallic tin remaining in the ampoule. Similar results were obtained if tetrahydrofuran was used as the solvent for the reaction.

The reaction between stannane and trimethylphosphonium methylid was also investigated by low temperature ^1H NMR. Me_3PCH_2 (0.07 mmol) was condensed into a NMR tube, followed by d^8-tetrahydrofuran, and allowed to dissolve. SnH_4 (0.075 mmol) was then added, the tube sealed off with a hand torch, then warmed to -78°C. A white precipitate instantly formed, which persisted on warming to -40°C inside the NMR spectrometer. The spectrum recorded is shown in Figure 3.11. The NMR tube was subsequently allowed to warm to room temperature, the white precipitate turning brown with effervescence of a colourless gas.

Interpretation of the low temperature NMR spectrum recorded of the reaction between stannane and Me_3PCH_2 is less satisfying than that for the analogous

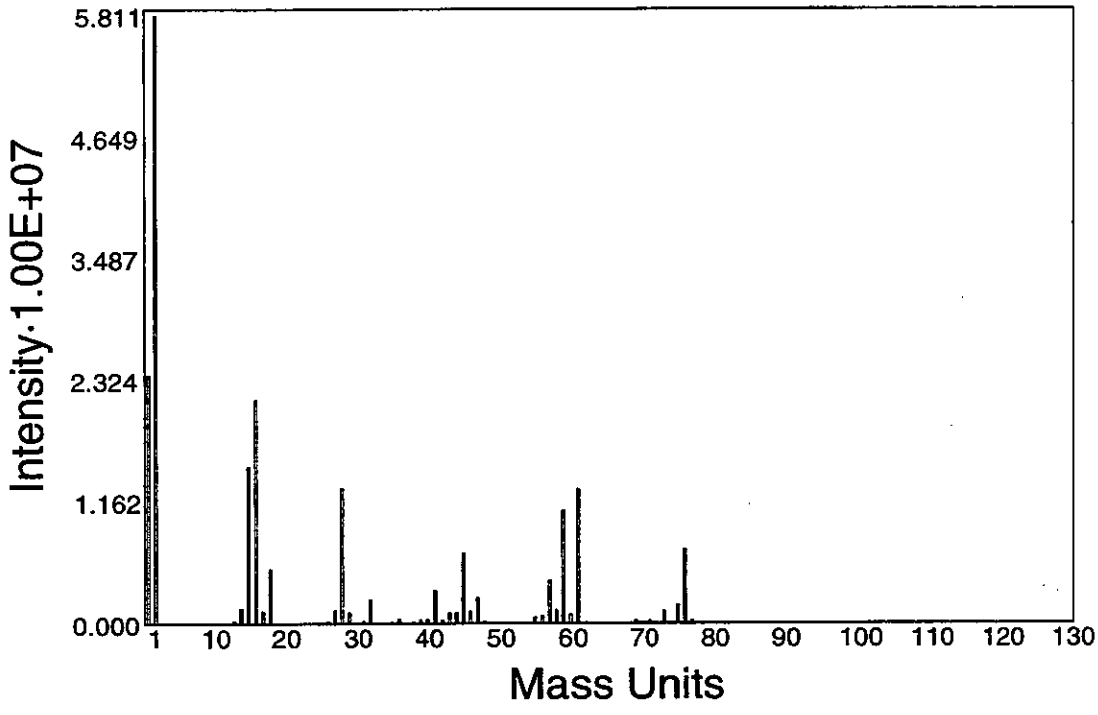

Figure 3.10. Mass Spectrum of the Decomposition Products of the Reaction between Me_3PCH_2 and SnH_4 in Tetrahydrofuran.

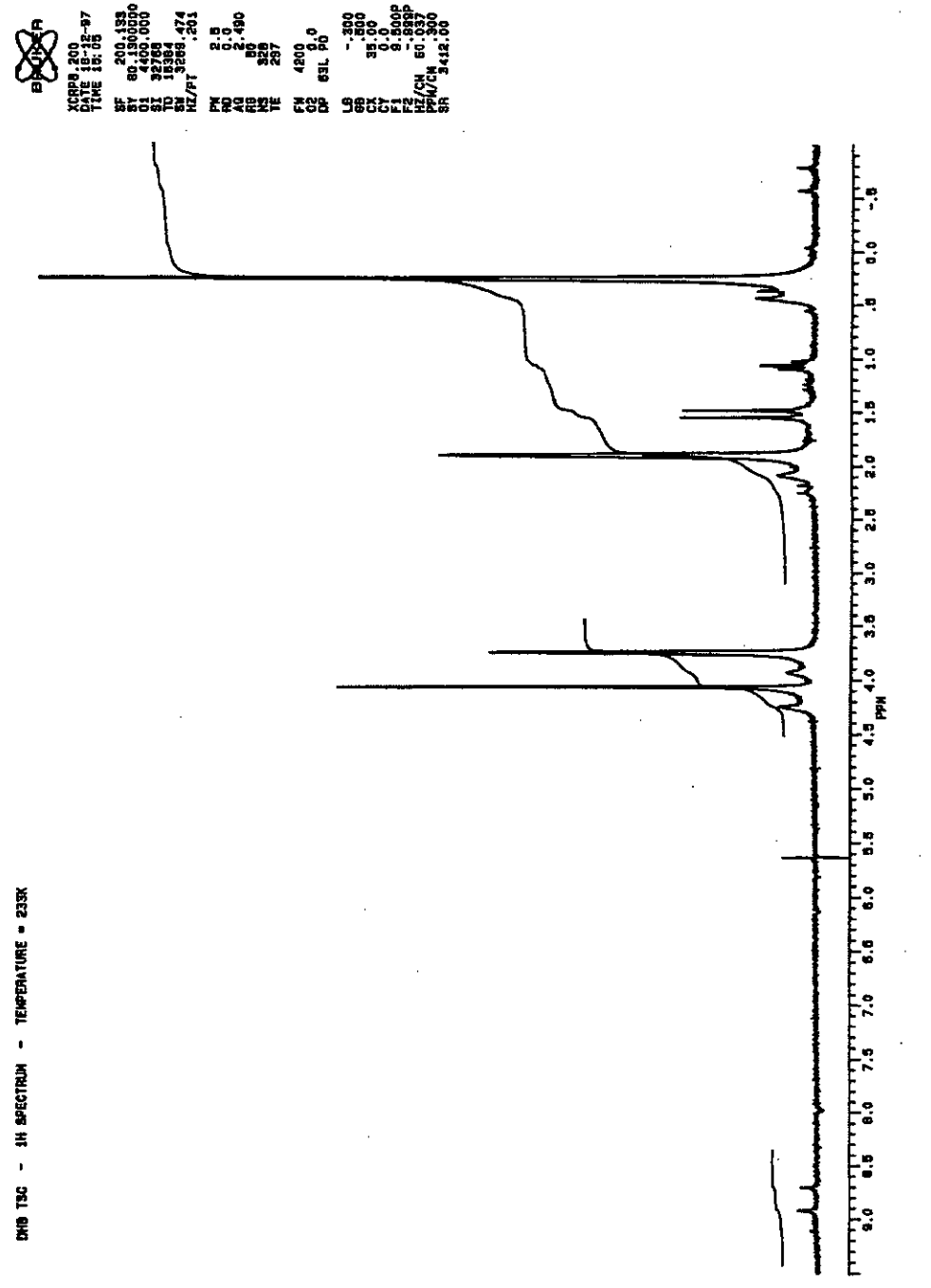

Figure 3.11. The ^{1}H-NMR Spectrum of a mixture of Me_3PCH_2 and SnH_4 at -40°C.

reaction between Me_3SnH and Me_3PCH_2. The presence of solid in the NMR tube results in a shimming error manifesting itself as shoulders of small intensity to high frequency of peaks in the spectrum. Solvent resonances at $\delta = 3.74$ and 1.90 may also be discounted, leaving three features in the spectrum to be accounted for.

The peak at $\delta = 4.06$, showing a $^1J_{^{119}Sn-H}$ coupling of 1942 Hz may be assigned to stannane.[59] The resonance at $\delta = 1.52$ shows a $^2J_{P-H}$ coupling of 13.1 Hz, which may be assigned to Me_3PO as before, and the peak at $\delta = 0.26$ to silicone grease.

Thus, no evidence for the formation of Me_4P^+ SnH_3^- is present in the spectrum, despite the observation of large quantities of a white precipitate in the NMR tube. The persistence of this precipitate at room temperature suggests that it has a low solubility in tetrahydrofuran, and the intensity of the solvent peaks in the NMR experiment and the relatively large amount of noise still present in the spectrum (after 328 scans) confirms that little is present in solution, despite the relatively large amounts of reactants that were present.

It would therefore appear that Me_4P^+ SnH_3^- has little solubility in tetrahydrofuran at -40°C and for that reason was not detected in the low temperature NMR experiment. As no other solvent potentially suited to the task is both available in a fully deuterated form and economically accessible, it seems that the investigation of Me_4P^+ SnH_3^- in solution by ^1H NMR is not currently feasible.

The Reactions between $MeSnH_3$, Me_2SnH_2 and Me_3PCH_2

$MeSnH_3$ + Me_3PCH_2 Trimethylphosphonium methylid (0.06 mmol) and a slight excess of methylstannane were condensed into an ampoule containing tetrahydrofuran and warmed to -78°C. A white precipitate formed that dissolved at around 0°C to give a colourless solution that gradually turned yellow, then orange on standing at room temperature while slowly effervescing.

The ampoule was then cooled back to -78°C and the solvent slowly pumped to the high vacuum line. Orange, needle-like crystals formed at the liquid–vacuum interface, decomposing on warming above about -50°C to a black solid.

Me_2SnH_2 + Me_3PCH_2 Trimethylphosphonium methylid (0.06 mmol) and a slight excess of dimethylstannane were condensed into an ampoule containing tetrahydrofuran and warmed to -78°C. A white precipitate formed that dissolved on further warming, giving a colourless solution that slowly effervesced and turned bright yellow at room temperature.

Interpretation The reactions between methylstannane, dimethylstannane and trimethylphosphonium methylid can be interpreted as the low temperature infrared spectra described previously suggest, as acid–base reactions giving stannyl anions. The Me_2SnH^-, and $MeSnH_2^-$ formed in this way then decompose on warming to give highly coloured species resembling those formed in reactions between stannanes and alkyl lithium, and alkali metal hydride reagents. It therefore seems plausible that polymeric $(MeSnH)_x$ and $(Me_2Sn)_x$ are formed here during decomposition.

The analysis of the decomposition products of $Me_4P^+\ SnH_3^-$ suggests reduction of the cation by the anion from phosphorus(V) to phosphorus(III) as the decomposition pathway.

$$Me_3PCH_2 + SnH_4 \xrightarrow{\text{thf, -78°C}} Me_4P^+\ SnH_3^- \qquad (26)$$

$$Me_4P^+\ SnH_3^- \xrightarrow{\Delta} Me_3P + CH_4 + Sn + H_2 \qquad (27)$$

$$Me_3PCH_2 + MeSnH_3 \xrightarrow{\text{thf, -78°C}} Me_4P^+\ MeSnH_2^- \qquad (28)$$

$$Me_4P^+\ MeSnH_2^- \xrightarrow{\Delta} Me_3P + CH_4 + (MeSnH)_x + H_2 \qquad (29)$$

$$(MeSnH)_x \xrightarrow{\Delta, \text{ in absence of thf}} MeH + Sn \qquad (30)$$

$$Me_3PCH_2 + Me_2SnH_2 \xrightarrow{\text{thf, -78°C}} Me_4P^+\ Me_2SnH^- \qquad (31)$$

$$Me_4P^+\ Me_2SnH^- \xrightarrow{\Delta} Me_3P + CH_4 + (SnMe_2)_x + H_2 \qquad (32)$$

The absence here of the colour changes observed during the decomposition of the alkali metal salts of SnH_3^- is possibly a result of the high temperature at which decomposition takes place, any hydride containing species produced having little stability at that temperature, and so quickly decomposing to tin metal and hydrogen gas.

3.5.4 The Reaction between Stannanes and Triphenylphosphonium Methylid

The reactions between triphenylphosphonium methylid, Ph_3PCH_2 and the stannanes Me_xSnH_{4-x} (x = 0–3) were investigated in the hope that they would follow a similar pattern to those reported above with Me_3PCH_2. The relative ease with which Ph_3PCH_2 can be prepared and manipulated in comparison to Me_3PCH_2 suggested that if it reacted similarly, then the synthetic utility of the resulting salts could be exploited in a straightforward manner.

The Reaction between Me_3SnH and Ph_3PCH_2

Me_3SnH + Ph_3PCH_2 in tetrahydrofuran Triphenylphosphonium methylid (1 mmol) and trimethylstannane (1 mmol) were stirred over night in tetrahydrofuran solution at room temperature. After 18 hours, the yellow colour of the ylid had faded away, leaving an almost colourless solution.

A similar reaction was performed using 0.2 mmol Ph_3PCH_2 and 0.3 mmol Me_3SnH in d^8-tetrahydrofuran. ^{13}C, ^{1}H, ^{31}P, and ^{119}Sn NMR spectra were recorded, and the data collected are shown in Table 3.14.

^{119}Sn:	δ = -28.1 (s), -106.8 (s).
^{31}P:	δ = -25.4 (s).
^{13}C:	δ = -11.5 (s), -11.0 (s), 11.4 (d, $^{1}J_{C-P}$ = 15.3 Hz), δ = 131.5 (d, $^{2}J_{C-P}$ = 18.8 Hz), 127.7 (broad s).
^{1}H:	δ = 0.42 (s, $^{2}J_{^{119}Sn-H}$ = 48.8 Hz, $^{3}J_{^{119}Sn-H}$ = 16.2 Hz), 0.46 (s, $^{2}J_{^{119}Sn-H}$ = 55.3 Hz), δ = 1.75 (d, $^{2}J_{P-H}$ = 4.0 Hz), 7.4–7.5 (m), 7.5–7.7 (m).

Table 3.14. NMR Data from the Reaction between Me_3SnH and Ph_3PCH_2 in d^8-thf.

Me_3SnH + Ph_3PCH_2 in pentane Triphenylphosphonium methylid (1 mmol) and trimethylstannane (1 mmol) were stirred over night in pentane giving a colourless solution. This was reduced *in vacuo* to give a small amount of a relatively non-volatile liquid, which was transferred (through judicious use of a

heat gun) to an NMR tube and dissolved in d^8-tetrahydrofuran. ^{1}H, ^{31}P, and ^{119}Sn (with, and without proton decoupling) were recorded, and the results are shown in Table 3.15.

^{119}Sn:	δ = -28.1 (poorly resolved decet, $^2J_{^{119}Sn-H} \simeq 54$ Hz).
^{31}P:	δ = -25.4 (s), -3.6 (s).
^{1}H:	δ = 0.46 (s, $^2J_{^{119}Sn-H}$ = 55.3 Hz), δ = 1.75 (s, $^2J_{P-H}$ = 4.0 Hz), δ = 7.4–7.5 (m), δ = 7.5–7.7 (m).

Table 3.15. NMR Data from the Reaction between Me_3SnH and Ph_3PCH_2 in pentane.

Me_3SnH + Ph_3PCH_2 in hexane Triphenylphosphonium methylid (1 mmol) and trimethylstannane (1.1 mmol) were stirred over night at room temperature in hexane, producing a colourless solution to which was added 1.1 mmol trimethylsilyl chloride. After stirring for a further 3 hours, the colourless solution was left for a further 48 hours, and then distilled through traps held at -31°C, and -196°C to the high vacuum line. A small quantity of a colourless liquid condensed in the -31°C trap which was dissolved in d^8-tetrahydrofuran and submitted for analysis by ^{1}H, ^{13}C, and ^{119}Sn NMR spectroscopy (see Table 3.16).

^{119}Sn:	δ = -28.0 (s), -106.6 (s)
^{13}C:	δ = -11.1 (s), 127.5 (s), 127.6 (2), 135.2 (s)
^{1}H:	δ = 0.44 (s, $^2J_{^{119}Sn-H}$ = 55.3 Hz), δ = 0.38 (s, $^2J_{^{119}Sn-H}$ = 48.8 Hz, $^3J_{^{119}Sn-H}$ = 16.2 Hz), δ = 7.40–7.50 (m), δ = 7.60–7.65 (m).

Table 3.16. NMR Data of the Volatile Product of the Reaction between Me_3SnH and Ph_3PCH_2 in hexane.

Me_3SnH + Ph_3PCH_2 in Et_2O Triphenylphosphonium methylid (1 mmol) and trimethylstannane (1 mmol) were mixed in diethyl ether and left to stand in a Young's tap ampoule for three months. The solution remained yellow throughout this time, eventually forming a small quantity of a black precipitate.

Interpretation The reaction between Ph_3PCH_2 and Me_3SnH does not resemble the reaction between Me_3PCH_2 and Me_3SnH. In diethyl ether solution no reaction is observed, as indicated by the persistence of the yellow colour due to the ylid over time. In tetrahydrofuran and hydrocarbon solvents the yellow colour slowly fades, in both cases producing a small quantity of a colourless liquid with a low vapour pressure at room temperature. The NMR data collected by performing the reaction in a sealed NMR tube indicate the presence of two tin containing species, but only one phosphorus containing species.

Comparison of the data with that collected in the literature (see Table 3.17) suggests the presence of Ph_2PMe. The variety of solvents used in the literature complicates the comparison of chemical shift data, but the general fit is good, and the agreement between observed and literature C–P and H–P coupling constants is excellent.

Nucleus	Chemical Shift	Solvent	Ref.
^{31}P:	δ = -27.7	C_6D_6	83
^{13}C:	δ = 12.7 ($^1J_{C-P}$ = 15.4 Hz),	C_6D_6	83
	δ = 141.5 ($^1J_{C-P}$ = 14.1 Hz),		
	δ = 132.6 ($^2J_{C-P}$ = 18.8 Hz),		
	δ = 128.8 ($^3J_{C-P}$ = 6.4 Hz),		
	δ = 128.7 ($^4J_{C-P}$ not resolved).		
^1H:	δ = 1.6 (s, $^2J_{P-H}$ not resolved),	$CDCl_3$	84
	δ = 7.3 (m), 7.4 (m)		

Table 3.17. Literature NMR Data for Ph_2PMe.

The tin species present can also be identified by comparison with the literature. In the reaction between Ph_3PCH_2 and Me_3SnH in an NMR tube, both $Me_3SnSnMe_3$ and $PhSnMe_3$ are formed. Their NMR parameters are shown in Tables 3.18 and 3.19. Again, the comparison of observed and literature chemical shifts is made difficult due to solvent effects, but the agreement between coupling constants is very good.

The isolation of $PhSnMe_3$ as a major product of the reaction is confirmed by its distillation from the product mixture and observation by ^{119}Sn NMR. The ^{119}Sn and ^{13}C chemical shifts recorded here correspond exactly to that of the tin

Nucleus	Chemical Shift	Solvent	Ref.
^{119}Sn:	δ = -108.7	$CDCl_3$	79
	δ = -91.5 ($^2J_{^{119}Sn-H}$ = 51.6 Hz, $^3J_{^{119}Sn-H}$ = 17.7 Hz)		78
^{13}C:	δ = -10.22	$CDCl_3$	79

Table 3.18. Literature NMR Data for $Me_3SnSnMe_3$.

Nucleus	Chemical Shift	Solvent	Ref.
^{13}C:	δ = -9.7, 128.4, 128.7, 135.8, 142.1	$CDCl_3$	85
^{1}H:	$^2J_{^{119}Sn-H}$ = 54.6 Hz	CCl_4	86

Table 3.19. Literature NMR Data for $PhSnMe_3$ (bottom).

species isolated simply by pumping off the reaction solvent, and transferring the liquid remainder to an NMR tube. The proton-coupled ^{119}Sn NMR spectrum of that species gave an even number of peaks, indicating the presence of either one or three methyl groups bound directly to tin. Examination of the integration of the ^{1}H spectrum suggests a ratio of approximately 6 phenyl protons to 10 alkyl protons, allowing us to discard the possibility of the presence of Ph_3SnMe, and suggest $PhSnMe_3$ as the major tin containing reaction product. The presence of a small quantity of $Me_3SnSnMe_3$ is probably a result of the use of an excess of the stannane in each reaction.

Ph_3PCH_2 and Me_3SnH therefore slowly react to give Ph_2PMe and Me_3SnPh.

$$Ph_3PCH_2 + Me_3SnH \xrightarrow{18\ h} Ph_2PMe + Me_3SnPh \qquad (33)$$

The Reactions between SnH_4, $MeSnH_3$, Me_2SnH_2 and Ph_3PCH_2

SnH_4 + Ph_3PCH_2 Triphenylphosphonium methylid (0.2 mmol) was transferred to a Young's tap ampoule in the dry box. On the high vacuum line, diethyl ether was condensed into the ampoule followed by stannane (0.35 mmol). The resulting mixture was warmed to -78°C at which point the yellow ylid dissolved

giving a colourless solution. On warming to approximately -50°C the solution began to effervesce, darkening in colour, and forming a tin mirror above the liquid surface in the ampoule.

$MeSnH_3$ + Ph_3PCH_2 Triphenylphosphonium methylid (1 mmol) was transferred to a Young's tap ampoule in the dry box. On the high vacuum line, the ylid was dissolved in tetrahydrofuran, and methylstannane (1.1 mmol) added. On warming to -78°C a deep red solution was formed that on warming to room temperature turned orange then yellow, while very slowly effervescing. After a few seconds at room temperature the solution gradually began to darken in colour, effervescing more rapidly and turning brown then almost black with the formation of a black precipitate.

Me_2SnH_2 + Ph_3PCH_2 Triphenylphosphonium methylid (0.3 mmol) was transferred to a Young's tap ampoule in the dry box. On the high vacuum line, the ylid was dissolved in tetrahydrofuran and an equivalent of dimethylstannane added. On warming to -78°C, the resulting solution turned deep red in colour, forming an orange solution and precipitate on warming to room temperature.

Interpretation

The observations of the reactions between Ph_3PCH_2, and SnH_4, $MeSnH_3$, and Me_2SnH_2 are, at least in their later stages reminiscent of those between the stannanes and Me_3PCH_2, suggesting that a similar pattern of reactions takes place. The formation of a deep red solution when Ph_3PCH_2 was mixed with $MeSnH_3$, and Me_2SnH_2 is intriguing, and perhaps indicative of the formation of a stannane–ylid complex of some kind at low temperature. Further characterisation is therefore required before the products of these reactions can be identified with greater certainty.

$$Ph_3PCH_2 + SnH_4 \longrightarrow [Ph_3PCH_3]^+ SnH_3^- \quad (34)$$

$$Ph_3PCH_2 + MeSnH_3 \longrightarrow [Ph_3PCH_3]^+ MeSnH_2^- \quad (35)$$

$$Ph_3PCH_2 + Me_2SnH_2 \longrightarrow [Ph_3PCH_3]^+ Me_2SnH^- \quad (36)$$

3.6 Summary and Suggestions for Further Work

1. Stannane reacts with sodium hydride, and potassium hydride to give salts containing SnH_3^-. The thermal stability of the salt is dependent upon cation size, $NaSnH_3$ decomposing at -15°C, $KSnH_3$ at 0°C, and the cryptate K[2,2,2-crypt]SnH_3 at room temperature.

2. Methyl-, dimethyl-, and trimethylstannane, and stannane itself react with trimethylphosphonium methylid to give Me_4P^+ $MeSnH_2^-$, Me_4P^+ Me_2SnH^-, Me_4P^+ Me_3Sn^-, and Me_4P^+ SnH_3^- respectively.

3. Me_2SnH^-, $MeSnH_2^-$, and SnH_3^- decompose on warming via highly coloured species. Analogy with the previously characterised highly coloured $(Me_2Sn)_x$ and $(Bu_2Sn)_x$ suggests that these species are most probably the polymers $(Me_2Sn)_x$, $(MeSnH)_x$, and $(SnH_2)_x$, but further characterisation is required before these suggestions can be made less tentative.

4. Methyl-, dimethyl-, and trimethylstannane react with methyl lithium by elimination of lithium hydride, producing dimethylstannane, trimethylstannane, and tetramethyltin respectively.

5. Trimethylstannane and Ph_3PCH_2 react to give Ph_2PMe and $PhSnMe_3$.

6. Me_4P^+ $SnMe_3^-$ reacts with Me_3SiCl to give $Me_3SiSnMe_3$ and Me_4PCl.

7. The organostannyl anions SnH_3^-, $MeSnH_2^-$, and Me_2SnH^-, as synthesised by reaction of the appropriate stannane with Me_3PCH_2 probably react similarly with electrophiles, providing potentially straightforward routes to species such as Me_3SiSnH_3, $In(SnH_3)_3$, and Me_3SnSnH_3. Their chemistry promises to be rich, and warrants substantial further investigation.

8. The structural chemistry of the organostannyl anions has so far been limited to anions with three organic substituents, and so the solid state structures of the organostannyl anions described here are of great interest, and worthy of determination despite the experimental challenges involved. A combination of neutron and X-ray diffraction techniques (as described in Chapter 6) may be usefully applied to this purpose.

Chapter 4

The Chemistry of Monochlorostannane

4.1 Introduction

The monohalostannanes, SnH_3X(where X = Cl, Br, or I), are colourless, air and moisture sensitive, highly thermally fragile vapours,[87,88] which decompose rapidly at room temperature to stannane, dihydrogen, and SnX_2. As a result of their thermal fragility, very little is known about their chemical properties, and experimental work to date has concentrated on the detailed study of their infra-red spectra. They do, however, represent the simplest known compounds containing the stannyl group.

4.1.1 Preparation

Monochlorostannane, SnH_3Cl, was first prepared by Amberger[88] in 1960, by the reaction of stannane with anhydrous hydrogen chloride at -70°C.

$$SnH_4 + HCl \xrightarrow{\text{-70°C, } AlCl_3} SnH_3Cl + H_2 \qquad (1)$$

His description of the product as a colourless vapour, substantially less stable than the germanium analogue, remained the only report of this species until 1971, when investigations by Jolly of the stannyl cation,[89] SnH_3^+, led him naturally onto the preparation of the chloro-, bromo-, and iodostannanes,[87] and their

characterisation by gas phase, and solid infra-red spectroscopy, and by mass spectrometry.

The monohalostannanes, prepared by reaction of stannane with the appropriate hydrogen halide at -78°C in a sealed tube, begin to decompose above -40°C, the rate of decomposition depending slightly upon the halide used. In their studies of the infra-red spectra of these molecules, Betzel and Bürger report complete decomposition at room temperature after 5 minutes for SnH_3Cl, 15 minutes for SnH_3Br, and 10 minutes for SnH_3I. However, distillation under high vacuum and continuous pumping can be performed, but usually results in decomposition of around 10% of the sample.

4.1.2 Structural Characterisation

The Raman spectra of the solid monohalostannanes are very similar. Bands are observed at 1880cm^{-1}(strong, symmetric stretch), and 733cm^{-1}(weak, tentatively assigned to the in-plane bending vibration) in the spectra of SnH_3Cl, and SnH_3Br; the spectrum of SnH_3I also contains a band at 1880cm^{-1}, but that at 733cm^{-1} is missing, presumed too weak to be observed.[87] In all three spectra, a strong absorption at around 30-50cm^{-1} is ascribed to a lattice vibrational mode.

These similarities, and the absence in the solid state of any absorption characteristic of a tin-terminal halogen stretching mode, suggest a structure consisting of chains of relatively independent SnH_3^+ cations, linked by bridging halide anions, resulting in essentially five coordinate tin. Examples of such structures are well known.[90]

The infra-red spectra of the monohalostannanes have been studied exhaustively in the gas phase,[91–93] and point conclusively to a C_{3v} structure for all three molecules. Microwave studies of all three have also been performed,[94–96] providing accurate determinations of the rotation constant B_0. To define completely the structure of the monohalostannanes in the gas phase, three independent pieces of structural information are required, giving the Sn-H, and Sn-X bond lengths, and the X-Sn-H bond angle. Only one piece of information can be derived from a single rotational constant (see Figure 4.1), and as A_0 cannot be determined experimentally from pure rotational spectra, two extra are required therefore before

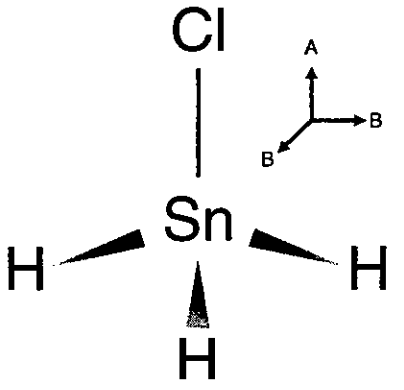

Figure 4.1. The Axes of Rotation of SnH_3Cl.

the structure can be determined fully.

The conventional solution to this problem - the determination of the rotation constants of isotopically substituted variants of the molecules in question - does not succeed for the monohalostannanes. This is not due to any difficulties in the preparation of isotopically enriched species, for both microwave and infrared studies of these molecules require the use of mono-isotopic tin, chlorine, and bromine. Rather, the problem lies in the large difference in mass between the hydrogen atom, and those of tin and the halogens. This results in a very small dependence of B_0 on the geometry of the SnH_3 top, requiring an alternative solution to be attempted.

Betzel and Bürger[93] have attempted to determine the geometry of the monohalostannanes in the gas phase using a relation between $\overline{\nu}(SnH)$ and $r_0(SnH)$ similar to that devised by McKean[97] for C-H, Si-H, and Ge-H bonds resulting in the parameters given in Table 4.1.

The accuracy of these parameters, unestimated by the authors, is dependent upon the validity of the relationship used in the determination of the Sn-H bond length. This, in turn, relies upon a strong correlation between the stretching frequency of the Sn-H bond, and its length. As the Sn-H stretching frequency and corresponding bond length have been determined for only stannane, and the diatomic, Sn–H, the reliability of the monohalostannane geometries derived from it, as Betzel and Bürger point out, must be questioned.

	SnH_3Cl	SnH_3Br	SnH_3I
r(Sn–H)/pm	1.696	1.698	1.701
r(Sn–X)/pm	2.328	2.470	2.675
<(H–Sn–X)/°	105.5	106.0	107.1

Table 4.1. The Gas Phase Structure of the Monohalostannanes from Microwave and Infra-red Data[93]

4.1.3 SnH_3^+ in solution.

The solution chemistry of the monohalostannanes has not been explored widely. Jolly[89] attempted a synthesis in aqueous media using stannane dissolved in eutectic mixtures of water and HCl, HBr, and HI, and explored the resulting reactions *via* NMR experiments, and by careful measurement of any hydrogen gas evolved. Noting a positive correlation between reaction rate, and the pK_a of the acid used, he then went on to study the chemistry of stannane when dissolved in neat fluorosulphonic acid, HSO_3F. The ^{119}Sn NMR spectrum of the resulting solution provides convincing evidence of the existence of SnH_3^+ in the solution phase and has since been investigated in considerable detail.[98]

Stannane reacts with fluorosulphonic acid in the following manner,

$$SnH_4 + HSO_3F \xrightarrow{\text{-78°C, liq. } HSO_3F} SnH_3^+ + SO_3F^- + H_2 \qquad (2)$$

On warming, no more hydrogen is evolved, the solution instead turning a light blue colour. The colour can be reproduced by the addition of elemental sulphur to fluorosulphonic acid, and is indicative of the presence of sulphur polycations in solution. At room temperature, sulphur dioxide may be pumped off the reaction mixture; this is known to be reduced to elemental sulphur by dihydrogen in HSO_3F solution, and strongly suggests a redox reaction as the decomposition pathway of SnH_3^+.

The ^{119}Sn NMR spectrum of stannane dissolved in fluorosulphonic acid gives a quartet at -192 ppm, significantly deshielded from the quintet observed for stannane dissolved in toluene, at -493 ppm. On warming, the quartet slowly decays, until at room temperature the only resonance observable is a singlet at -1780 ppm, corresponding to a solution of $Sn(SO_3F)_2$ in HSO_3F.

The ^{119}Sn-H coupling constant in SnH_3^+ is about 2960 Hz. Jolly *et al.*[89] suggest that this is not unreasonable for a planar SnH_3^+ cation with a fairly high positive charge on the tin centre for the following reasons. It is well established that the Sn–H coupling constant in neutral tin-containing species is proportional to the s-character of the tin orbital involved in bonding.[59,99,100] In stannane itself, $^1J_{^{119}Sn-H} = 1933$ Hz, suggesting that $^1J_{^{119}Sn-H}$ in a species containing sp^2 hybridised tin should be around 4/3 of that, or about 2570 Hz. That the observed Sn–H coupling constant is somewhat larger, at 2960 Hz is not surprising, given the high positive charge on the tin atom.

4.1.4 Aims of the Present Research

The current body of knowledge concerning the stannyl group suggests that it takes on a planar configuration in the solid and in solution. In the gas phase, it adopts a C_{3v} geometry. No reliable Sn–H bond distances are available for the monohalostannanes or the stannyl group in the solid, and solution phases. Moreover, owing to the thermally fragile nature of the monohalostannanes, their chemistry has not been explored.

Herein are presented the results of a brief exploration of the chemistry of monochlorostannane with the aim of developing a high yielding synthesis of distannane, and of an investigation of its structure by gas phase electron diffraction.

4.2 The Chemistry of Monochlorostannane

4.2.1 Synthesis

Monochlorostannane was synthesised according to the method of Jolly[87] and equation (3). Equimolar amounts of stannane and hydrogen chloride (typically 1 mmol) were condensed *via* the high vacuum line in an all-glass ampoule equipped with a break-seal cooled to -198°C. The ampoule was then sealed off under vacuum, and immersed in a dry ice/acetone bath for one hour, after which the reaction was judged to be complete.

$$SnH_4 + HCl \xrightarrow{\text{-78°C, liq. HCl}} SnH_3Cl + H_2 \qquad (3)$$

The ampoule was then cooled to -196°C, and attached to an all-glass train of taps. After opening the break seal, hydrogen gas produced in the reaction was pumped away, and the ampoule warmed slowly to room temperature, during which time the monochlorostannane vapourised and was trapped at -116°C.

4.2.2 The Synthesis of Distannane, Sn_2H_6

Introduction

In the past forty years, two preparations of distannane have been reported. The first of these, by Jolly[101] in 1961, involved the isolation of distannane as a very minor by-product of a low-yield synthesis of stannane using aqueous tetrahydroborate,[12]

$$SnO_2^- + BH_4^- \xrightarrow{6M\ HCl(aq.)} SnH_4 + Sn_2H_6 + \ldots \qquad (4)$$

The yield of distannane based on the tin starting material was *ca.* 0.06%.

Repeated preparations enabled Jolly to collect sufficient distannane for elemental analysis, and for a solid phase infra-red spectrum to be recorded. Both of these provide convincing evidence for his isolation of the molecule.

In 1997, Åserud and Lampe[13] observed the formation of small quantities of distannane during a vacuum-ultraviolet photodecomposition of SnH_4. Study of the decomposition kinetics of distannane by mass spectrometry at a variety of temperatures allowed them to propose a first order rate law, with a half life of distannane at room temperature of around four seconds.

In view of the low yield of the first preparation, and before the second preparation was published, it was decided to investigate whether alternative preparative routes could be developed for generating distannane in significant quantities. A starting point for this work was a consideration of the synthetic routes to hexaorganodistannanes.

Hexaorganodistannes are commonly in use in synthetic organic chemistry as a means of introducing the trialkytin group. Two standard synthetic methods are commonly employed in their preparation,[102] exploiting the reaction between either a trialkyltin halide and sodium metal, or a trialkyltin anion. For example, hexaethylditin may be prepared in the following way,[103]

$$2\ Et_3SnBr + 2\ Na \xrightarrow{120°C,\ Et_2O} Et_3Sn{-}SnEt_3 \qquad (5)$$

Hexaphenylditin may be synthesised using a trialkyltin anion,[104]

$$Ph_3SnLi + Ph_3SnBr \xrightarrow{Et_2O} Ph_3Sn{-}SnPh_3 \qquad (6)$$

It seemed reasonable, therefore, to adapt these methods to the formation of distannane, by either passing monochlorostannane vapour over sodium metal, or by allowing it to react in solution with a stannyl anion. Both methods were attempted, and are described below.

The Reaction between Monochlorostannane and Sodium Metal

A sample of monochlorostannane (ca. 1 mmol) was prepared as detailed previously, and attached to apparatus consisting of a glass coil passing directly into a quadrupole mass spectrometer.

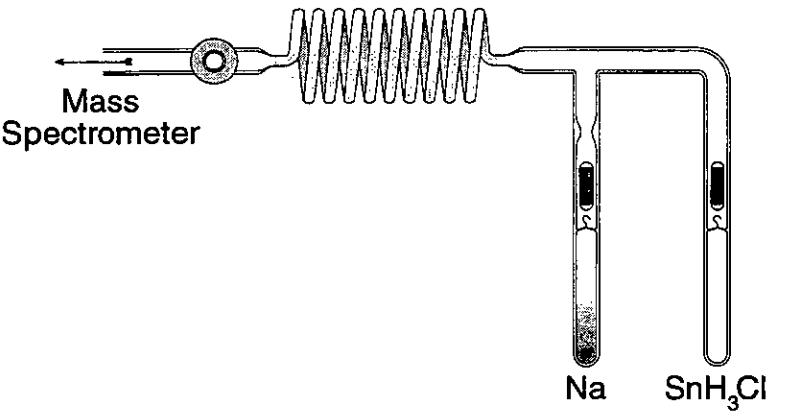

Figure 4.2. Apparatus for the Reaction between SnH_3Cl Vapour and Sodium Metal.

A sample of sodium metal in a break-seal ampoule was also attached, and the apparatus evacuated. The ampoule containing monochlorostannane was then opened, and warmed to -112°C, at which point any hydrogen gas and excess reactants present were pumped off. The break-seal to the ampoule containing sodium was then also opened, and the sodium inside distilled into the apparatus,

so as to cover as much of the surface of the glass coil as possible. The remainder of the apparatus was also "flamed out", and the remains of the sodium ampoule sealed off from the vacuum line.

Finally, the ampoule of monochlorostannane was warmed to -78°C, and then slowly to room temperature, while a series of mass spectra were recorded.

Initially, only peaks due to SnH_x^+ were observed in the mass spectrum, but as the temperature of the monochlorostannane ampoule rose, a darkening of the sodium mirror inside the coil was noted, accompanied by generation of peaks centered on 240 m/z, and 158 m/z. After further warming, the peaks at 240 m/z decreased in intensity, while those at 158 m/z remained. At this point, the sodium in the glass coil was completely covered in a dull grey sheen.

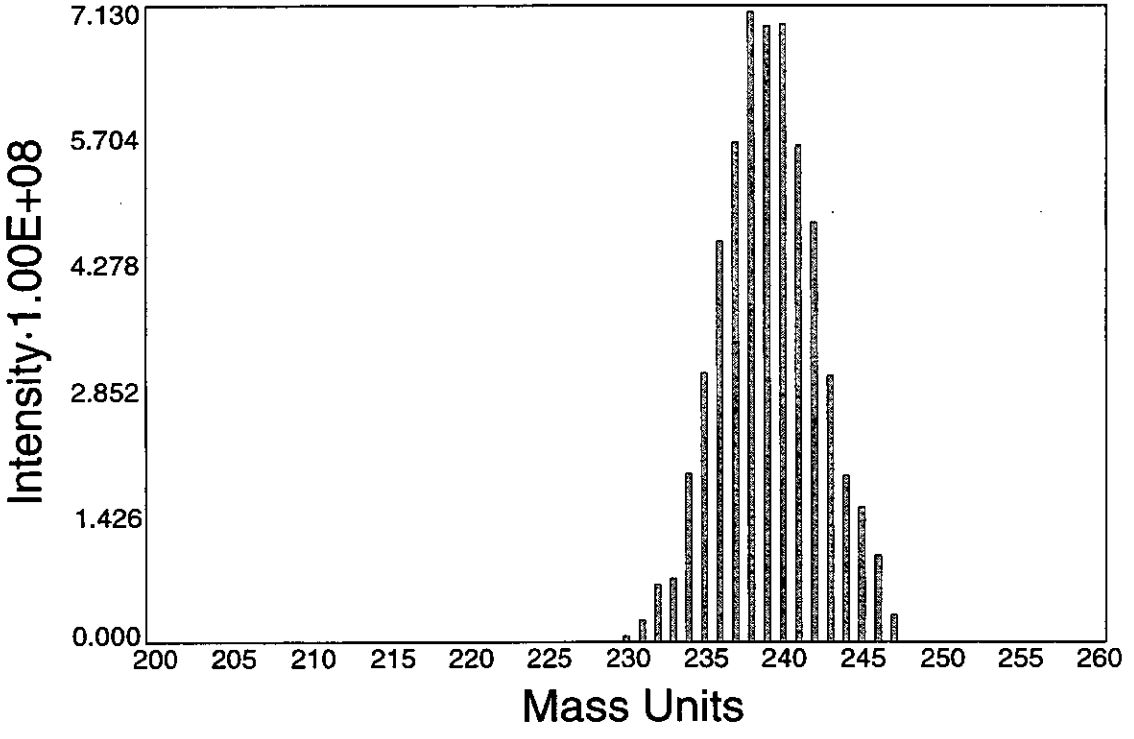

Figure 4.3. Mass Spectrum of the Reaction between SnH_3Cl and Na

These results can be interpreted in terms of two competing reactions, one

between monochlorostannane and sodium at the sodium surface, producing distannane ($m/z(^{120}Sn_2H_6) = 246$) and sodium chloride, and the other involving decomposition of both reactant and product at the sodium surface, forming a thin covering layer of tin metal.

$$2\ SnH_3Cl + 2\ Na \longrightarrow Sn_2H_6 + 2\ NaCl \qquad (7)$$

Once completely covered, further reaction between monochlorostannane and sodium metal ceased, excess SnH_3Cl ($m/z(^{120}SnH_3{}^{35}Cl) = 158$) passing unchanged into the mass spectrometer.

The observation in the mass spectrum of a multiplet centered at $m/z = 240$, rather than 246 can be rationalised in terms of the presence of daughter ions of distannane of the form $Sn_2H_x{}^+$ in the mass spectrometer. The alternation of intensity present in the predicted mass spectra[105] of $Sn_2{}^+$ and $Sn_2H_6{}^+$ (see Figures 4.4 and 4.5, respectively) is therefore not observed here due to overlap between the spectra of the daughter ions, which differ in mass by a single unit only.

To provide further insight into the reaction taking place, a similar experiment was performed using an identical apparatus, but with a sodium mirror covering only the end of the glass coil furthest from the mass spectrometer. Monochlorostannane vapour was passed over the mirror, and the relative intensities of peaks due to Sn_2H_6, and SnH_3Cl were observed as various parts of the glass coil were warmed to 50°C with a heat gun.

Initially, the end of the coil closest to the mass spectrometer was heated, through which the reaction products, and unchanged SnH_3Cl were thought to be passing. As heat was applied, the intensity of the signal due to SnH_3Cl decreased, while that due to Sn_2H_6 remained virtually unchanged (see Figure 4.6). A white deposit also formed on the heated glass, as would be expected during the thermal decomposition of monochlorostannane,[87]

$$2\ SnH_3Cl \xrightarrow{\Delta} SnH_4 + SnCl_2 + H_2 \qquad (8)$$

$$3\ SnH_3Cl \xrightarrow{\Delta} 2\ SnH_4 + SnCl_2 + HCl \qquad (9)$$

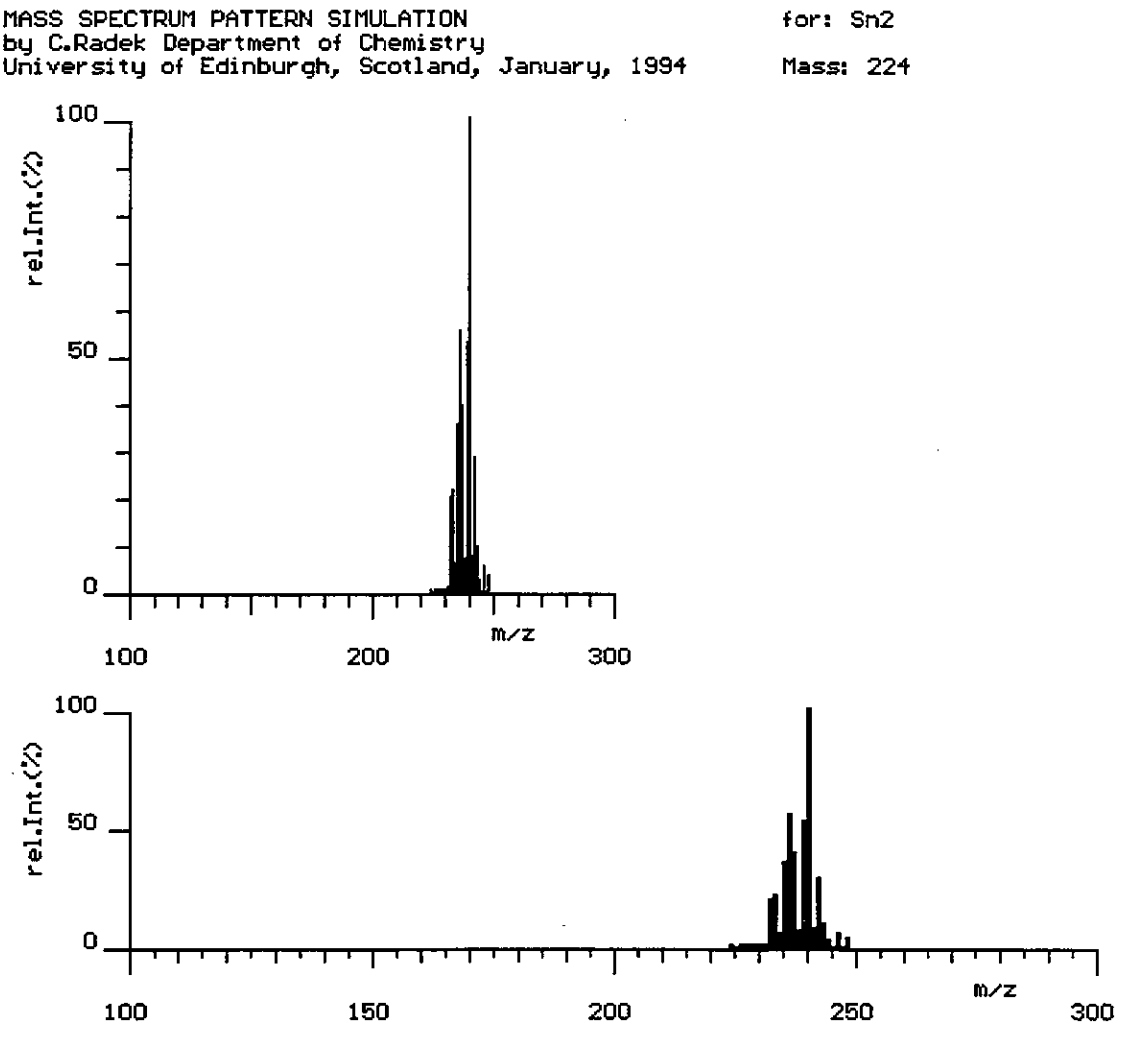

Figure 4.4. The Predicted Mass Spectrum of Sn_2^+.

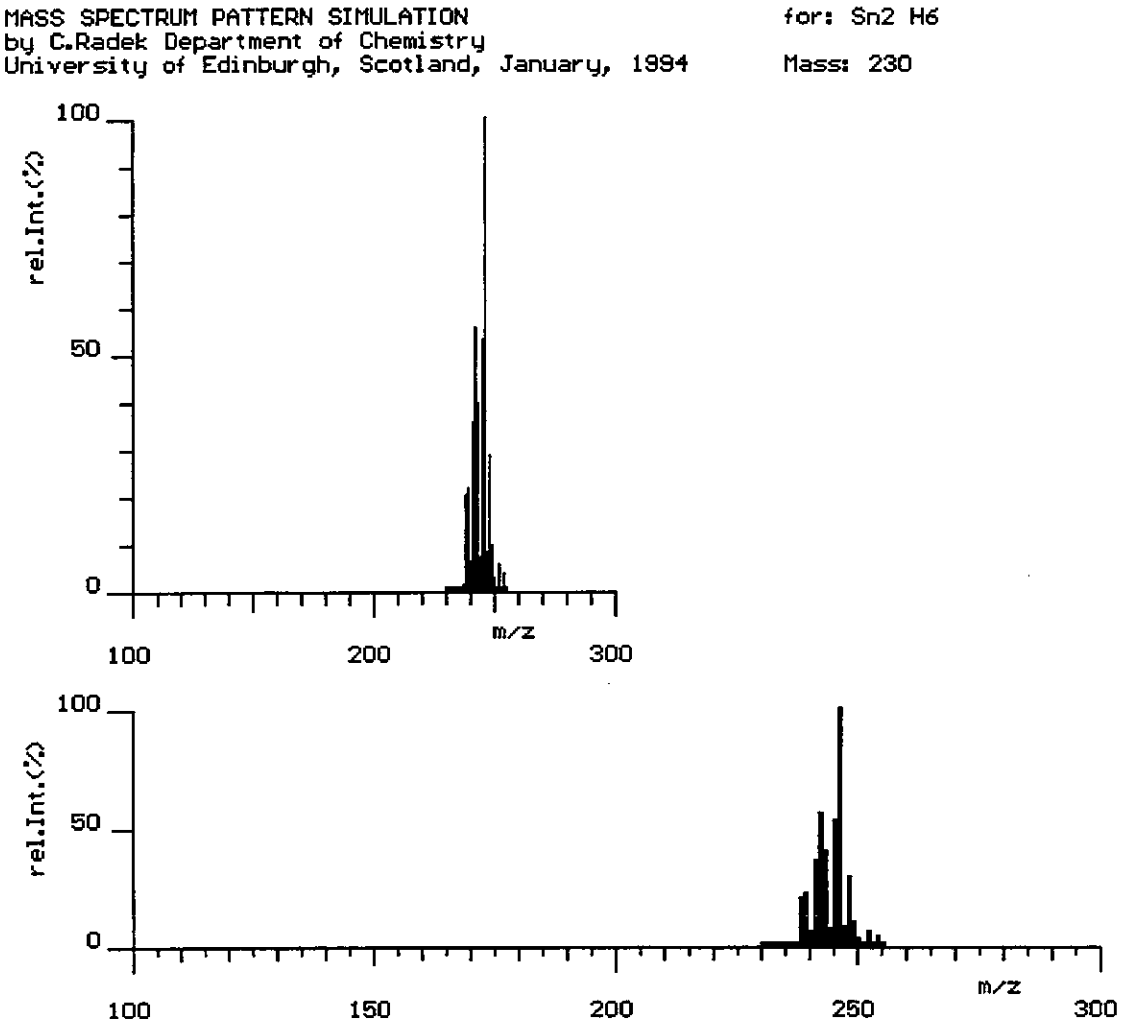

Figure 4.5. The Predicted Mass Spectrum of $Sn_2H_6^+$.

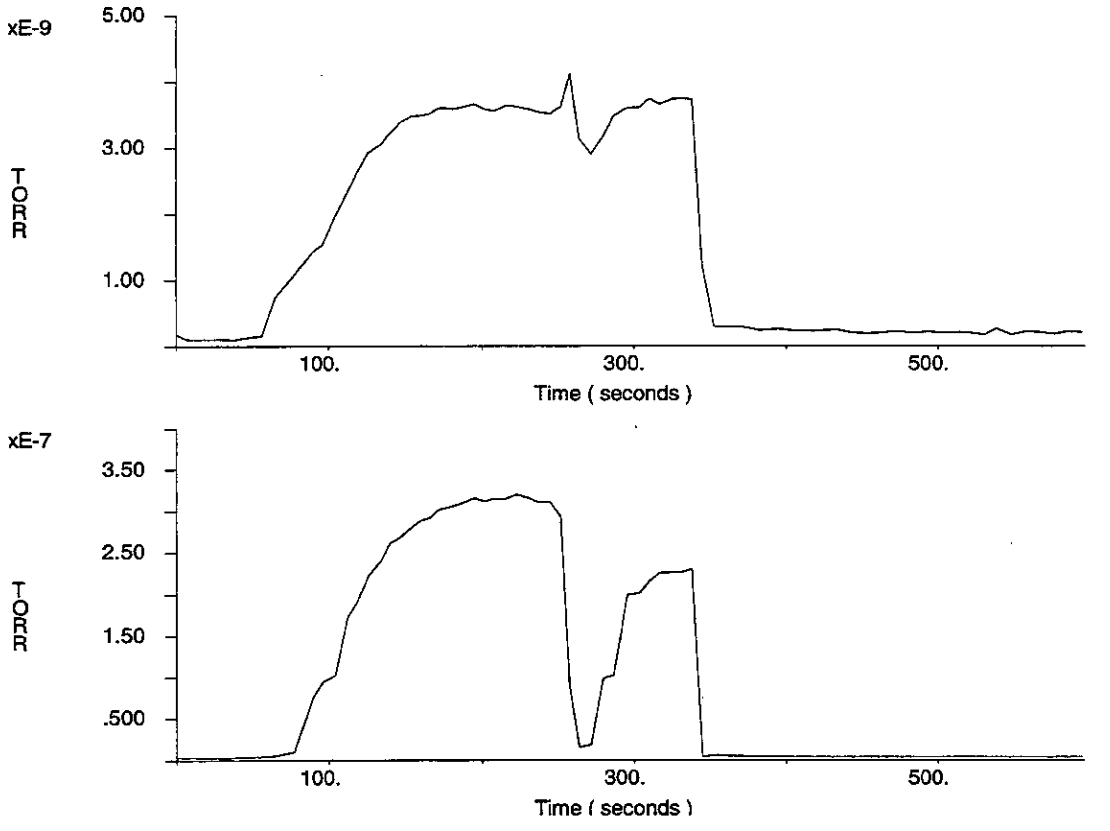

Figure 4.6. The decomposition of SnH_3Cl (bottom graph) in the presence of Sn_2H_6 (top graph) on heating. Heating commenced at around 270 s, at lasted for a few seconds only.

When the sodium mirror was heated, the intensity of the signals due to both monochlorostannane and distannane dropped sharply.

These results suggest that the presence of sodium is required for the generation of distannane and that it is not produced simply by the thermal decomposition of monochlorostannane, or by subsequent reaction of its decomposition products, but by reaction between monochlorostannane and sodium at the sodium surface.

No attempt was made to scale up this reaction to produce synthetically significant amounts of distannane. Performing the reaction using the apparatus described above but on a larger scale would be unsuccessful, as the amount of distannane produced is dependent upon the surface area of sodium metal available. As this is rapidly reduced by covering with tin metal, a significant increase in the yield of distannane would not be achieved.

This technique can be used to generate small quantities of distannane for mass spectrometric purposes, but cannot easily be scaled up to provide amounts sufficient for analysis by other structural techniques, such as gas-phase electron diffraction.

The Reaction between SnH_3Cl and SnH_3^-

Potassium hydride (0.2 mmol) and [2,2,2-crypt] (0.2 mmol) were loaded under dry nitrogen into the left-hand finger of the apparatus shown in Figure 4.7. The apparatus was then attached to the high vacuum line, and a sample of monochlorostannane (0.2 mmol) prepared in the right-hand finger. After this reaction was complete, the finger was cooled in liquid nitrogen while 2–3 ml tetrahydrofuran, and 0.2 mmol stannane were condensed onto the potassium hydride. The left hand finger was then warmed to -63°C, and shaken to aid reaction.

One hour later, after excess stannane, hydrogen chloride, and any hydrogen gas were pumped from the right hand finger, the central tap was opened, and the solution of K^+ SnH_3^- poured from the left hand finger into the right. On mixing, an orange colouration was observed in the tetrahydrofuran solution. The left part of the apparatus was then sealed off under vacuum, and the right part warmed to -78°C for one hour to allow reaction to complete.

The contents of the right hand finger, now a deep red-brown colour, were then

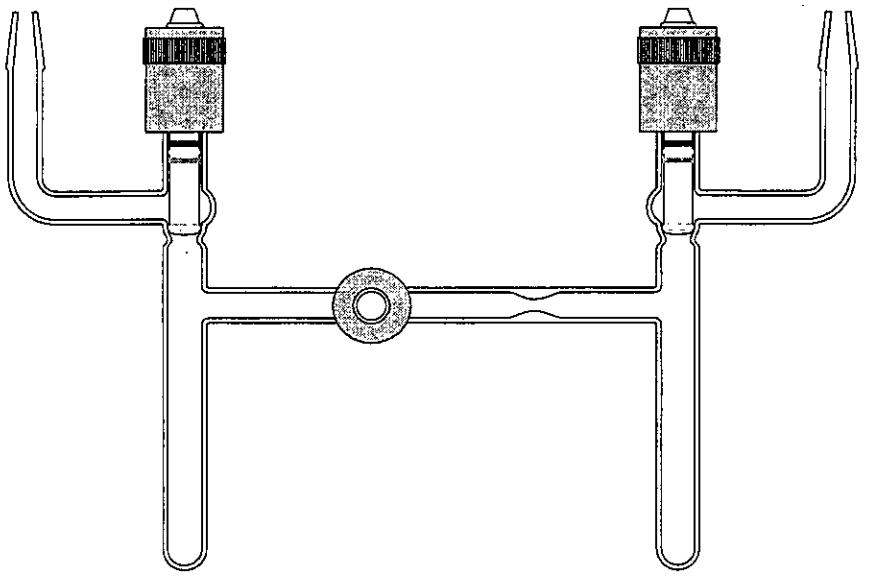

Figure 4.7. Apparatus for the Preparation of Sn_2H_6 from SnH_3Cl and SnH_3^-.

distilled at -78°C, through traps at -112°C, and -196°C to high vacuum. Analysis of the contents of the -112°C trap by mass spectrometry showed no tin containing species. However, when the contents of the -196°C trap were warmed to -78°C, and allowed to pass into the mass spectrometer, an intense multiplet centered at 240 m/z was observed.

These observations can be interpreted in terms of a reaction between SnH_3^- and SnH_3Cl, producing distannane, decomposition of stannane, distannane, and monochlorostannane in the presence of residual base and any tin metal present producing the colour changes observed.

$$SnH_3^- + SnH_3Cl \xrightarrow{\text{-78°C, thf}} Sn_2H_6 + Cl^- \qquad (10)$$

A second preparation, using sodium hydride rather than potassium hydride, also generated sufficient distannane for mass-spectrometric analysis (see Figure 4.8).

Scaling up this reaction to produce significant quantities of distannane would be difficult as the reaction requires substantial experimental agility. Transfer

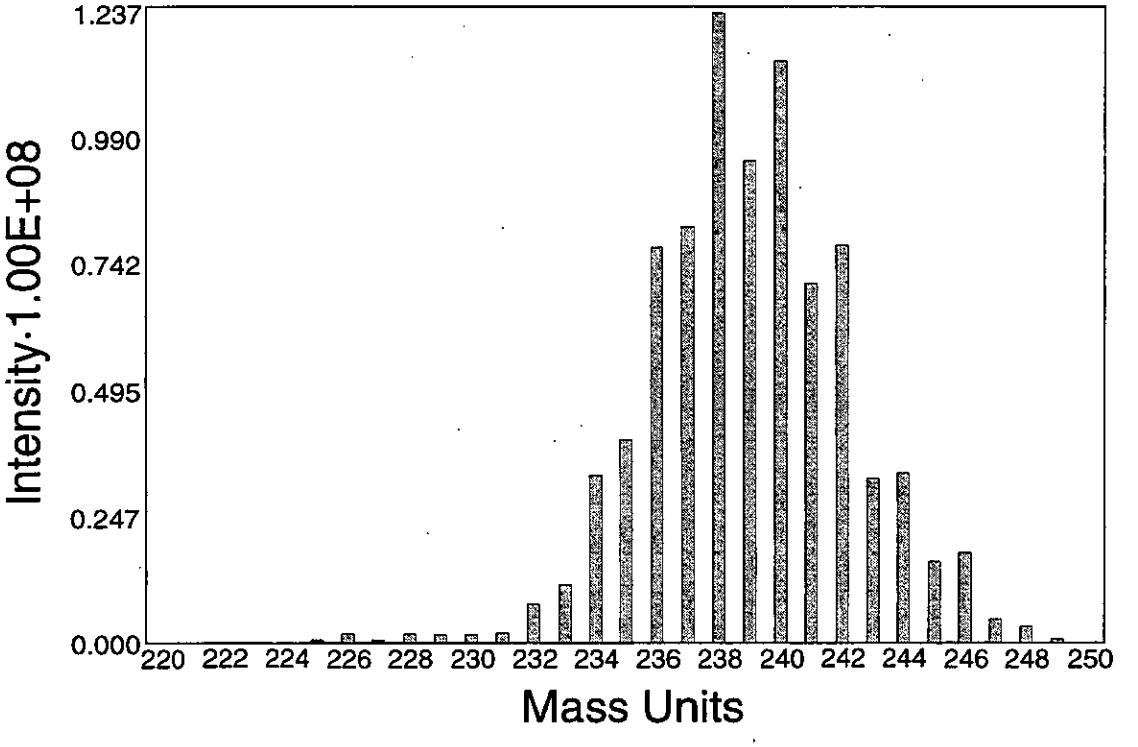

Figure 4.8. Mass Spectrum of the Reaction between SnH_3Cl and Na^+ SnH_3^-.

of the ethereal solution of K^+ SnH_3^- from one finger of the apparatus to the other inevitably entails a small amount of decomposition, even if the apparatus is cooled as much as possible using a cold bath, or by application of liquid nitrogen. The presence of tin metal in the final reactant mixture is therefore unavoidable, leading to catalytic decomposition of the majority of any distannane produced.

Although performing the reaction on a larger scale would possibly lead to the generation of a larger amount of distannane, the absolute quantity produced would still be insufficient for further experimental work.

4.3 The Structure of SnH_3Cl as Determined by Gas Phase Electron Diffraction

4.3.1 Introduction

The structure of monochlorostannane in the gas phase has been investigated, by infra red, and microwave techniques. However, the information derived from these measurements was insufficient to determine completely the structure of the molecule. To rectify this situation, a structural investigation *via* gas-phase electron diffraction (GED) was attempted, the results of which are outlined below.

4.3.2 Experimental

A sample of monochlorostannane was prepared by Cormack,[74] and submitted for diffraction at the E.P.S.R.C. GED service at the University of Edinburgh, on an apparatus originally constructed at Cornell University by Professor S. H. Bauer.

Two diffractograms were recorded on Kodak Electron Image plates, at two different nozzle-to-plate distances, by passing monochlorostannane vapour at -5°C through an all-glass inlet into a beam of electrons accelerated to 40–55 keV. After an exposure time of approximately two minutes, the plates were removed, washed with water, and left overnight before developing in order to minimise the fogging effect of the strongly reducing vapour.

The patterns on the exposed plates were traced and digitised at the E.P.S.R.C. facility at Daresbury using a Joyce-Loebl MDM6 microdensitometer. Elastic

atomic scattering contributions to the resultant scattering intensities were then subtracted using the complex scattering factors of Fink and Ross,[106] leaving a set of experimentally observed molecular scattering intensities suitable for structure refinement.

4.3.3 Structure Refinement

The structure of monochlorostannane in the gas phase was explored using a least squares refinement procedure in which the observed molecular scattering intensities were compared to theoretical intensities derived from a model structure.

The original model used in the refinement consisted solely of SnH_3Cl, assumed to have C_{3v} symmetry. It soon became apparent, however, that scattering due to monochlorostannane alone was insufficient to reproduce the observed scattering pattern. In particular, a peak was observed in the experimental radial distribution curve at around 3.7 Å, attributable to scattering by $Cl\cdots Cl$ in SnH_2Cl_2, suggesting that the sample provided for GED analysis was either impure, or had decomposed slightly on the way into the electron diffraction chamber.

An *ab initio* study of both SnH_3Cl, and SnH_2Cl_2 was therefore undertaken using the Gaussian 94 package,[42] to provide an initial geometry of the SnH_2Cl_2 molecule to allow its inclusion in the GED refinement. The results of this study are presented in Table 4.2.

A contribution due to dichlorostannane was then included in the theoretical model using starting parameters derived from the *ab initio* study. The Sn–Cl, and Sn–H distances in both SnH_2Cl_2 and SnH_3Cl were restrained by the difference in their values as calculated, with uncertainties on these restraints assigned according to the variation in the calculated distances with the level of theory used.

Least squares refinements using a variety of SnH_3Cl : SnH_2Cl_2 mole ratios were then performed, allowing the bond lengths of both molecules to vary as necessary, but with the interbond angles of both mono- and dichlorostannane fixed at their *ab initio* (DZ(P)/MP2) values. A ratio of 15 mole% SnH_2Cl_2 to 85 mole% SnH_3Cl was found to provide the best fit between theoretical and experimental data.

SnH_2Cl_2	Sn-H	Sn-Cl	Cl-$\hat{S}$n-Cl	Cl-$\hat{S}$n-H	H-$\hat{S}$n-H	E/E_H
DZ(P)/HF	1.691	2.3161	107.56	108.03	116.82	-33.9352
DZ(P)/MP2	1.706	2.3170	107.92	107.98	116.70	-34.2612
A-DZP/HF	1.708	2.3417	107.36	108.08	116.82	-6942.73
A-DZP/MP2	1.700	2.3346	107.69	107.99	116.87	-6943.19
A-TZP/HF	1.716	2.3394	106.73	108.24	116.73	-6942.97
A-TZP/MP2	1.713	2.3246	106.82	108.34	116.29	-6943.46

SnH_3Cl	Sn-H	Sn-Cl	Cl-$\hat{S}$n-H	E/E_H
DZ(P)/HF	1.6999	2.3401	106.56	-19.7345
DZ(P)/MP2	1.7124	2.3366	106.75	-19.9335
A-DZP/HF	1.7158	2.3651	106.55	-6483.78
A-DZP/MP2	1.7040	2.3532	106.65	-6484.11
A-TZP/HF	1.7235	2.3618	106.56	-6483.98
A-TZP/MP2	1.7176	2.3414	106.85	-6484.34

Table 4.2. The Structures of SnH_3Cl and SnH_2Cl_2 by *ab initio* calculation. Bond lengths are in Ångstroms, and angles in degrees.

Moreover, it was found that if information contained in the diffractogram collected at the long camera distance was excluded from the refinement, the estimated standard deviations of the bond lengths of SnH_2Cl_2 and SnH_3Cl decreased, suggesting that that data set contained no useful information concerning the structure of SnH_3Cl.

Unfortunately, the R factor for the refinement at this point was still unacceptably large ($R_G = 17.4\%$) suggesting that although the data collected contained a certain amount of information on the structure of monochlorostannane, insufficient information was present to allow concurrent refinement of two different molecules using a single data set.

This is almost certainly due to the nature of the photographic process chosen to record diffraction data for monochlorostannane. In a standard electron diffraction experiment, silver cations present in the electron image plates used are reduced by the diffracted electron beam, producing amounts of silver metal proportional to the intensity of the incident electron beam.

Monochlorostannane is also capable of reducing Ag^+ to silver metal, producing a fogging of the plate should it come into contact with the plate surface. The diffractogram recorded at the long camera distance seems to have been substantially fogged in this way, and therefore contains little useful structural information.

At this point it was decided that no further progress could be made without new experimental information, preferably taken from a sample not containing dichlorostannane, and using a detection process not dependent upon a photographic technique. The structure of SnH_3Cl best fitting the experimental data collected to date is given in Table 4.3, and the corresponding radial distribution curve and molecular scattering curves are shown in Figures 4.9, and 4.10.

SnH_3Cl	Sn-H/Å	Sn-Cl/Å	Cl-$\hat{S}$n-H(°)
GED(exptal)	1.685(28)	2.328(3)	106.75 (fixed)

Table 4.3. The Structure of SnH_3Cl as determined by Gas Phase Electron Diffraction ($R_G = 17.4\%$).

Nozzle to plate distance (mm)	Δs (Å^{-1})	s_{min}(Å^{-1})	sw_1 (Å^{-1})	sw_2 (Å^{-1})	s_{max} (Å^{-1})
202.93	0.4	4.0	6.0	17.2	20.0

Correlation (p/h)	Scale factor k	Electron Wavelength (Å)
0.0614	0.304(9)	0.05697

Table 4.4. Experimental Details for the Electron Diffraction Pattern of SnH_3Cl

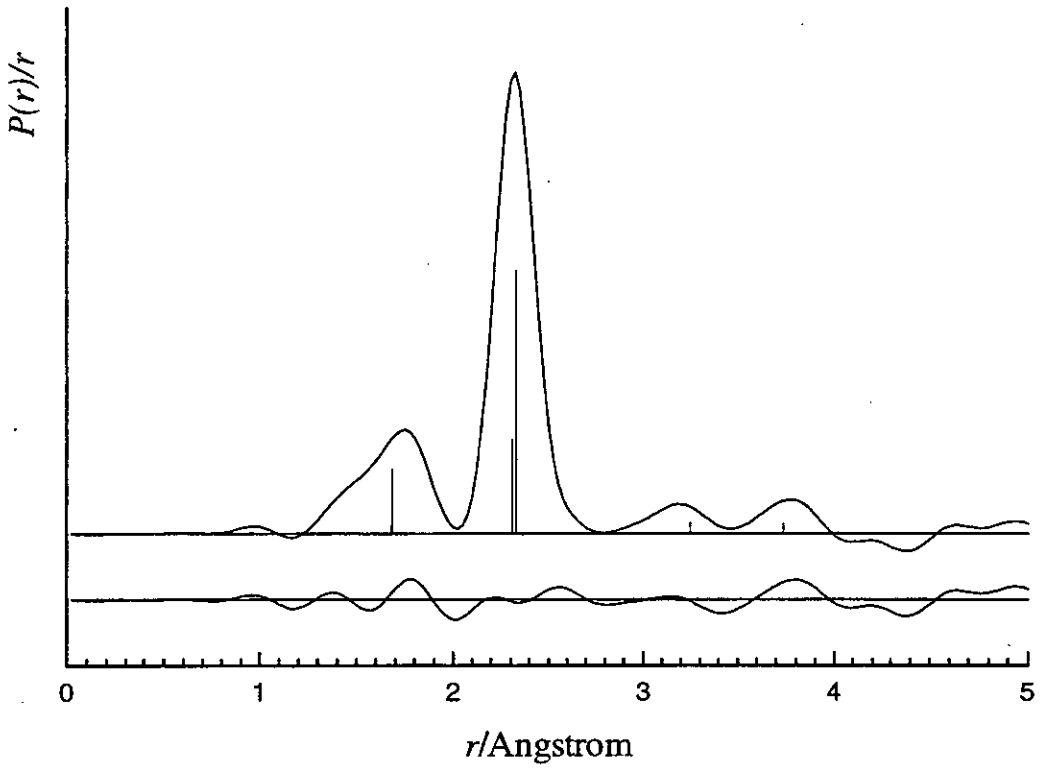

Figure 4.9. Observed and difference radial distribution curves, P(r)/r against r, for SnH_3Cl vapour. Before Fourier inversion, the data were multiplied by $s.\exp[(-0.00002s^2)/(Z_{Sn} - f_{Sn})(Z_{Cl} - f_{Cl})]$.

SnH_3Cl		SnH_2Cl_2			
r(Sn–Cl)	r(Sn–H)	r(Sn–Cl)	r(Sn–H)	k	
100	-8	27	-8	0	r(Sn–Cl)
-8	100	-7	98	31	r(Sn–H)
27	-7	100	-7	-6	r(Sn–Cl)
-8	98	-7	100	31	r(Sn–H)
0	31	-6	31	100	k

Table 4.5. Least Squares Correlation Matrix (x100) for the Analysis of the Electron Diffraction Pattern of SnH_3Cl

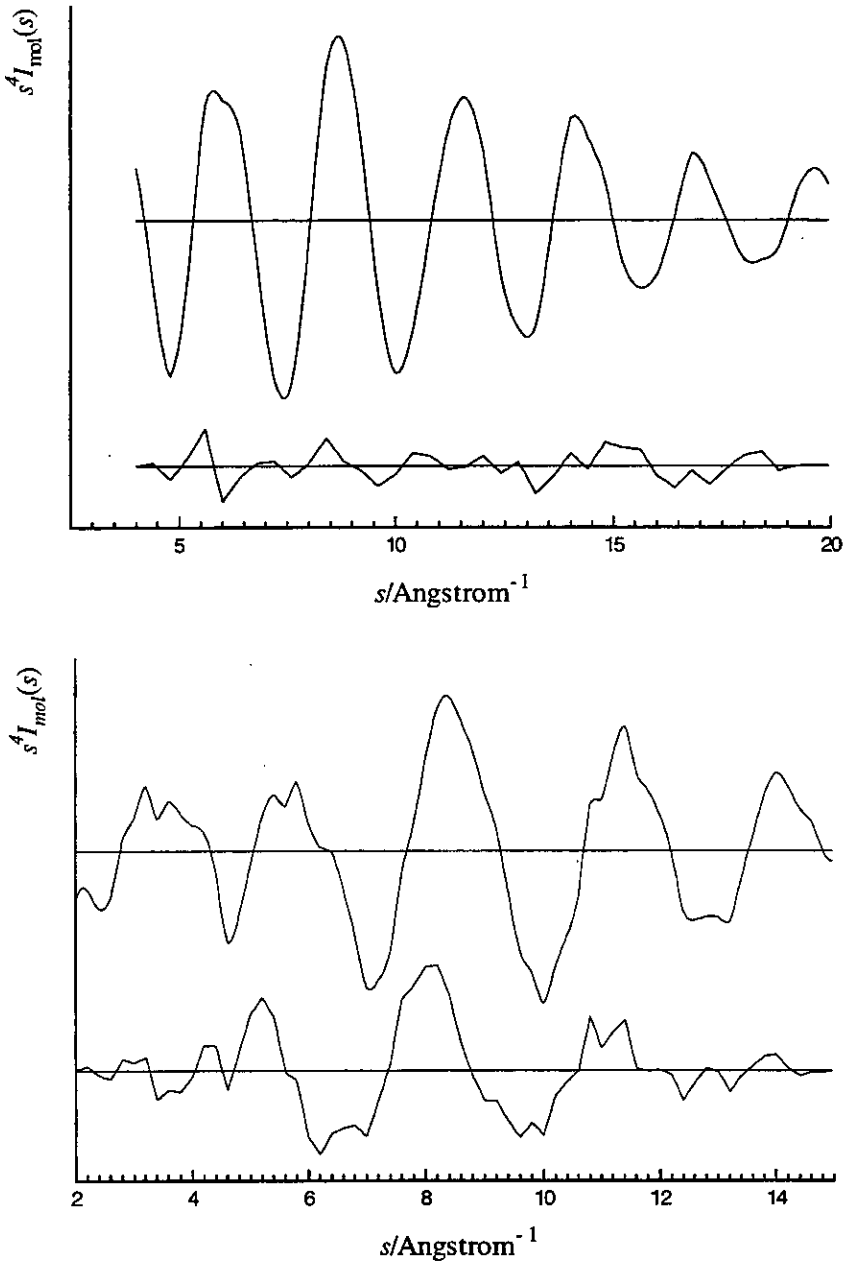

Figure 4.10. Experimental and final difference molecular scattering curves for SnH_3Cl. Nozzle-to-plate distances were 202.933 mm (top) and 263.670 mm (bottom).

SnH_3Cl		SnH_2Cl_2	
r(Sn–Cl)	2.328(3)	r(Sn–Cl)	2.308(5)
r(Sn–H)	1.685(28)	r(Sn–H)	1.678(28)
Cl–Sn–H	106.75 (fixed)	Cl–Sn–Cl	107.92 (fixed)
		Cl–Sn–H	107.98 (fixed)

Table 4.6. Molecular Parameters derived from the Analysis of the Electron Diffraction Pattern of SnH_3Cl

SnH_3Cl		Vibrational Amp. ($Å^{-1}$)	SnH_2Cl_2		Vibrational Amp. ($Å^{-1}$)
Sn–Cl	2.328(3)	0.048	Sn–Cl	2.308(5)	0.047
Sn–H	1.685(28)	0.093	Sn–H	1.678(28)	0.092
Cl···H	3.243(20)	0.147	Cl···H	3.245(21)	0.146
H···H	2.794(46)	0.161	H···H	2.857(48)	0.158
			Cl···Cl	3.733(7)	0.122

Table 4.7. Distances derived from the Analysis of the Electron Diffraction Pattern of SnH_3Cl, and corresponding Vibrational Amplitudes. The Amplitudes were fixed in the refinement.

4.4 Summary

1. Distannane has been synthesised in small quantities by two different synthetic routes, involving the reaction of SnH_3Cl with sodium metal, and SnH_3^- respectively,

$$2\,SnH_3Cl + 2\,Na \longrightarrow Sn_2H_6 + 2\,NaCl \qquad (11)$$

$$SnH_3Cl + SnH_3^- \xrightarrow{\text{-78°C, thf}} Sn_2H_6 + Cl^- \qquad (12)$$

   The distannane produced was identified by mass spectroscopy. The yields of these syntheses do not represent an improvement over the existing literature method,[101] and their potential to be scaled up is limited by either the nature of the synthesis, or by the low thermal stability of the reactants used.

2. The structure of monochlorostannane has been investigated in the gas phase by electron diffraction, and by *ab initio* calculation. The results of this study indicate that the sample submitted for GED by Cormack[74] also contained roughly 15% dichlorostannane, complicating the refinement sufficiently to preclude a definitive result. A final R_G of 17.4% corresponded to a Sn–Cl bond length of 2.328(3) Å, and a Sn–H bond length of 1.685(28) Å. The Cl-$\hat{\text{Sn}}$-H bond angle was fixed at the *ab initio* value.

Chapter 5

Crystal Structures of Low Melting Compounds

5.1 Introduction

Structural studies of simple alkyltin hydrides have so far been confined to the gas phase, Me_3SnH, and Me_2SnH_2 being examined by electron diffraction,[31] and $MeSnH_3$ through the use of microwave spectroscopy.[32] These compounds are all liquids even at temperatures below -100°C, and so no attempts have been made to probe their structures in the solid phase.

The vibrational spectra of the methyltin hydrides in the solid phase (see Chapter 3) suggest that they exist as discrete molecular entities, and do not form bridges, or chains with neighbouring molecules as is the case with the methyltin fluorides.[107,108] This suggests that if their solid state structures could be determined, useful comparisons could be drawn with those already obtained in the gas phase, and an insight then gained into the influence of the phase of a molecule on its geometry.

The determination of the structures of the methyltin hydrides in the solid phase would allow a number of areas of interest to be explored. These include,

1. Comparison of their solid and gas phase structures,
2. Examination and exploration of the techniques available for the growth of crystals on a diffractometer from very low melting samples,

3. Provision of a basis for further analysis by neutron diffraction (see Chapter 6).

This chapter describes the techniques used in the determination of the structures of very low melting compounds, and their application to the structures of the methyltin hydrides and the simplest isolable phosphorus ylid, Me_3PCH_2.

5.2 Experimental

5.2.1 The Growth of Single Crystals at the Diffractometer.

Samples for X-ray crystallography were condensed *via* the high vacuum line into Pyrex capillaries approximately 2–3 cm long and not more than 0.3 mm in diameter, which were then sealed off using a hand torch. After storage in liquid nitrogen, the capillary was transferred to a four circle Stoë Stadi-4 diffractometer equipped with an Oxford Cryosystems variable-temperature device,[109] and attached to a Tufnol mount using epoxy resin and polymethylmethacrylate cement. The mount was then inserted into a goniometer head and the head attached to the diffractometer, so placing the sample in a stream of cooled nitrogen of a precisely controlled temperature, flowing from the variable temperature device. This arrangement is outlined in Figure 5.1.

The temperature of the nitrogen stream was then reduced to just below the melting point of the sample, causing all of the sample to freeze. The temperature of the gas stream was then raised slowly to the melting point of the sample, the crystalline mass observed throughout this procedure using a microscope, plane polarised light, and a polarising filter. At the point at which only a tiny seed crystallite remained in the capillary, slow cooling (0.5 K/min) of the sample was initiated. In this way, a single crystal was grown in the capillary.

Difficulties Inherent in the Technique.

This technique of single crystal growth at the diffractometer is successful in the vast majority of cases, although complications sometimes arise from two general

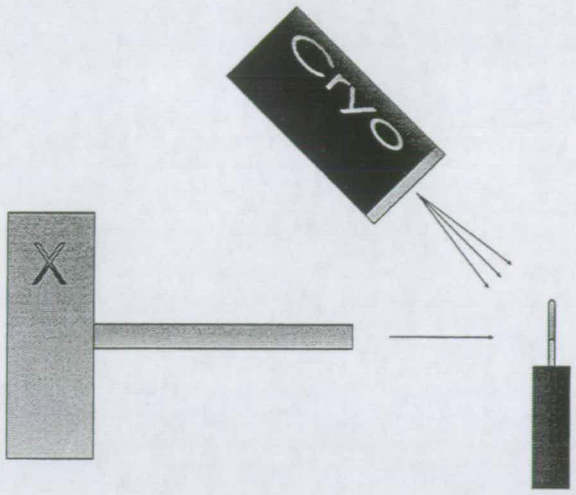

Figure 5.1. Apparatus for the Growth of Single Crystals at the Diffractometer.

areas - in the design of the apparatus used, and in the nature of the sample to be studied.

The design of the apparatus places a number of constraints on the samples that can be studied in this way. Firstly, the use of a gas stream derived from boiling liquid nitrogen places a lower limit on the melting points of samples to be studied of around 120 K. Helium cooling systems do exist,[110] but are currently not designed to allow visual inspection of their contents during operation. As monitoring of the growth of a single crystal requires visual inspection, this makes the study of samples with melting points below 120 K currently unfeasible.

Secondly, the shape of the capillaries used places a physical constraint on the form of the single crystals that can be grown. This poses a problem only for samples that would usually take a needle-like habit. Crystal growth along the axis of the capillary then becomes so facile that twinning often occurs, complicating to a sometimes intractable degree the process of single crystal data collection and refinement.

The sample, as in the case above, can also introduce complications, both in mounting on the diffractometer, and during the crystal growth process.

The *in situ* crystal growth technique is often applied to samples of very low

melting point, and low thermal stability. Both these properties complicate the sample mounting procedure, as in some cases the time taken to remove the sample from liquid nitrogen storage, attach it to the Tufnol mount, and then place it in the gas stream is sufficient for the sample either to boil and shatter the capillary, or to degrade thermally so as to make it unsuitable for further study.

In these cases, the problem may be reduced by transferring the sample directly from storage to a bath of liquid nitrogen contained in a copper block into which a small hole has been drilled. The capillary may then be transferred from the container and placed vertically in the hole in the copper block without raising its temperature much above 77 K. Sample mounting can then be performed with one end of the capillary cooled in the block, while the other is glued to the Tufnol mount. Rapid transfer to the gas stream at the diffractometer is then sufficient to maintain the integrity of the capillary and the sample within.

The difficulties encountered with the sample in the *in situ* growth process are expressed either as a tendency of the sample to produce twinned crystals on cooling, or as a failure to produce crystals at all. Glass formation can occur if the process of warming from a polycrystalline mass goes too far, and no seed crystal remains to initiate single crystal growth on subsequent cooling. Supercooling below the normal melting point of the sample can then result, ending either in a sudden transition back to a polycrystalline mass, or in the formation of a glass.

In this case, cooling to well below the normal melting point of the sample is usually enough to ensure transition from the glass to a polycrystalline mass suitable for a further attempt at single crystal growth. In some cases, however, the formation of a glass in preference to a single crystal is dictated by the sample itself, rather than by experimental agility. Samples of this type cannot be studied in this manner.

A final complication arises in the final stage of sample preparation, when the single crystal so carefully grown is cooled to sufficiently far below the sample melting point to ensure its mechanical stability, and to reduce the thermal motion of the atoms therein. It sometimes happens that during this cooling process the sample changes phase, reducing the single crystal of one phase to a polycrystalline mass of another.

This can be avoided by collecting data if possible above the temperature of

the phase change. In some cases, however, the transition temperature is only a few degrees below the normal melting point of the sample. Here, it is sometimes possible to exploit the supercooling mentioned above to bypass the phase change, growing crystals of the low temperature phase only. This requires a sample of melting point significantly above the low temperature limit of the gas stream.

The Application of the *in situ* Crystal Growth Technique to the Study of the Methyltin Hydrides, and to Me_3PCH_2.

Samples of stannane, methyl-, dimethyl-, and trimethylstannane, and trimethylphosphonium methylid were submitted to Dr. Simon Parsons at the University of Edinburgh for analysis in this way.

Attempts to grow single crystals of stannane and methylstannane failed, in part due to their tendency to form very thin, needle like crystals, and also owing to their melting points lying at the low extreme of the stable temperature range of the nitrogen stream. In both cases, it proved impossible to grow sufficiently large, single crystals. Powder patterns showing a high degree of preferred orientation were observed instead.

Single crystal data were recorded for dimethyl- and trimethylstannane and the ylid by Dr. Parsons, who then proceeded to solve and refine[111] their structures. The results of these analyses are presented below, and the refinement details in Appendices at the end of this thesis.

5.3 The Solid State Structures of Me_2SnH_2 and Me_3SnH.

5.3.1 Me_2SnH_2

Dimethylstannane exists as discrete molecules in the solid state, crystallising in a triclinic space group, with each unit cell containing two formula units. The Sn–C bond length of 2.14 Å, is typical - an analysis of 693 structural fragments[112,113] containing $R_3Sn\text{-}CH_3$ gives a tin–carbon bond distance of 2.14(4)Å. The C–Sn–C angle of 111.8° suggests approximately tetrahedral coordination around the

tin atom. The positions of the hydrogens bound to tin have been determined, but are subject to substantial uncertainty. This is not surprising considering the markedly different electron densities associated with the tin and hydrogen centres. The Sn–H bond length, of 1.63 Å, is again not unusual. The salient features of the solid state structure are summarised in Table 5.1, and graphically in Figure 5.2.

Crystal system	Triclinic
Space group	$P\bar{1}$
Unit cell dimensions	a = 6.1460(12)Å, α = 102.68(3)°
	b = 6.4270(13)Å, β = 92.40(3)°
	c = 6.8310(14)Å, γ = 107.79(3)°
Sn–C(1)	2.138(4)Å
Sn–C(2)	2.140(4)Å
Sn–H(1)	1.63(5)Å
Sn–H(2)	1.62(5)Å
C(1)–Sn–C(2)	111.8(2)°
C(1)–Sn–H(1)	112(2)°
C(1)–Sn–H(2)	109(2)°
C(2)–Sn–H(1)	108(2)°
C(2)–Sn–H(2)	107(2)°

Table 5.1. The Geometry of Me_2SnH_2 by Single Crystal X-Ray Diffraction

The structure of Me_2SnH_2 has also been determined in the past by gas phase electron diffraction,[31] and in this work by *ab initio* methods. The structural parameters obtained in this way are compared with those in the solid state in Table 5.2.

Given that the X-Ray experiment determines centres of electron density, whereas both GED and *ab initio* experiments determine the positions of nuclei, the differences between the theoretical, gas phase, and solid phase structures are not large. The largest variation, in the C–Sn–C bond angle can be ascribed to shrinkage effects unaccounted for in the GED study.

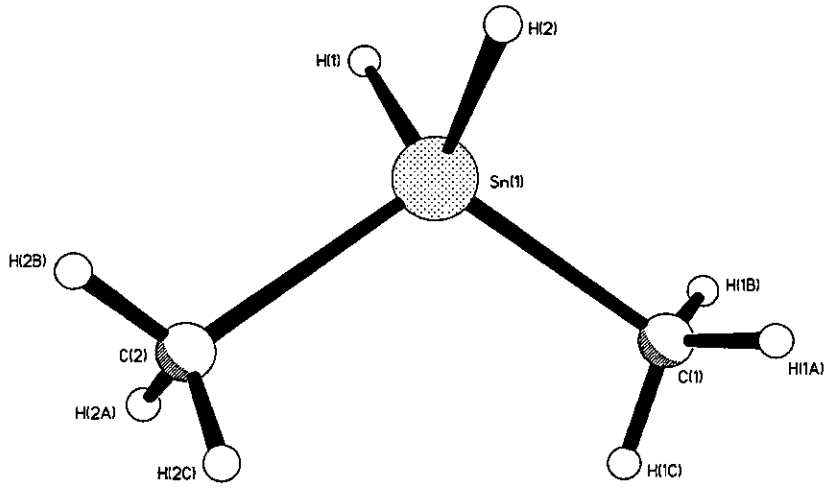

Figure 5.2. The Structure of Me_2SnH_2 by Single Crystal X-Ray Diffraction.

Parameter	X-Ray	GED[31]	DZ(P)/MP2
Sn–C/Å	2.140(4)	2.150(3)	2.1469
Sn–H/Å	1.63(5)	1.680(15)	1.7270
C–Sn–C(°)	111.8(2)	104.8(5)	110.00
C–Sn–H(°)	108(2)	108.0(15)	109.73

Table 5.2. Geometrical Parameters of Me_2SnH_2 from X-Ray, GED, and *ab initio* studies.

Comparison of the solid state structure of Me_2SnH_2 with analogous dimethyltin compounds is difficult, as few crystal structures of this kind have been reported. Of the halides, only the structures of the difluoride[108] and dichloride[114] are known, and only the dichloride consists of relatively discrete Me_2SnX_2 units. A structure of Me_2SnBr_2 cocrystallised with 1,4-dithiane has also been reported,[115] and is included for comparison in Table 5.3.

Compound	Sn–C/Å	C–$\widehat{Sn}$–C(°)	Sn–X/Å	X–$\widehat{Sn}$–X(°)
Me_2SnH_2	2.140(4)	111.8(2)	1.63(5)	109(3)
Me_2SnF_2	2.06(1)	180	2.12(1)	90
Me_2SnCl_2	2.21(8)	123.5(45)	2.40(4)	93(2)
Me_2SnBr_2	2.14(1)	140.0(6)	2.577(2), 2.518(2)	95.24(6)

Table 5.3. Geometrical Parameters of Me_2SnX_2, X = H, F, Cl, Br, by X-Ray diffraction.

The effects of intermolecular forces on the structures of the dichloride and the dibromide are highlighted by their comparison to the structure of the dihydride, in which intermolecular interaction (as evidenced by its low melting point) is weak, and to the polymeric structure of the difluoride. Me_2SnF_2, melting at more than 360°C,[116] adopts a structure similar to SnF_4 in which the tin is six coordinate, the methyl groups occupying positions trans to each other. The four equatorial positions are taken by fluorine, corner sharing then creating a plane containing only tin and fluorine, with the methyl groups coordinating above and below.

The structure of the dichloride and to a certain extent, the dibromide, can be viewed as lying somewhere between these extremes. The X–Sn–X angles in both halides come close to the 90° observed for the difluoride, but the C–Sn–C angles are still significantly far from the 180° required if the difluoride structure were completely adopted.

5.3.2 Me_3SnH

Trimethylstannane also crystallises as isolated molecules in a triclinic space group, each unit cell containing two formula units. Salient features of the structure are

displayed in Table 5.4, and drawn in Figure 5.3.

Crystal system	Triclinic twin
Space group	$P\bar{1}$
Unit cell dimensions	a = 6.2620(13)Å, α = 67.41(3)°
	b = 6.8220(14)Å, β = 80.92(3)°
	c = 8.640(2)Å, γ = 62.62(3)°
Sn–C(1)	2.145(11)Å
Sn–C(2)	2.140(10)Å
Sn–C(3)	2.145(10)Å
C(1)–Sn–C(2)	109.4(5)°
C(1)–Sn–C(3)	109.8(4)°
C(2)–Sn–C(3)	109.7(4)°

Table 5.4. The Geometry of Me_3SnH by Single Crystal X-Ray Diffraction

The Sn–C bond lengths again are typical, and the C–Sn–C angles suggest tetrahedral geometry around the tin centre. The location of the hydrogen bound directly to tin could not be determined from the data collected.

The structure of Me_3SnH as determined by *ab initio* and GED methods is compared with that found in the solid state in Table 5.5.

Parameter	X-Ray	GED[31]	DZ(P)/MP2
Sn–C/Å	2.14(1)	2.147(4)	2.1480
Sn–H/Å		1.705(67)	1.7310
C–Sn–C(°)	109.7(4)	107.5(6)	109.78
C–Sn–H(°)		111.5(20)	109.16

Table 5.5. Geometrical Parameters of Me_3SnH from X-Ray, GED, and *ab initio* studies.

Again, the C–Sn–C bond angle measured by GED deviates substantially from those calculated, and those observed in the solid state, the variation being ascribed to shrinkage effects not compensated for in the gas phase study.

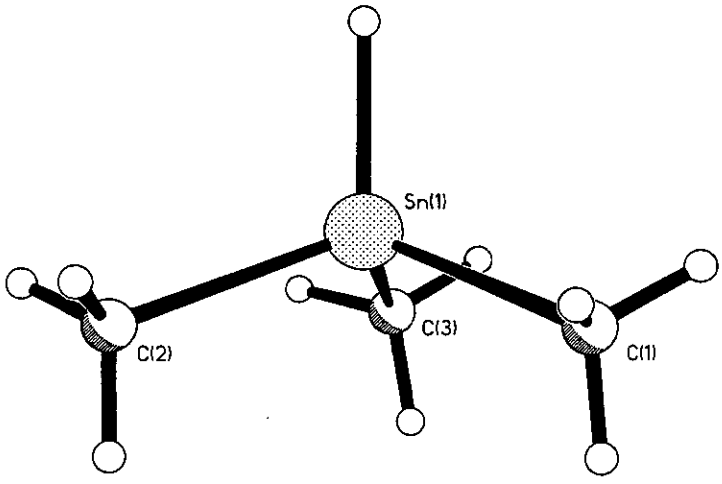

Figure 5.3. The Structure of Me_3SnH by Single Crystal X-Ray Diffraction.

Only one other example of a trimethyltin compound that contains discrete Me_3SnX units has been recorded in the solid state. The fluoride[107] is disordered and probably polymeric, leaving only the chloride, as determined by Lefferts *et al.*[117] for comparison purposes. Parameters for both structures are presented in Table 5.6.

Compound	Sn–C/Å	C–$\widehat{Sn}$–C(°)	Technique
Me_3SnH	2.140(10)	109.8(4)	X-ray
	2.149(4)	107.5(6)	GED[31]
Me_3SnCl	2.119(7)	117.1(3)	X-ray[117]
	2.106(6)	114.9(1.6)	GED[31]

Table 5.6. Geometrical Parameters of Me_3SnX, X = H, Cl, by GED, and single crystal X-Ray diffraction.

Here, as for the dimethyltin derivative, the C–Sn–C bond angle is larger in the chloride than in the hydride. Lefferts points to the presence of Cl···Sn–Cl chains in the chloride structure as a justification for this, the C–Sn–C angle widening due to interaction between tin and the chlorine of a neighbouring molecule. The

C–Sn–C angle observed in the gas-phase, though only slightly smaller, is artificially inflated due to shrinkage, suggesting that its increase on transition to the solid state is indeed due to intermolecular effects.

5.4 The Solid State Structure of Me_3PCH_2.

5.4.1 Introduction

Ylids have a fundamental importance in organic chemistry, particularly in the field of stereoselective alkene synthesis,[118–120] and therefore have been the subject of intense investigation from theoretical, synthetic, and structural standpoints.

The nature of the ylidic bond, and as a consequence, the coordination geometry of the ylidic carbon has been of substantial structural interest. It has been found that attaching delocalising groups to this carbon atom generally produces a roughly planar coordination sphere, while non-delocalising groups generate pyramidal coordination.[121] For example, the sum of angles around the ylidic carbon in triphenylphosphonium methylid[122] is 346.3°, indicating a pyramidal carbon, while that in triphenylphosphonium benzylid[123] is 359.9°, suggesting an almost perfectly planar geometry.

The ylid which has been subject to the most intense structural scrutiny is triphenylphosphonium methylid, first synthesised by Schmidbaur and Tronich in 1968.[124] Simpler ylids have received significantly less attention, triisopropylphosphonium methylid[125] being the smallest to be characterised in the solid phase.

Herein the solid state structure of the simplest isolable phosphonium ylid, Me_3PCH_2, is described and compared with a previous gas-phase determination,[126] and that predicted by *ab initio* methods.

5.4.2 Results and Discussion

Me_3PCH_2 crystallises in a monoclinic space group, each unit cell containing two formula units. Structural parameters are outlined in Table 5.7, the labelling scheme shown in a graphical representation of a single formula unit in Figure 5.4.

A crystallographic mirror plane runs through the C(2)–P–C(5) plane of the

Crystal system	Monoclinic
Space group	$P2_1/m$
Unit cell dimensions	a = 6.086(1)Å, $\alpha = 90°$
	b = 7.615(2)Å, $\beta = 92.55(2)°$
	c = 6.457(2)Å, $\gamma = 90°$
P–C(2)	1.678(2)Å
P–C(5)	1.791(2)Å
P–C(9)	1.808(1)Å
C(2)–H(3)	0.92(3)Å
C(2)–H(4)	0.74(3)Å
C(5)–H(6)	0.92(2)Å
C(5)–H(7)	0.96(3)Å
C(9)–H(10)	0.94(2)Å
C(9)–H(11)	1.00(2)Å
C(9)–H(12)	0.94(2)Å
C(2)–P–C(5)	110.7(1)°
C(2)–P–C(9)	115.69(6)°
C(5)–P–C(9)	105.40(6)°
C(9)–P–C(9A)	102.9(1)°
P–C(2)–H(3)	110.5(17)°
P–C(2)–H(4)	118(3)°
H(3)–C(2)–H(4)	118(3)°
H(4)–C(2)–H(4A)	71(5)°

Table 5.7. The Geometry of Me_3PCH_2 by Single Crystal X-Ray Diffraction

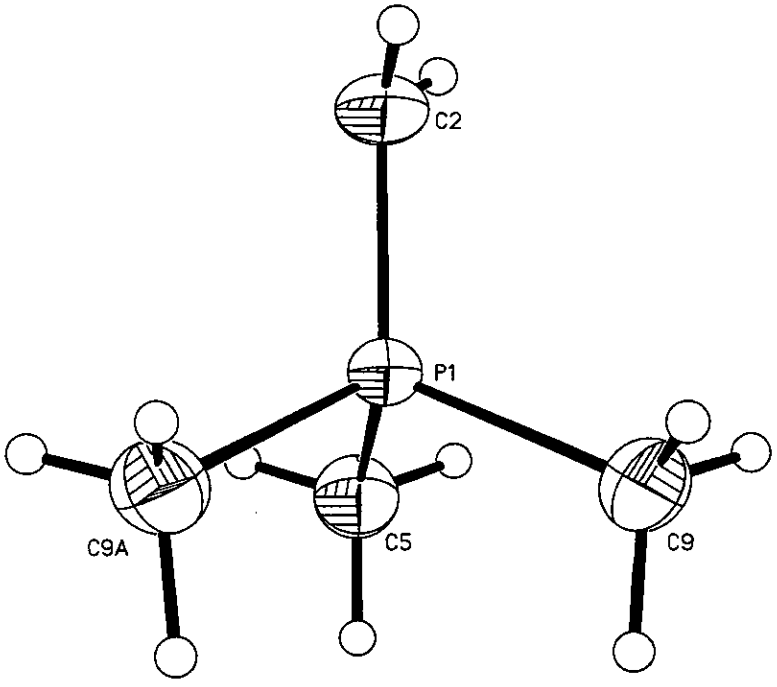

Figure 5.4. The Structure of Me_3PCH_2 by Single Crystal X-Ray Diffraction.

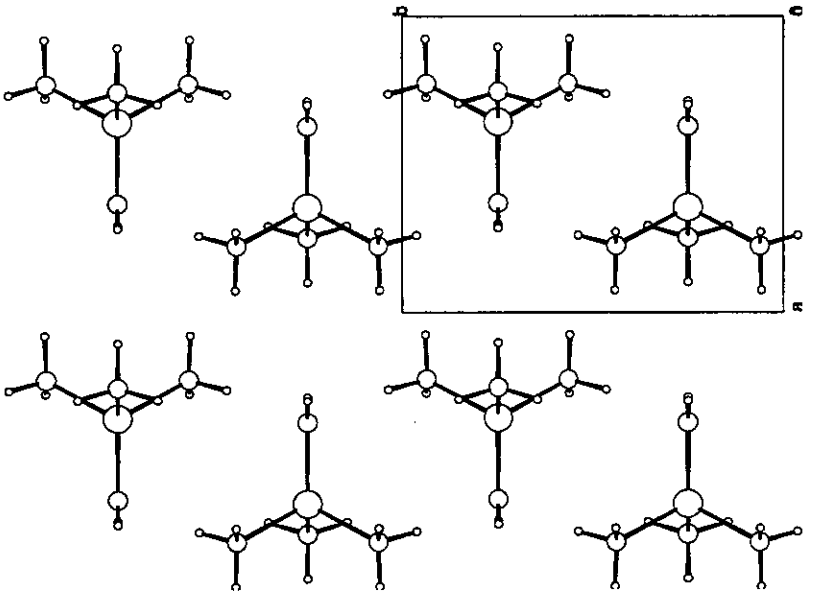

Figure 5.5. The Packing of Me_3PCH_2 in the Solid State.

molecule, generating two equivalent methyl groups, and enforcing a staggered conformation at C(2). Only one of the ylidic protons lies in the mirror plane, the other lying substantially out of the plane, being disordered between two equivalent sites generated by reflection. The position of one of these sites can be clearly seen in Figure 5.4, the two sites forming an angle with C(2) of 71(5)°. Thus, the geometry around the ylidic carbon is not planar, the sum of angles being 346(7)°. This is to be expected for an ylid carbon lacking delocalising substituents.

The minimum energy geometry of Me_3PCH_2 according to *ab initio* methods is substantially different from that observed in the solid state, although C_s symmetry is retained. In the global minimum structure, the ylidic protons lie out of the mirror plane, the bond lengths and angles around phosphorus being substantially different from those in the solid state as a result. The ground state structure is shown in Figure 5.6.

To estimate the energy difference between the ground state *ab initio*, and the observed solid state structure, a second set of calculations was performed in

which the ylidic protons were fixed in the mirror plane of the molecule. Calculation of the vibrational force field of this structure yielded 42 vibrations, 41 with real frequencies, but one with an imaginary frequency. This indicated that the structure calculated was not at the global minimum of the molecular potential energy surface, but corresponds to a transition state. The structure of Me_3PCH_2 in this configuration is shown in Figure 5.7, and the geometrical parameters of both this, and the global minimum structure are compared to those observed in the solid state in Table 5.8.

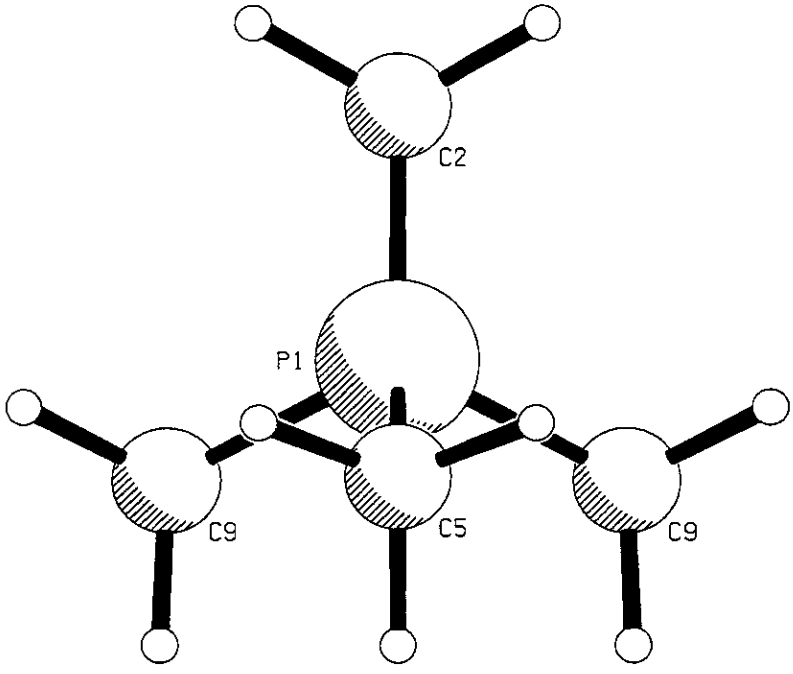

Figure 5.6. The Ground State Structure of Me_3PCH_2 as calculated by *ab initio* techniques.

There is a strong similarity between the transition state and solid state structures. The energy difference between the global minimum and the transition state is also small (5.25 kJ/mol), suggesting that packing effects may be sufficient to turn the transition state calculated in the gas phase into the observed solid–state structure.

A structural study of Me_3PCH_2 in the gas phase by electron diffraction was

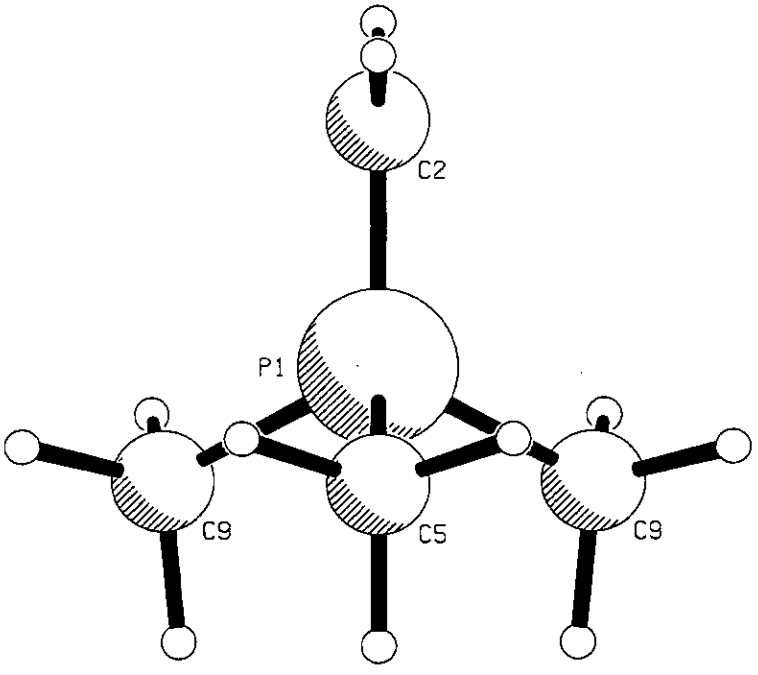

Figure 5.7. A Transition State Structure of Me_3PCH_2 as calculated by *ab initio* techniques.

performed in 1977,[126] but assumed that a C_{3v} structure was adopted. The calculations presented above, and the structure observed in the solid state suggest that this is a poor assumption, a C_s model being much more appropriate. Mitzel[127] has since re-refined the electron diffraction data collected in the original study in terms of a C_s model using an improved GED methodology.[128,129] The refinement finally converged with $R_G = 3.95\%$ (compared to the previous R_G of 13%), indicating that the assumption of C_s over C_{3v} symmetry is a good one. The resulting structure resembles the calculated global minimum state, with the ylidic hydrogens perpendicular to the C(2)–P–C(5) plane, and is outlined in Table 5.8.

		MP2/6-311G*		
Parameter	X-Ray	Minimum	T. S.	GED
P–C(2)/Å	1.678(2)	1.6773	1.6648	1.656(2)
P–C(5)/Å	1.791(2)	1.8494	1.8141	1.837(6)
P–C(9)/Å	1.808(1)	1.8171	1.8348	1.809(3)
C(2)–P–C(5)	110.7(1)°	123.93	110.26	122.4(7)
C(2)–P–C(9)	115.69(6)°	110.44	117.50	111.4(13)
C(5)–P–C(9)	105.40(6)°	101.66	104.76	101.0(20)
C(9)–P–C(9A)	102.9(1)°	107.36	100.52	108.3(14)
P–C(2)–H(3)	110.5(17)°	117.02	121.65	118.2(4)
P–C(2)–H(4)	118(3)°	117.02	119.01	118.2(4)
E(MP2)/E_H		-499.2713	-499.2693	

Table 5.8. The Geometry of Me_3PCH_2 by X-Ray, GED, and *ab initio* techniques.

The large variation in structure caused by a 90° rotation about the ylidic C–P axis is surprising, considering the small calculated energy difference between the global minimum and the transition state. During this rotation, the C(2)–P–C angles vary by between 3 and 13 degrees, and the H_3C–P bond lengths alter by up to 0.04Å. This is presumably a result of the changing position of the carbanionic lone pair on C(2), the methyl groups moving to remain as far away from it as is possible.

In the global minimum, the angles C(9)–P–C(9A) and C(2)–P–C(5) are large, the lone pair residing in the mirror plane. The opposite situation is the case in the

transition state, in which the lone pair points out of the mirror plane. This forces the C(9) methyl groups closer together, increasing C(5)–P–C(9), and decreasing C(2)–P–C(5) as a result.

Chapter 6

The Structure of Trimethyllead Hydride

6.1 Introduction

The hydrides of lead, as noted in Chapter 1, are extremely poorly characterised, most probably due to the extreme care with which they must be handled, and the difficulties encountered in preparing them. Here we present the results of attempts to remedy this situation by determining the structure of trimethyllead hydride, Me_3PbH, in the solid state by powder neutron diffraction, and in the gas phase by electron diffraction, with the aim of thereby accomplishing the first ever experimental determination of a Pb–H bond length.

6.2 Experimental Techniques

6.2.1 Synthesis of Trimethyllead Hydride

Trimethyllead hydride was synthesised according to the method of Becker *et al.*[39]

In a typical preparation, 5–10 mmol of Me_3PbBr was transferred in the dry box to the first trap of the apparatus shown in Figure 6.1.

The trap was then attached to the Schlenk line, and cooled in liquid nitrogen. One quarter of the molar equivalent of lithium aluminium hydride was added

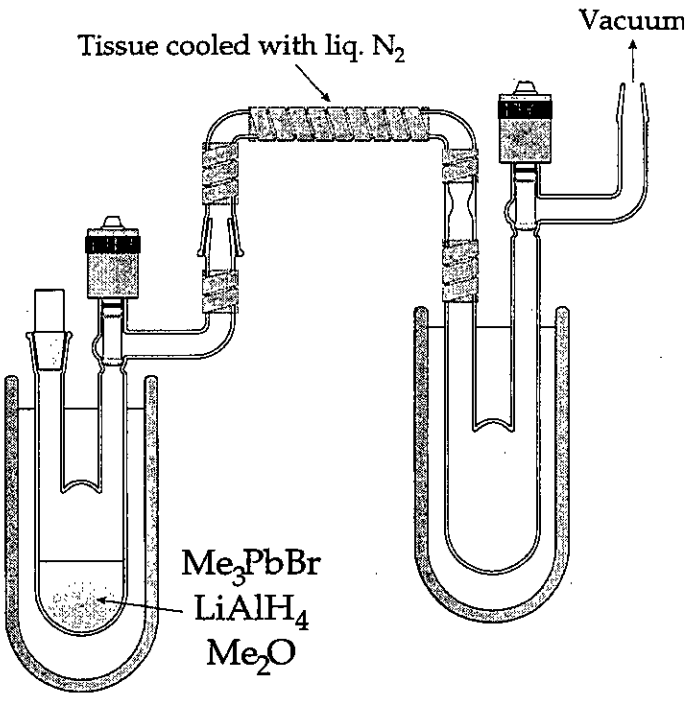

Figure 6.1. Apparatus for the Preparation of Me_3PbH.

under a nitrogen stream, and the trap sealed, evacuated, and connected to the remainder of the apparatus on the high vacuum line. As much of the glassware as possible was then "flamed out" to remove any water and other volatile contaminants present.

Dimethyl ether (5–10 cm^3) was condensed onto the solid mixture, and the trap containing the reactants sealed and warmed to -78°C with constant magnetic stirring. After 15 minutes a black colouration appeared in the solution, at which point the reaction was considered complete. The second trap was then cooled to -78°C, and the intervening glassware cooled by soaking the tissue coating with liquid nitrogen to minimise thermal decomposition of the product during distillation. The solution was then warmed to -45°C under continuous pumping, and Me_3PbH and some Me_4Pb condensed in the -78°C trap. Excess solvent and non-condensables were pumped away. The trap was then cooled in liquid nitrogen and sealed off under vacuum using a hand torch.

A second distillation from -45°C to -78°C using the above method was sufficient to separate the product from any Me_4Pb present, giving a yield of *ca.* 0.5–1 cm^3 Me_3PbH.

6.2.2 Synthesis of $(CD_3)_3PbD$

$(CD_3)_3PbD$was prepared in a manner similar to that of $(CH_3)_3PbH$, but using lithium aluminium deuteride, and $(CD_3)_3PbBr$ (prepared by Dr. Holger Fleischer) as starting materials.

Two preparations were attempted, using 2.0 g, and 2.57 g of $(CD_3)_3PbBr$ respectively, the products of which were condensed into a single quartz ampoule provided by the Rutherford Appleton Laboratory.

6.2.3 Powder Neutron Diffraction at ISIS

Introduction

The high resolution powder diffractometer (HRPD) at the ISIS facility, Rutherford Appleton Laboratory, in Oxfordshire is the highest resolution powder diffractometer in the world, allowing neutron diffractograms to be recorded up to a

resolution of $\Delta d/d = 4 \times 10^{-4}$.

Neutrons for the HRPD (and for the many other instruments at ISIS) are produced by the impact of a pulse of high energy protons from a synchrotron onto a heavy metal target (see Figure 6.2). The resulting neutron pulse passes through a liquid methane moderator, then up a 100 m wave guide to the diffractometer, in which the sample is mounted in a cryostat. Three detectors collect diffracted neutrons at different angles around the diffractometer allowing high resolution data to be recorded at d-spacings of up to 5–6 Å, and data of a lower resolution to be recorded up to, and beyond a d-spacing of 20 Å.

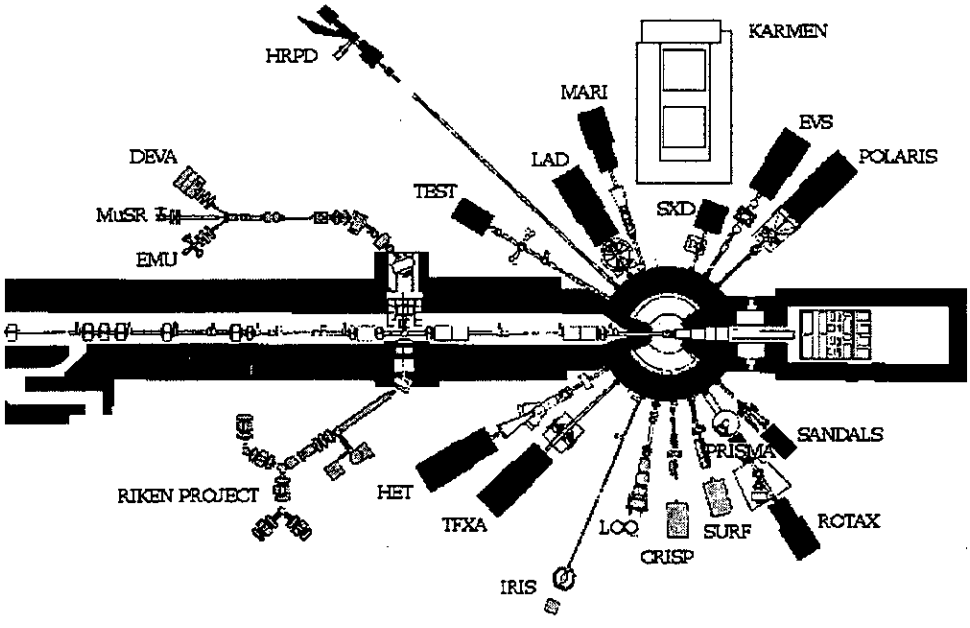

Figure 6.2. The ISIS Facility at the Rutherford Appleton Laboratory.

The neutron pulse entering the HRPD consists of neutrons of varying energy, and therefore varying wavelength. Instead of passing the pulse through a monochromator, filtering out all but a few neutrons of a single chosen wavelength, the HRPD adopts an alternative approach dependent upon measuring the time of flight of each neutron arriving at a detector.

In the standard X-ray diffraction experiment, an X-ray source of a single,

accurately known wavelength is used. Diffraction data are then collected by observing X-ray intensity at various angles formed between the source, the sample, and the detector. Information on d-spacings in the sample is subsequently derived from the Bragg equation,

$$n\lambda = 2d\sin(\theta)$$

in which the d-spacing, d, is calculated from the wavelength, λ, of the X-ray source, and the angle, θ, between source, sample, and detector.

At the HRPD, the detectors used are mounted in fixed positions, and so the angle θ becomes the constant of the Bragg equation. Instead, the time between the formation of the neutron pulse at the spallation source, and the arrival of each neutron at the detector is used to calculate the speed at which the neutron was travelling, and therefore its energy, and effective wavelength. The output of the "Time of Flight" (TOF) experiment is a plot of diffracted intensity against time, from which sample d-spacings can be readily calculated.[130]

The TOF method allows every neutron available in a single pulse to contribute to the resulting diffractogram, greatly reducing the measuring time required to collect high quality diffraction data for a sample.

Data collected in this way may be analysed using standard powder diffraction software packages. The principles behind this analysis, and the rationale for applying them to the study of Me_3PbH in the solid state, are outlined in the following section.

The Analysis of Powder Diffraction Data by Rietveld Refinement

The process of generating chemically useful structural information from diffraction data breaks down into four distinct steps,[131]

1. Indexing of the diffraction pattern and the determination of the crystal system and lattice parameters.

2. Identification of the space group.

3. Solution of the phase problem and determination of an approximate structure.

4. Refinement of the structure.

For single crystal X-ray diffraction data, overlap between individual reflections is relatively uncommon, allowing the easy measurement of peak intensity. Indexing usually takes place at the diffractometer as one of the first steps in data collection, sometimes automatically, but usually with some input from the crystallographer to confirm predicted unit cells as sensible and realistic. Subsequent data collection then uses reflection positions calculated from the chosen unit cell to increase the efficiency of the process, and to decrease the time taken to collect a data set sufficient for subsequent analysis.

Advances in computing power, and the software available for the solution and refinement of single crystal diffraction data have made the final two steps in the process almost straightforward, allowing the entire process to be performed for routine samples in a matter of a few days at most.

For powder diffraction data, the process is not so straightforward. The random orientation of the crystallites within the sample reduces the pattern of 'spots' observed in the single crystal experiment to a set of rings, compressing a two dimensional data set into a single dimension. Peaks in a powder diffractogram frequently overlap one another, thereby introducing ambiguity into the indexing process, and complicating the assignment of intensity to individual peaks.

The indexing problem can in general be solved through the use of auto-indexing computer software.[132] Programs of this type require highly accurate d-spacing data and function most efficiently if that data extends to as high a d-spacing as possible. For both these reasons, results collected at the HRPD are highly suited to analysis in this way, peak indexing of high quality data rarely presenting a significant barrier to structure solution.

The problem of peak overlap has been tackled in two very different ways. The first requires knowledge of the intensity profile of the radiation source used to deconvolute individual peaks in the diffractogram, a least squares refinement procedure producing the best fitting allocation of intensity to individual reflections.[133] Refinement then proceeds as for the single crystal case.

The second, as developed by Rietveld,[134,135] uses knowledge of the intensity profile of the neutron source, coupled with an initial starting model of the structure in question to calculate a theoretical diffraction pattern. This is then compared with the experimental result, and the model structure modified using a least squares refinement procedure until the best fit between theory and experiment is obtained. This approach can only succeed if the starting model used is of reasonable quality. It is therefore not a structural solution method, and is only effective in cases where fairly accurate knowledge of the structure to be refined already exists.

The advantage of Rietveld refinement over an *ab initio* approach lies in the use of the experimental data collected. The least squares approach to intensity assignment uses only those parts of the data set collected in which individual peaks can be adequately deconvoluted and assigned. The Rietveld method, on the other hand, compares the entire experimental data set to one calculated on the basis of the model used. This allows information stored in every data point collected to contribute to the final structure, even if the information gained is simply that reflections are not observed in certain parts of the diffractogram.[136]

For situations in which a good starting model for a Rietveld refinement is available, this method becomes the method of choice for the analysis of powder diffraction data.

The Application of Rietveld Refinement to the Structure of Me_3PbH.

In 1996, Fleischer *et al.*[137] successfully grew a diffraction quality single crystal of Me_3PbH on an X-ray diffractometer using the techniques described in Section 5.2.1. The resulting structure, shown in Figure 6.3, contains no information concerning the location of hydrogen atoms in the molecule due to the nature of the diffraction experiment.

X-rays are scattered by electrons, and not by individual atomic nuclei. Therefore the solution of a diffraction experiment is a map of electron distribution in the sample being studied. Atom positions and types are then assigned to centres of electron density, resulting in the generation of a molecular structure that best fits the electron density observed. The position of a hydrogen atom (Atomic Number

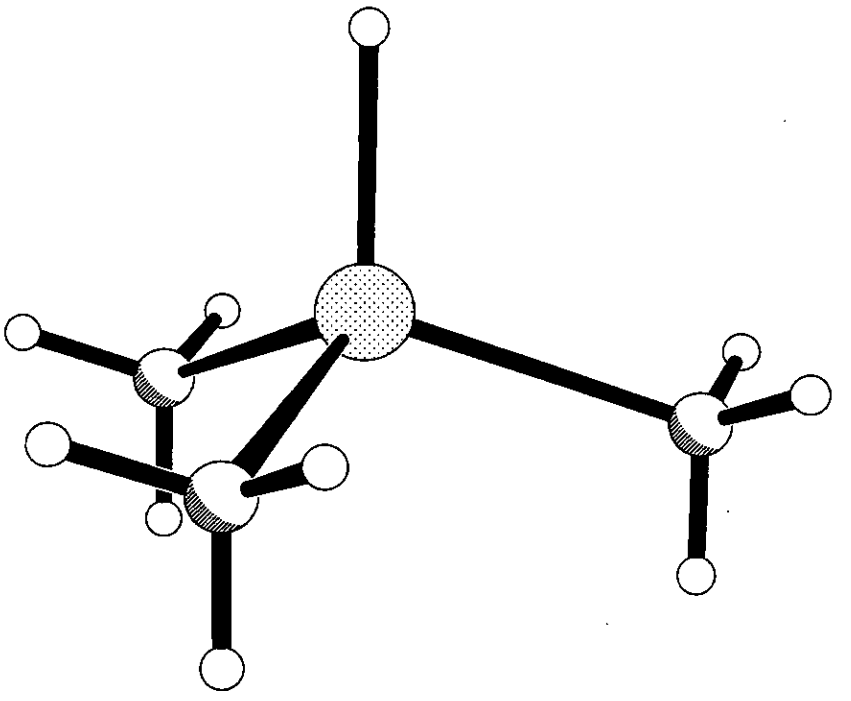

Figure 6.3. The Structure of Me_3PbH by X-ray Diffraction.[137] Hydrogens are shown at idealised positions.

1) close to a lead atom (Atomic Number 82) cannot be accurately determined by this technique, therefore.

Neutrons, on the other hand, are scattered by atomic nuclei, and not by the electrons that surround them. Neutron scattering intensities are expressed in terms of the scattering lengths of individual atoms, which depend not only upon the atomic number of the atom, but upon the number of neutrons in the nucleus as well. Neutron scattering length is not a simple function of atomic number, e.g. the scattering length of a proton is -3.94 fm, and for a deuteron is 6.67 fm.

The complex variation in neutron scattering length with atom type can be exploited in the search for hydrogen positions, particularly in the case of Me_3PbH. Here, only three types of atoms scatter, with lengths Pb = 9.4 fm, C = 6.65 fm, and D = 6.67 fm. Carbon and deuterium scatter neutrons to an approximately equal extent, and have only two-thirds the scattering power of lead, allowing the positions of the deuteria in $(CD_3)_3PbD$ to be determined by neutron diffraction with a high degree of precision.

Unfortunately, owing to the low melting point of Me_3PbH, and its extreme thermal instability, growth of a single crystal of the compound suitable for neutron diffraction at the diffractometer was thought to be technically unfeasible. However, the handling problems associated with mounting a polycrystalline sample on the diffractometer were surmountable, and so a neutron powder diffractogram of $(CD_3)_3PbD$ was recorded at 4 K on the HRPD at ISIS by Dr. Kevin Knight, data being collected at $2\theta = 168.33°$ and 90.0°.

A Rietveld refinement was then attempted, using the single crystal structure of Me_3PbH as a starting model. The results of this attempt are detailed in the following sections.

6.3 The Structure of Me_3PbH by Neutron Powder Diffraction

6.3.1 Structure Refinement

The diffraction data collected at the HRPD were refined using the "General Structure Analysis System" (GSAS), by Larson and von Dreele[138] developed for the analysis of TOF and other data from the Neutron Scattering Centre at Los Alamos. GSAS is currently in common use world-wide, its ability to refine concurrently data collected from both X-ray and neutron experiments enabling the first unambiguous structural determination of $YBa_2Cu_3O_{7-x}$, for example.[139]

Three approaches were used in the refinement process, using

1. an unrestrained model, in which all atom positions were allowed to refine freely,
2. a constrained model, in which the geometry of the three methyl groups in $(CD_3)_3PbD$ was assumed to be pyramidal, with identical C–D bond lengths,
3. difference Fourier maps to determine the positions of deuterium atoms.

The results of each refinement are detailed in the following sections.

6.3.2 Refinement using an Unrestrained Model

The diffraction data collected at $2\theta = 90.0°$, and 168.3°, and instrument parameters appropriate to the HRPD were entered into GSAS in the usual manner, and a starting model created using the space group, and lattice parameters shown in Table 6.1 and atomic positions from Table 6.2.

The refinement then proceeded in the manner suggested by Young,[136] in which the histogram scale factors, background function, and lattice parameters were refined in turn until a stable minimum was reached.

Next, the shape of the diffraction peak profile was refined using a set of isolated reflections as a guide to the experimental peak shape. Once a satisfactory fit had

Crystal system	Monoclinic
Space group	P $2_1/n$
Z	4
Unit cell dimensions	a = 6.287(3)Å,
	b = 15.859(10)Å, β = 115.96(4)°
	c = 6.850(3)Å
Pb–C(1)	2.26(2)Å
Pb–C(2)	2.22(2)Å
Pb–C(3)	2.22(2)Å
C(2)–Pb–C(3)	108.6(7)°
C(2)–Pb–C(1)	109.7(7)°
C(3)–Pb–C(1)	110.5(7)°

Table 6.1. The Geometry of Me_3PbH by Single Crystal X-Ray Diffraction[137]

	Unit cell coordinates		
Atom	a	b	c
Pb	0.13527	0.84594	0.49703
H	0.24639	0.74408	0.50639
C1	-0.22163	0.83807	0.50030
H11	-0.20503	0.80986	0.63352
H12	-0.33057	0.80587	0.37389
H13	-0.28426	0.89505	0.49490
C2	0.09952	0.90970	0.19593
H21	-0.01099	0.87801	0.06927
H22	0.25442	0.91224	0.19417
H23	0.03933	0.96703	0.19134
C3	0.38643	0.91918	0.78063
H31	0.40394	0.89169	0.91497
H32	0.32555	0.97649	0.77463
H33	0.54063	0.92170	0.77745

Table 6.2. Unit cell coordinates of the atoms in Me_3PbH by single crystal X-ray diffraction.[137] The hydrogen positions are idealised.

been obtained, the positions of individual methyl groups were allowed to vary. It was found that if large changes in atom positions were permitted at this stage, a convergent refinement was rarely obtained, and so a high damping factor was applied to the motion of every refining atom in the molecule.

After a substantial number of refinement cycles involving the motion of various combinations of methyl groups and the D–PbC_3 skeleton, a relatively stable structure was obtained, providing an acceptable fit to the data observed at 168.3°($R_{wp} = 6.7\%$), and a less good fit to the data collected at 90°($R_{wp} = 18.4\%$). The predicted and observed diffractograms for both data sets are shown in Figure 6.4, and the geometrical parameters of the Me_3PbH model required to produce this fit are shown in Table 6.3.

a = 6.207Å	b = 15.46Å	β = 116.59°	c = 6.833Å
Pb–D	2.166Å	Pb–C1	2.229Å
Pb–C2	2.160Å	Pb–C3	2.336Å
D11–C1	1.91Å	D11–C1–Pb	104.3°
D12–C1	1.30Å	D12–C1–Pb	Not calculated
D13–C1	1.47Å	D13–C1–Pb	99.2°
D21–C2	0.93Å	D21–C2–Pb	123.0°
D22–C2	0.57Å	D22–C2–Pb	117.4°
D23–C2	1.22Å	D23–C2–Pb	109.6°
D31–C3	Not calculated	D31–C3–Pb	Not calculated
D32–C3	1.49Å	D32–C3–Pb	81.4°
D33–C3	0.57Å	D33–C3–Pb	121.9°

Table 6.3. The Geometry of $(CD_3)_3PbD$ from a Rietveld Refinement with Unconstrained Deuterium Positions.

The results of this refinement highlight many of the problems associated with this form of structure analysis in general, and a number of the difficulties inherent in the refinement of the structure of $(CD_3)_3PbD$ in particular.

The first and most obvious conclusion from a brief study of the geometrical

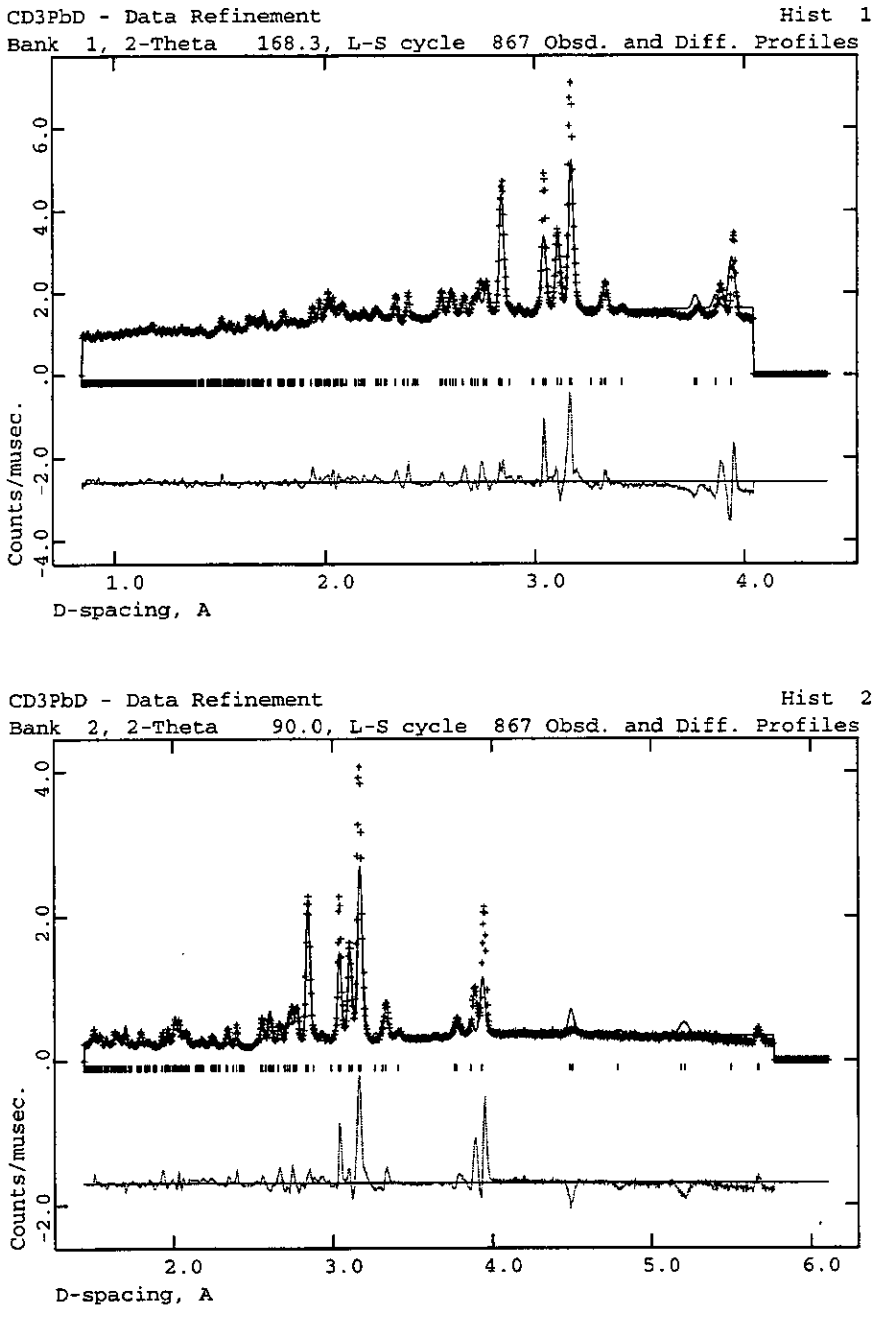

Figure 6.4. Predicted and Observed Diffractograms for the Rietveld Refinement of $(CD_3)_3PbD$, with Unconstrained Deuterium Positions.

parameters shown is that they make little chemical sense. Many of the Pb–C–D bond angles, and nearly all the C–D bond lengths are implausible - there is no reason to expect these to differ widely from an approximately tetrahedral angle (109.4°), and a bond length between 0.84–1.10Å.

However, the positions of the lead and carbon atoms are little different from those in the starting model. This suggests one possible reason for the unlikely deuterium positions generated by the refinement : the idealised structure used as the starting model has a roughly correct PbC_3 skeleton, but the hydrogen positions are wrong. This would not be unreasonable given the low temperature of the neutron refinement. At 4 K, rotation about the Pb–C bond should be minimal, allowing the individual methyl groups to adopt eclipsed or staggered conformations, or a lower energy conformation somewhere between the two extremes. The possibility of disorder at the methyl groups also exists, thereby introducing added complications.

Two highly disturbing features are present in the graphical output of the refinement. The first manifests itself at a d-spacing of about 3.9Å, while the other is only visible in the data collected at 90°.

A magnification of the 168.33° data set at around 3.9Å is shown in Figure 6.5, the solid line therein corresponding to the predicted diffraction pattern, and the crosses marking the observed intensities. Underneath these, black tick marks represent reflection positions predicted on the basis of the unit cell parameters currently used.

It is clear that the predicted and observed reflection positions do not coincide, the predicted ones appearing at a slightly smaller d-spacing. As the reflection positions are calculated directly from the lattice parameters, this implies that at least one of the lattice parameters is incorrect. This parameter can be determined from the indexing of the reflection positions between 3.6Å and 4.0Å as predicted by GSAS; this is shown in Table 6.4.

The d-spacing for a monoclinic space group is given by,

$$\frac{1}{d_{hkl}^2} = \frac{h^2}{a^2 \sin^2\beta} + \frac{k^2}{b^2} + \frac{l^2}{c^2 \sin^2\beta} - \frac{2hl\cos\beta}{ac\sin^2\beta}$$

From this it is apparent that the erroneous lattice parameter is b. This is the

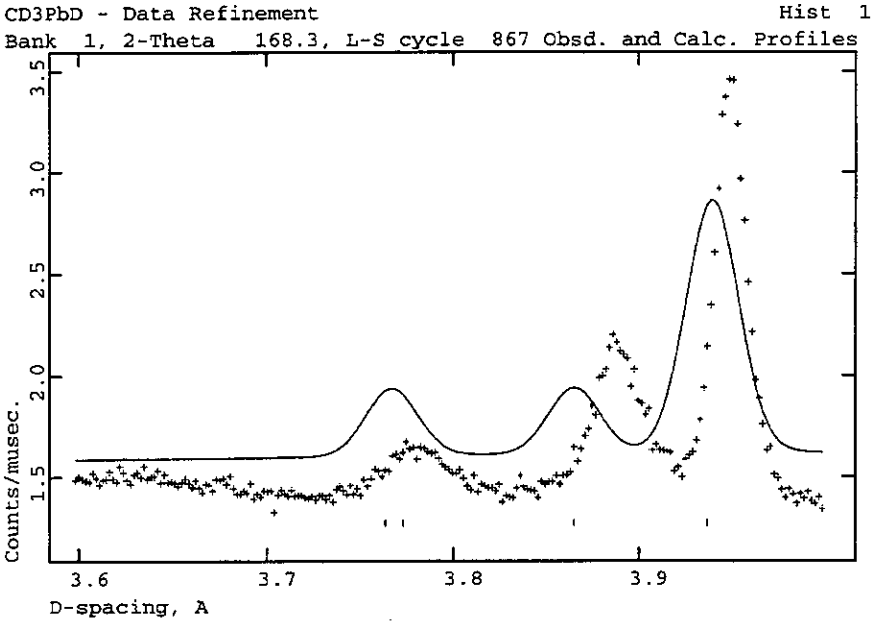

Figure 6.5. Predicted and Observed Diffraction Patterns for $(CD_3)_3PbD$ for a d-spacing of 3.6–4Å

d-spacing/Å	(hkl)
3.77	$13\bar{1}$
3.78	130
3.86	040
3.94	031

Table 6.4. Predicted Indexing for Reflections between 3.6Å and 4.0 Å

only parameter governing the position of the (040) reflection, and as it is also more than twice as large as both a and c, its effect on the positions of the other reflections in Table 6.4 is dominant.

It was found by a trial-and-error approach that fixing the value of b to 15.54Å while allowing the other lattice parameters to refine freely, reduced to a minimum the difference between the observed and predicted reflection positions in this region.

The second problem observed in the graphical output underlines the poor quality of the structural model generated by this refinement. At d-spacings of approximately 4.5Å, and 5.2Å in the data collected at 90.0°, peaks are predicted to appear by the model used that are not actually present in the experimental data. The presence of these unobserved peaks, and the other problems mentioned above suggest that an alternative approach be taken to the Rietveld refinement in which the positions of the methyl deuteria are fixed, at least initially, in chemically reasonable positions. The implementation of this approach using GSAS, and the results obtained from it, are detailed in the following section.

6.3.3 Refinement using a Constrained Model

The second approach to the Rietveld refinement of the structure of $(CD_3)_3PbD$ concentrates on the geometries of the methyl groups in the molecule. The previous section outlines the result of a refinement in which the deuteria of the methyl groups were allowed to refine to any position in the unit cell, and comments on the unacceptability of the resulting structure. Here is described an approach in which the deuterium atoms are constrained to take reasonable positions around the methyl carbons.

GSAS provides two functions for this purpose, in which geometrical parameters are either fixed ("constrained") or allowed to refine within certain limits ("restrained"). The restraint function simply involves the specification of the magnitude and error of the interatomic distance to be restrained. This method is not ideally suited to the specification of the bond lengths and angles required to define the geometry of a methyl group, and so was discarded after a small amount of experimentation. The second, called the "rigid body" approach, was

explored in some detail, and is described below.

The "Rigid Body" Approach to Geometric Constraint.

Rigid bodies were built in to GSAS to allow the definition of simple, highly symmetric structures using only a small number of refinable parameters. For example, the determination of the deuterium positions in ND_4^+ counter-ions of an ionic material is a problem ideally suited to this technique. Although the adaptation of the rigid body definition to the constraint of molecular fragments, rather than molecules or ions as a whole is less straightforward, it is still more effective than an approach using restraints.

The definition of a rigid body within GSAS begins at an abstract, geometrical level. Firstly, an atom within the structural fragment to be constrained is chosen as the origin for the coordinate system within which the rigid body is to be defined. For ND_4^+, this would be the nitrogen; for the definition of a methyl group, the carbon atom is the sensible choice.

Next, the geometry of the rigid body is determined, relative to this origin by the calculation of vectors starting at the origin, and terminating at the other atoms to be included in the body. For the ND_4^+ cation, four vectors would be calculated from nitrogen to the four deuteria, giving a tetrahedral geometry, and in the case of a methyl group, three vectors are required to define the three methyl hydrogen positions. The position of the carbon atom is also defined in this way, using a vector of zero length. The vectors used to define a pyramidal methyl group are detailed in Table 6.5.

Atom	x	y	z
C	0.00000	0.00000	0.00000
D	0.00000	-0.94281	-0.33333
D	-0.81650	0.47140	-0.33333
D	0.81650	0.47140	-0.33333

Table 6.5. Unit vectors for the definition of a pyramidal methyl group using a GSAS rigid body. D–C–D = 109.47°

This completes the definition of the geometry of a GSAS rigid body, creating

a model which can be used as the geometric basis for the independent constraint of as many fragments within the model structure as is appropriate. Each use of a rigid body requires the specification of six additional parameters, giving its position and orientation within the model. Each methyl group in $(CD_3)_3PbD$ may be located and oriented independently, therefore, although each shares the same geometrical definition.

In total, six parameters are required for the complete specification of each methyl group, giving 18 in all. An extra parameter defines the scaling of the geometrical model, fixing the length of the C–D bond in $(CD_3)_3PbD$ at a single value. This brings the total number of parameters needed to define the positions of the atoms in the three methyl groups to 19, substantially less than the 36 required without the use of rigid bodies.

The final step in the use of rigid bodies in GSAS is to determine the values of the positional and orientational parameters of each rigid body. For the methyl groups of $(CD_3)_3PbD$, this involves calculating the appropriate rotations and translation to move each methyl group from the origin to their appropriate places within the unit cell.

The positional parameters are best used to define the locations of the carbon atoms of $(CD_3)_3PbD$ as each carbon lies at the origin of its rigid body. The values used are then simply the unit cell coordinates of each carbon atom taken from the X-ray structure. The orientational parameters are then used to define rotations about the carbon atom to place the deuterium atoms bound to it in positions roughly corresponding to those predicted by the X-ray study.

The determination of the orientational parameters defining the positions of the deuterium atoms of the methyl groups is the most time consuming part of the process. The parameters are expressed as rotations about the X, Y, and Z axes used in the definition of the geometry of the rigid body, rather than as a torsion angle about, say, a Pb–C vector. In the case of ND_4^+, this is not particularly serious, but for the location of the three methyl groups of $(CD_3)_3PbD$, this requires an iterative, trial and error approach using manually estimated rotations, and an external software package[140] to view graphically the results of each attempt.

Once each rigid body has been manoeuvred into an appropriate position, refinement then proceeds in the normal fashion, with the magnitude, positions,

and rotations of each rigid body as refinable parameters. The use of rigid bodies has a severe impact on the time taken to perform a least squares refinement cycle, however. For the refinement of $(CD_3)_3PbD$ using three rigid bodies, the time taken for each cycle increased from roughly 100 s to about 550 s.

The Rietveld Refinement of $(CD_3)_3PbD$ using the "Rigid Body" Approach.

The refinement outlined in Section 6.3.2 was modified for the introduction of methyl groups defined using the rigid body technique described above. A starting model based on the single crystal structure of Me_3PbH was used, with the methyl hydrogens lying approximately in the idealised positions shown in Figure 6.3.

Refinement then proceeded with the heavy atom skeleton, and then each methyl group in turn being allowed to refine singly, then all at once until a minimum position was reached. The structural parameters defining this minimum are shown in Table 6.6 and Figure 6.6, and the corresponding diffractograms are shown in Figure 6.7.

a = 6.204Å, b = 15.54Å, β = 116.74°, c = 6.831Å					
	Pb–D	2.346Å	Pb–C1	2.260Å	
	Pb–C2	2.030Å	Pb–C3	2.458Å	
D–Pb–C1	83.0°	D–Pb–C2	135.8°	D–Pb–C3	144.0°
	D–C–D	109.47°	D–C	1.035Å	
D11–C1–Pb	107.8°	D21–C2–Pb	114.0°	D31–C3–Pb	131.7°
D12–C1–Pb	119.3°	D22–C2–Pb	85.6°	D32–C3–Pb	100.2°
D13–C1–Pb	100.8°	D23–C2–Pb	125.4°	D33–C3–Pb	94.7°

Table 6.6. The Geometry of $(CD_3)_3PbD$ from a Rietveld Refinement with Constrained Deuterium Positions.

The refinement converged with R_{wp} = 7.0% for the data collected at 168.33°, and R_{wp} = 19.2% for that at 90.0°. The poorer fit to the 90.0° data set was also

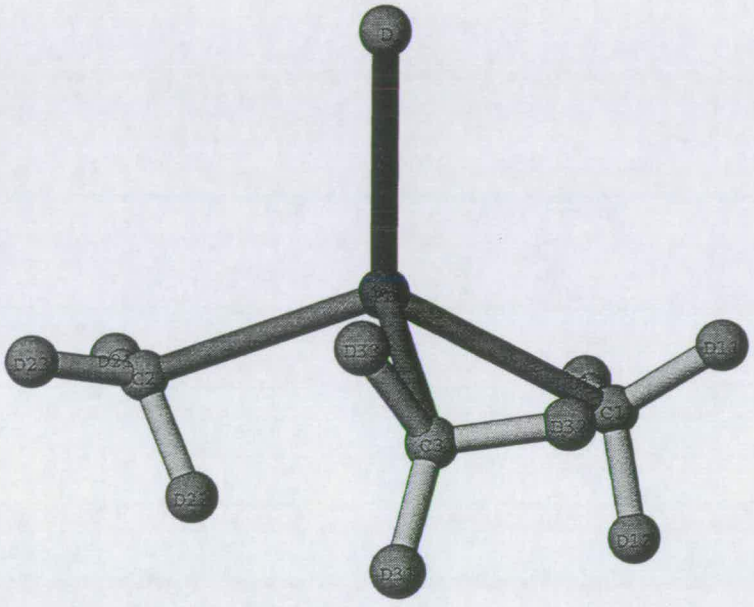

Figure 6.6. The Structure of $(CD_3)_3PbD$ by Rietveld Refinement with Constrained Deuterium Positions.

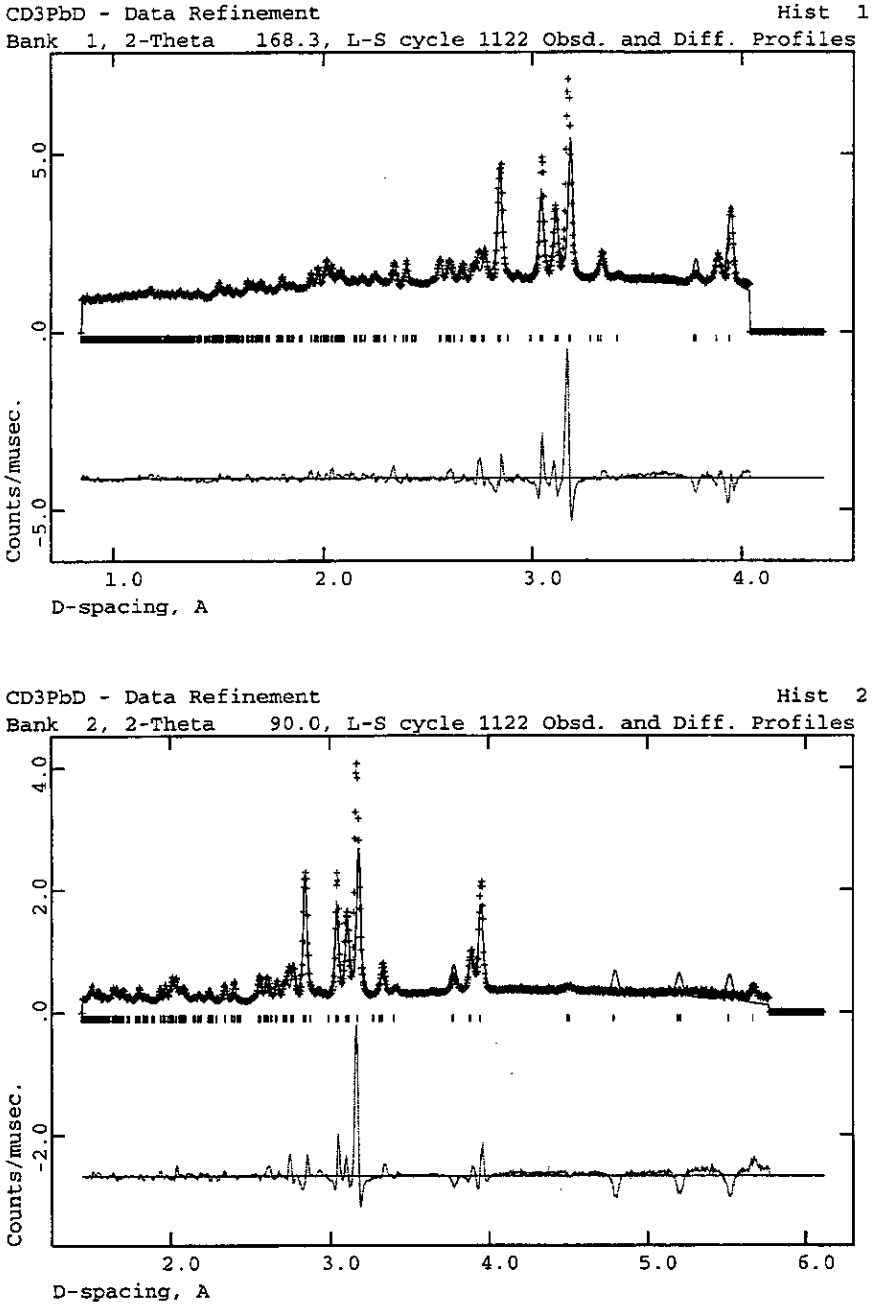

Figure 6.7. Predicted and Observed Diffractograms for the Rietveld Refinement of $(CD_3)_3PbD$, with Constrained Deuterium Positions.

observed in the previous refinement attempt, in which deuterium positions were allowed to refine freely. This suggests that this is not due to the use of rigid bodies, but rather due to a more fundamental mismatch between theory and experiment. The presence of peaks in the theoretical diffraction curve between 4.8Å and about 5.5Å that are not observed in the experimental data is the probable source of the increase in R_{wp}, as these mismatches would have a substantial effect on the quality of fit of the 90.0° data, but no effect at all on R_{wp} for the 168.33° data set.

The geometrical parameters derived from the final structure are more reasonable than those from the previous refinement. In view of the constraints placed on the positions of nine of the fourteen atoms in $(CD_3)_3PbD$, this is not surprising. However, the differences observed in the three Pb–C bond lengths, and in the Pb–C–D bond angles are substantial, and as there is no obvious chemical justification for this, the final structure cannot be regarded as acceptable.

The single largest manifestation of the errors in the structural model derived through the use of rigid bodies is highlighted in the difference curves for both data sets at about 3.2Å. This peak, present to a certain degree throughout all the refinements tried so far, is shown in magnification in Figure 6.8.

The peaks at 3.8–4.0Å, highly mismatched in the previous refinement, are now predicted at appropriate positions, although the match between theoretical and observed intensity is still not entirely acceptable. The peaks at around 3.18Å, however, are misplaced, occurring at a slightly larger d-spacing than is experimentally observed. The indexing of these reflections, as predicted by GSAS, is shown in Table 6.7.

d-spacing/Å	(hkl)
3.110	$12\bar{2}$
3.121	121
3.177	$14\bar{1}$
3.181	140

Table 6.7. Predicted Indexing for Reflections between 3.1Å and 3.2Å

It would appear that the positions of these peaks are affected by the value of the b lattice parameter in a manner similar to those around 3.9Å. In fixing the

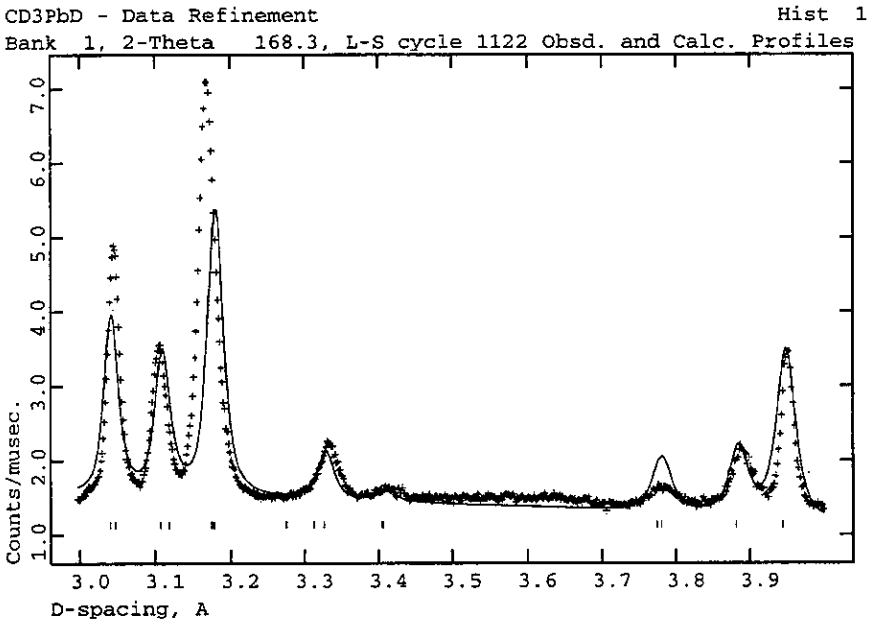

Figure 6.8. Predicted and Observed Diffraction Patterns for $(CD_3)_3PbD$ for d-spacings of 3.6–4.0Å

value of b at a certain value, we have ensured that the overlap between predicted and experimental reflection positions is maximised at 3.9Å, but at the expense of the overlap between theory and experiment at 3.18Å.

There would appear to be no value of the b lattice parameter that gives a satisfactory fit in both regions of the diffractogram. If the value of b is allowed to refine freely using the results of the rigid body refinement as a starting model, it inevitably drops to about 15.46Å, representing the best compromise between the two extremes. In this situation, the peaks at 3.18Å are fitted more satisfactorily, and the mismatch previously eliminated at 3.9Å is reintroduced.

This problem is a fundamental one. Without reliable lattice parameters, structure refinement using the Rietveld technique is not possible, and as seen above, gives implausible results. The problem strongly suggests that a basic assumption of the refinement is incorrect, the effects of this assumption manifesting themselves in the discrepancy between predicted and observed reflection positions.

The assumptions upon which the refinement is based are,

1. The sample is pure $(CD_3)_3PbD$, and is fully deuterated.

2. The data collected do not suffer from artifacts of the experimental process, such as "preferred orientation".

3. The structure of $(CD_3)_3PbD$ as observed by neutron diffraction is not significantly different to that observed by single crystal X-ray diffraction.

Problems due to sample purity and phase contamination can be ruled out by inspection of the experimental diffraction data. The presence of incomplete deuteration is signalled by a intense background due to substantial incoherent scattering by the hydrogens present. This is not observed in either data set.

The presence of other crystalline phases is detected by the observation of reflections not predicted by the structural model. In contrast, the single crystal X-ray model of Me_3PbH accounts for every reflection observed and predicts a few more besides, suggesting that the sample is either very pure, or highly impure. From a synthetic standpoint, the first alternative is the most likely as no signs of decomposition were observed as the sample ampoule was filled and sealed off.

The analysis of powder diffraction patterns assumes that the sample studied contains a large number of crystallites that are oriented randomly with respect to each other. In some cases, the crystallites adopt a "preferred orientation", in which one arrangement is adopted in preference to another. For example, crystals in a plate habit placed on a flat sample holder would tend to orient themselves so as to lie parallel to the holder.

Preferred orientation problems in the sample of $(CD_3)_3PbD$ submitted for neutron diffraction were side stepped in the sample preparation technique, in which $(CD_3)_3PbD$ was condensed straight into the sample holder at -196°C. No annealing step occurred, and no liquid phase was ever present, so no opportunity for the formation of crystallites with preferred orientations was ever presented to the sample. The small crystallite size that resulted from this style of sample preparation is evident in the low resolution of the diffraction data obtained.

It is possible, however, that the data collected by the single crystal and neutron diffraction experiments are inconsistent. The two experiments were performed at different temperatures, with the X-ray data collected at 100 K, and the neutron data at 4 K. It is possible that on cooling from 100 K to 4 K, Me_3PbH underwent a phase change of some kind, the structure of the molecule, or the manner of its packing changing in some way. This sort of change could be responsible for the problems encountered in the choice of lattice parameters for the neutron data set.

A number of structural changes occur on cooling. Rotation of the methyl groups would cease, for example, leaving the methyl deuteria either in the ideal positions shown for the single crystal study, or in a variety of other, semi–staggered orientations. As each methyl group is to some degree independent of the other, a variety of torsional angles around the Pb–C bond could be adopted, resulting in serious disorder of the deuterium positions. Alternatively, only a small distortion could occur, that would be best modelled by doubling one, or a number of the unit cell lengths, and adding a number of independently defined $(CD_3)_3PbD$ molecules to the model.

It is apparent that only a small number of minor structural distortions can be explored using Rietveld refinement, as the technique is not designed to solve unknown structures, but only to provide accurate structural parameters on the

basis of an already well defined model. In the hope that the distortion observed lay merely in the locations of the methyl deuteria, an attempt was made to tackle the problem using the difference Fourier method. The results of this attempt are outlined in the following section.

6.3.4 Refinement using the Difference Fourier Method.

The difference Fourier method is a structure refinement technique that, like Rietveld refinement, takes a model structure of the unit cell under examination, and uses it in combination with experimental diffraction data to derive information about the unit cell contents, and the quality of the model structure in use.[141]

The mechanism used by the difference Fourier method to achieve this is quite different to that used in Rietveld refinement, and is to some extent complementary.

The aim of Rietveld refinement is to determine accurately the crystal structure of the sample being studied. This aim is judged to be met when a theoretical model of the sample, including experimental effects, is created which can be used to calculate the observed experimental diffractogram to high precision.

The first part of this process involves using the model unit cell parameters, and the positions of atoms within to calculate "structure factors", F_{hkl} for the (hkl) range observed by experiment. Once the structure factor of a reflection is known, then its intensity profile can be calculated, and combined with the results of similar calculations for the other reflections, generating a theoretical diffractogram. The process of Rietveld refinement can therefore be reduced to the generation and modification of F_{hkl} until the best fit to experiment is obtained.

The structure factor can be used in an entirely different manner, however, to generate an electron density map of the proposed unit cell by Fourier synthesis,

$$\rho_c(\mathbf{r}) = \frac{1}{V} \sum_{\mathbf{h}} F_{\mathbf{h}}^c e^{-2\pi i \mathbf{h}\cdot\mathbf{r}}$$

in which the electron density, ρ, at point $\mathbf{r}$ in the unit cell is linked to the cell volume, V, and the calculated structure factor, $F_{\mathbf{h}}^c$, summed over every point $\mathbf{h}$ in reciprocal space.

A similar expression applies to $F_{\mathbf{h}}^{o}$, the observed structure factor at $\mathbf{h}$. Unfortunately, $F_{\mathbf{h}}^{o}$ is proportional to the square root of the observed diffraction intensity at $\mathbf{h}$, and so its sign cannot easily be determined. This is the crux of the "phase problem" so often referred to in crystallographic circles.

$F_{\mathbf{h}}^{o}$ is related to the observable quantity $|F_{\mathbf{h}}^{o}|$ by

$$F_{\mathbf{h}}^{o} = |F_{\mathbf{h}}^{o}| e^{i\phi_{\text{true}}}$$

in which ϕ represents the unknown phase. If ϕ were known, then the electron density distribution in the unit cell could be simply determined using the Fourier series shown previously, and structure solution would be a remarkably simple process.

However, although ϕ cannot be easily determined by experiment, it can be calculated using a model of the unit cell if the model is a sufficiently accurate one. The values of ϕ will, for the most part be correct, allowing an electron density calculation to be performed that combines theoretical and experimental information to best effect.

If this electron density is then subtracted from that produced solely using the theoretical model, any residual differences will correspond to defects in the theoretical model used,

$$\Delta\rho(\mathbf{r}) = \rho_o(\mathbf{r}) - \rho_c(\mathbf{r}) = \frac{1}{V}\sum_{\mathbf{h}}(F_{\mathbf{h}}^{o} - F_{\mathbf{h}}^{c})\, e^{-2\pi i \mathbf{h}\cdot\mathbf{r}}$$

Thus, peaks in $\Delta\rho$ will correspond to atoms missing in the structural model, and other fluctuations to atoms misplaced, or with incorrect thermal parameters, for example.

The effectiveness of the technique is determined by the quality of the theoretical model used. If this is wildly inaccurate then the phases predicted by it will be incorrect, and the resulting difference map will be of no use in the refinement process.

The Application of the Difference Fourier Method to the Refinement of the Solid State Structure of $(CD_3)_3PbD$.

The difference Fourier method was applied to the Rietveld refinement of the structure of $(CD_3)_3PbD$ by combining the single crystal information derived from the X-ray structure of Me_3PbH with the neutron diffraction data of $(CD_3)_3PbD$.

Difference electron density maps were calculated using the GSAS package, using the heavy atom positions from the single crystal structure as the theoretical model. The positions at which the twenty most intense peaks in the map were observed were then combined in a single file with the heavy atom positions and viewed using XP.[142]

The distances between the peaks in the difference map and the carbon atoms were then calculated, as were the angles formed between the peaks, carbon, and lead. If the results of the calculation for a single peak corresponded to a roughly tetrahedral angle, and a bond length of between 0.84Å and 1.10Å, the peak was judged to correspond to a methyl deuterium, and its position recorded as such in the GSAS model.

The process was then repeated, using the lead and carbon positions, and the newly found deuterium positions in the GSAS model, in an attempt to determine the positions of the remaining methyl deuterium atoms, and that of the deuterium bound to lead, until either a complete model was determined, or no further peaks in the difference map could reasonably be undiscovered deuterium atoms.

The results of this search, which finished without determining satisfactorily the methyl groups of $(CD_3)_3PbD$, are displayed in Table 6.8, and Figures 6.9, and 6.10.

Although the angles formed between deuterium, carbon, and lead are acceptably tetrahedral, and the D–C bond lengths derived are not atypical, the D–C–D angles are not consistent with a tetrahedral geometry about the methyl carbons. The diffractograms also display the features alluded to in earlier sections that suggest problems with the refinement. The misfits at 3.1Å, and the predicted, but unobserved peaks at 4.5–5.8Å all indicate a substantial problem with the theoretical model used.

The application of the difference Fourier method to the refinement of the

a = 6.209Å, b = 15.53Å, β = 116.66°, c = 6.828Å					
Pb–C1	2.230Å	Pb–C2	2.202Å	Pb–C3	2.182Å
D11-C1	0.88Å	D21–C2	0.85Å	D31–C3	0.91Å
D12-C1	0.84Å			D32–C3	0.88Å
D11–C1–Pb	107.2°	D21–C2–Pb	107.1°	D31–C3–Pb	108.6°
D12–C1–Pb	107.3°			D32–C3–Pb	116.1°
D11–C1–D12	131.7°			D31–C3–D32	128.6°

Table 6.8. The Geometry of $(CD_3)_3PbD$ using the Difference Fourier Method.

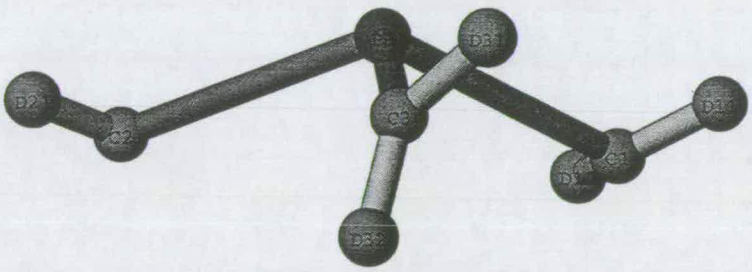

Figure 6.9. The Structure of $(CD_3)_3PbD$ using the Difference Fourier Method.

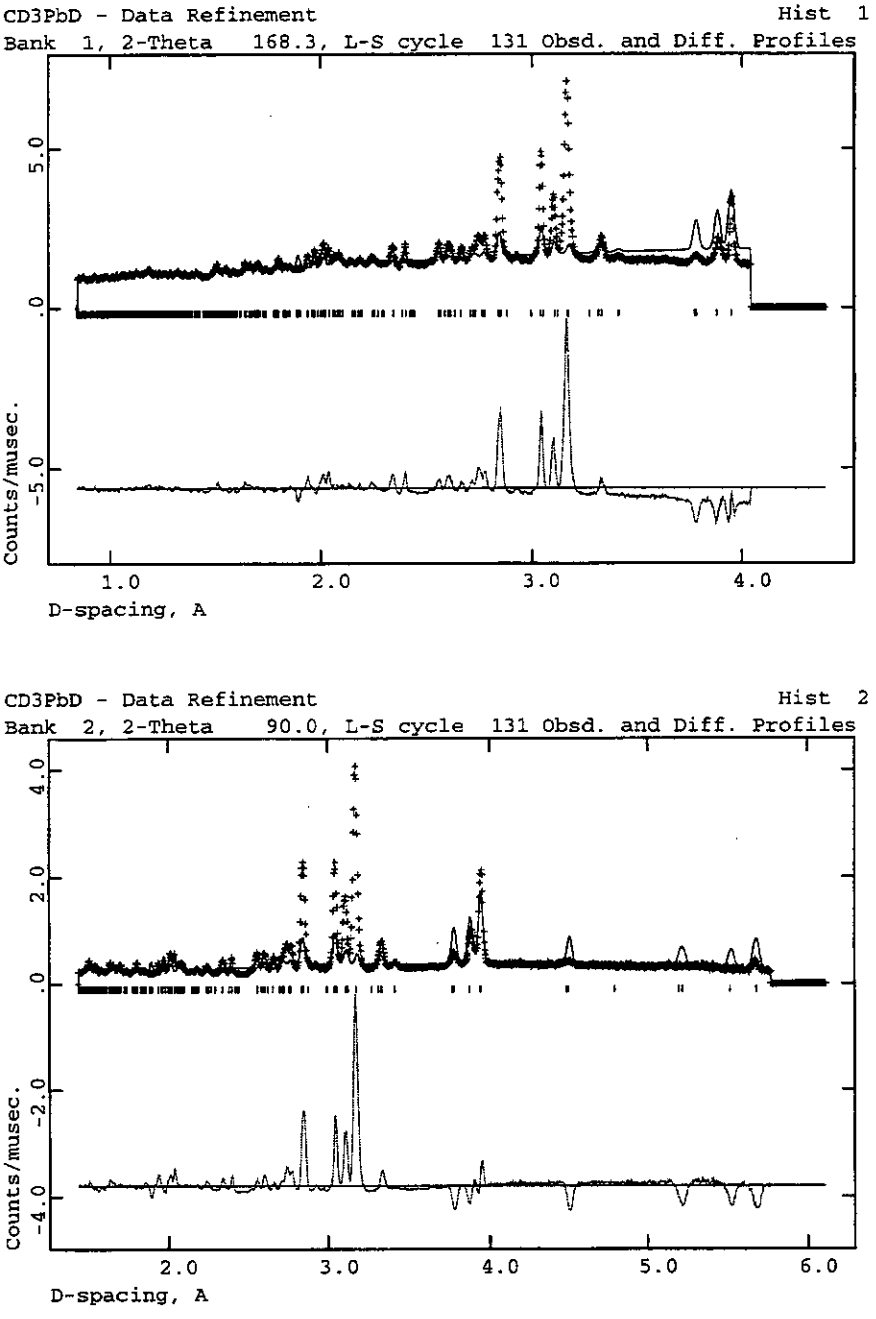

Figure 6.10. Predicted and Observed Diffractograms for the Rietveld Refinement of $(CD_3)_3PbD$, using the Difference Fourier Method.

structure of $(CD_3)_3PbD$ was as unsuccessful as the other approaches mentioned previously. This suggests that the reasons for the failure of the refinement lie not with the methods used, or their application, but with the experimental data collected.

It would appear that the neutron diffraction data collected at 4 K, and the X-ray single crystal data collected at 100 K are substantially inconsistent. As the consistency of the two data sets was one of the fundamental assumptions of the style of refinement undertaken, it is not surprising that the refinement failed.

6.3.5 Summary, and Suggestions for Further Work.

1. $(CD_3)_3PbD$ was synthesised according to a published method, and submitted for powder neutron diffraction on the high resolution powder diffractometer at the ISIS facility in Oxfordshire.

2. Various attempts at the determination of the structure of $(CD_3)_3PbD$ in the solid state, and thereby the length of the Pb–D bond, were made using the neutron diffraction data collected. These attempts were based on the Rietveld method of structure refinement, using the GSAS software package, and a single crystal X-ray structure of Me_3PbH as a starting model.

3. None of these attempts was successful owing to structural inconsistencies between the neutron diffraction data, and the single crystal X-ray model.

4. These inconsistencies were ascribed to a structural phase change presumed to occur on cooling from the temperature of the X-ray experiment (100 K) to that of the neutron experiment (4 K).

5. It is suggested that the neutron diffraction experiment be repeated at 100 K to generate experimental data consistent with the single crystal X-ray structure and therefore suitable for Rietveld refinement.

6.4 The Gas Phase Structure of Me_3PbH.

The sum total of structural knowledge concerning trimethyllead hydride until very recently consisted of a single NMR study,[40] and the assignment of the Pb–H stretching mode in its infra-red spectrum.[37]

The determination of the single crystal X-ray structure of Me_3PbH by Fleischer *et al.*[137] added significantly to the body of knowledge concerning the molecule in the solid state, and his NMR, and infra-red studies determined unequivocally the connectivity of the molecule in solution, and in the solid and gas phases.[143]

However, the detailed structure of Me_3PbH in the gas phase, and in particular the length of the Pb–H bond, remained unknown. An attempt was therefore made to determine the structure of Me_3PbH in the gas phase by electron diffraction. The results of this attempt are detailed in the remainder of this chapter.

6.4.1 Experimental

Two samples of Me_3PbH were prepared for analysis by GED using the preparative methods described in Section 6.2.2. After preparation, the samples were distilled into the all-glass ampoules shown in Figure 6.11, which were then carefully sealed off using a hand torch.

The ampoules of Me_3PbH were stored in liquid nitrogen, and transported to the University of Reading for analysis on the GED apparatus in the Chemistry Department[144] by Prof. David Rice and Dr. Elizabeth Page.

Three plates were recorded at a camera distance of 243.65 mm using an electron wavelength of 0.058778 Å (determined by calibration against diffraction patterns of benzene[145]), and a sample temperature of -19 to -23°C. A uniform darkening was observed on each plate, but no visible scattering pattern was noted. The plates were then traced on the Agfa Arcus II scanner of the Department of Chemistry, University of Oslo,[146] and one trace, although very faint, was judged to be suitable for inclusion in the subsequent refinement.

In a previous experiment, three plates had been recorded using a sample prepared by Dr. Holger Fleischer and held at -23 to -24°C, with a nozzle to plate distance of 494.50 mm, and an electron wavelength of 0.058703 Å. These were analysed in a similar fashion, and two of the resulting traces were judged suitable

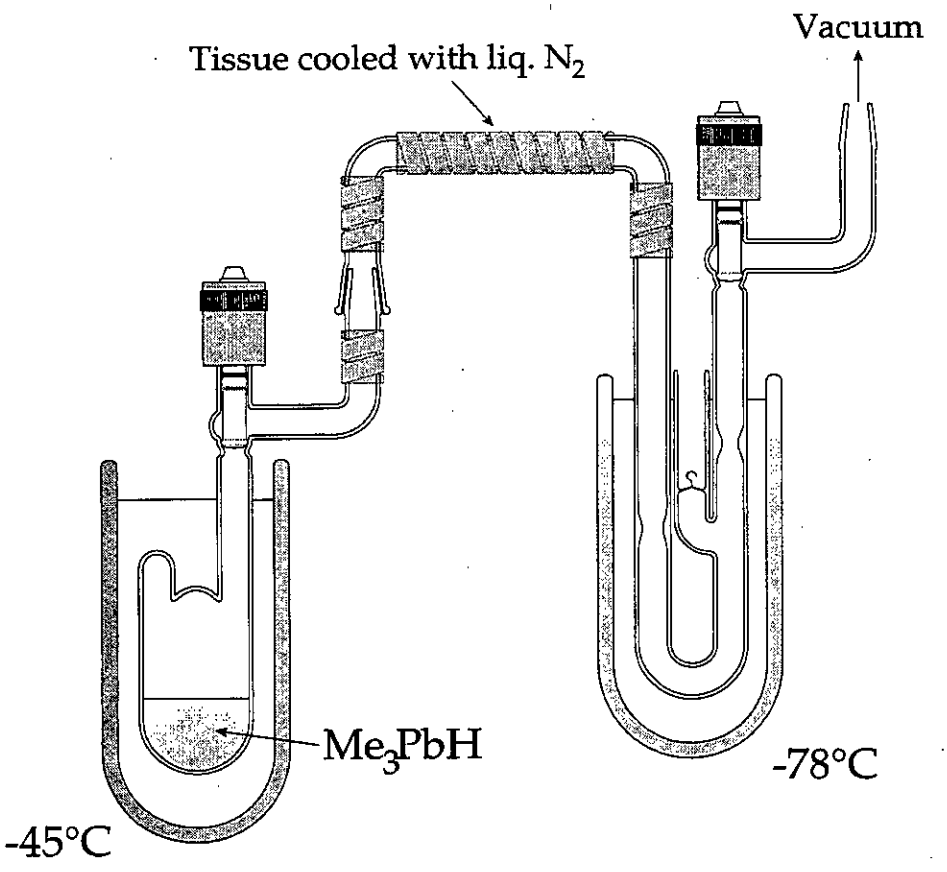

Figure 6.11. Apparatus for the Distillation of Me_3PbH into an All-Glass Ampoule suitable for GED.

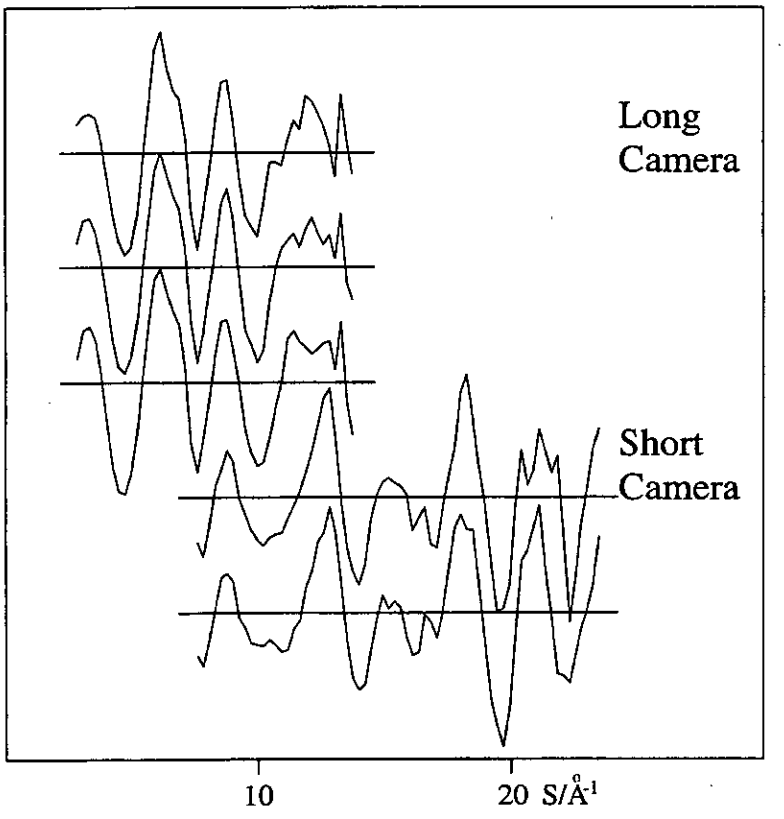

Figure 6.12. Experimental Molecular Scattering Curves for Me_3PbH

for inclusion in the refinement. A set of five plates was also recorded at that time using a nozzle to plate distance of 244.43 mm, but the resulting images were partially obscured by a shadow cast by a screen close to the nozzle, and so were excluded from the refinement.

The experimental molecular scattering curves for the plates collected at long and short camera distances are shown in Figure 6.12. Least squares refinements[147] were performed at the University of Reading by Drs. Elizabeth Page and Kirsten Aarset, using a molecular model of C_{3v} symmetry.

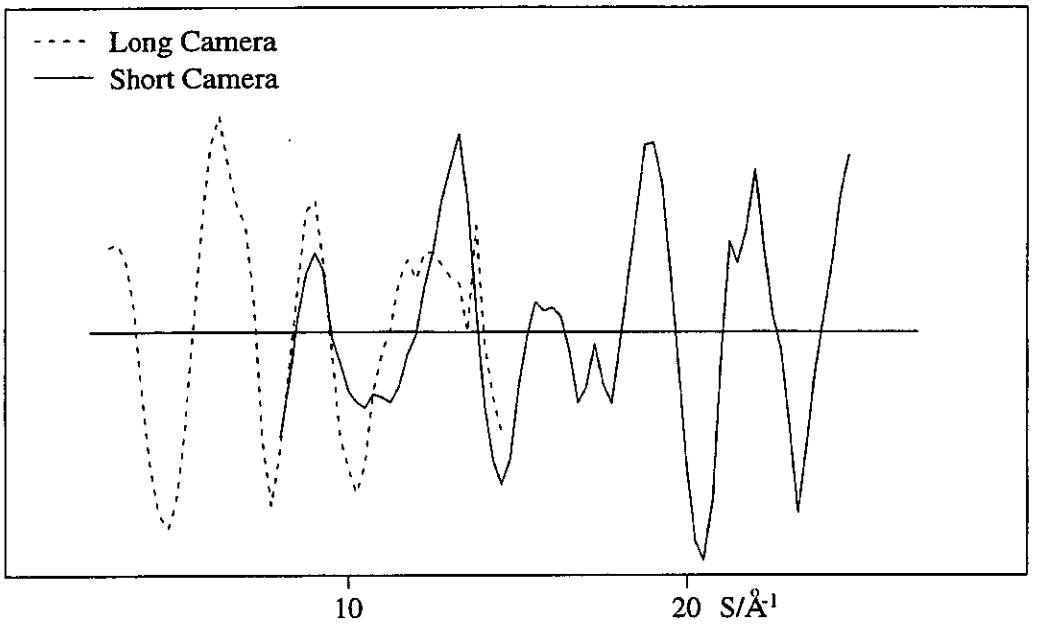

Figure 6.13. Overlapping Molecular Scattering Curves for Me_3PbH

6.4.2 Data Analysis

The analysis of a combination of short and long camera distance data was complicated by difficulties arising from the manner in which the two data sets were combined. The method chosen had a substantial impact on the Pb–H distance and the angles H–Pb–C and Pb–C–H derived from subsequent refinements, giving, for example, a Pb–H distance that varied between 1.73 and 1.85 Å, with an associated uncertainty of 0.20 Å. The Pb–C distance could be refined to an almost constant value, however, and was independent of the range of data chosen. The data from long and short camera distances are shown together in Figure 6.13.

The source of the problem encountered may lie in the low scattering intensity observed in the short camera distance experiment, or in the temperature at which the sample of Me_3PbH was held while electron diffraction was in progress. The similarities between the two short camera distance data sets shown in Figure 6.12 suggest that the scattering observed was real, and not an artifact of the measuring process. However, the proximity of the plate to the sample inlet, coupled

with the increased exposure time used at the short camera distance, may have resulted in significant reaction of Me_3PbH with the plate surface producing the uniform darkening observed at the time of the experiment. Exposure of photographic plates by chemical reduction has been observed previously during the determination of the gas phase structure of digallane by electron diffraction.[77] Darkening by this means reduces the accuracy with which a diffraction pattern can be recorded by limiting the dynamic range of the photographic plate.

If the temperature at which the sample was held was fractionally too high, some decomposition may have occurred as the sample moved through the cooled inlet system to the diffraction chamber, producing sufficient tetramethyllead to impact upon the resulting diffraction pattern. No corresponding lead deposits were observed in the inlet system, however, suggesting that if decomposition did occur, then it must have been to a very limited extent.

The temperature at which the sample is held in an electron diffraction experiment is chosen to maximise electron scattering, while keeping sample decomposition to a minimum. This is especially important when a small nozzle to plate distance is used, as it is at this distance that high angle, low intensity molecular scattering is recorded. The plate exposure times are longer, and sample vapour pressures higher than those used for a long camera distance experiment to ensure that the resultant scattering patterns are sufficiently intense. However, these conditions also maximise the degree to which chemical attack at the plate surface can occur.

For a thermally fragile, and highly reactive species such as Me_3PbH, the sample temperature chosen must provide a balance between the need to maximise molecular scattering intensity whilst keeping sample decomposition, and fogging effects to a minimum. In this case, the short camera distance experiment differed from that at the long camera distance through the use of a plate exposure time increased from two to four minutes, and a sample temperature raised by 2–4°C.

An accurate structural determination of Me_3PbH can only be performed in this way if reliable short camera distance data are available for use in the refinement. A third experimental attempt at recording these data is therefore required, using a sample temperature not greater than -23°C, and an exposure time substantially longer than the four minutes tried here. The Pb–H bond length in

Me_3PbH will only be established in the gas phase once this attempt reaches a successful conclusion.

Appendix A

Crystal Structure Refinements

A.1 Trimethylphosphonium methylid

Data collection, structure solution and refinement were performed by Dr. Simon Parsons from a single crystal grown *in situ* from a sample prepared by the author.

Table A.1. Crystal Data

Empirical formula	C4 H11 P1
	CH2=PMe3
Formula weight	90.10
Wavelength	0.71073 A
Temperature	120 K
Crystal system	Monoclinic
Space group	P21/m
Unit cell dimensions	a = 6.086(1) Å alpha = 90 deg.
	b = 7.615(2) Å beta = 92.55(2) deg.
	c = 6.457(2) Å gamma = 90 deg.
Volume	298.96 $Å^3$
Number of reflections for cell	46 (15 < theta < 17 deg.)
Z	2.00
Density (calculated)	1.00 Mg/m^3
Absorption coefficient	0.30 mm^{-1}
F(000)	100.19

Table A.2. Data Collection

Crystal description	Colourless cylinder developed in [001]
Crystal size	0.60 x 0.16 x 0.16 mm
Theta range for data collection	2.67 to 27.55 deg.
Index ranges	-7<=h<=7, -9<=k<=9, -8<=l<=8
Reflections collected	2957
Independent reflections	739 [R(int) = 0.04]
Scan type	Omega-theta with learnt-profile (Clegg)

Table A.3. Solution and Refinement

Solution	Direct Methods (SIR92)
Refinement type	Full-matrix least-squares on F
Program used for refinement	CRYSTALS version 10
Hydrogen atom placement	Difference map
Hydrogen atom treatment	Refined freely
Data / parameters	651/55
Goodness-of-fit on F^2	1.1168
R	0.0297
Rw	0.0324
Observed criterion	>2.00sigma(I)
Final maximum delta/sigma	0.013204
Weighting scheme	Chebychev 3-term polynomial
Largest diff. peak and hole	0.39 and -0.21 e.$A^{-}3$

Table A.4. Atomic coordinates (x10^4), equivalent isotropic displacement parameters (A^2 x 10^3) and site occupancies for Me_3PCH_2. U(eq) is defined as one third of the trace of the orthogonalized Uij tensor.

	x	y	z	U(eq)	Occ
P1	8546(1)	2500	1871(1)	21	1.00
C2	11306(3)	2500	1997(3)	29	1.00
H3	11830(4)	2500	3350(5)	48(8)	1.00
H4	11870(6)	1940(4)	1260(5)	40(1)	0.50
C5	7517(3)	2500	-771(3)	32	1.00
H6	8000(3)	1540(2)	-1480(3)	46(5)	1.00
H7	5940(5)	2500	-860(4)	40(7)	1.00
C9	7253(2)	643(2)	3064(2)	36	1.00
H10	7660(3)	-360(3)	2320(3)	38(4)	1.00
H11	5620(4)	760(3)	2980(3)	51(5)	1.00
H12	7700(3)	570(3)	4470(3)	51(5)	1.00

Table A.5. Anisotropic displacement parameters (A^2 x 10^3) for Me_3PCH_2. The anisotropic displacement factor exponent takes the form: $-2\pi^2[h^2a^{*2}U_{11} + \ldots + 2hka^*b^*U_{12}]$

	U11	U22	U33	U23	U13	U12
P1	19(1)	22(1)	23(1)	0	1(1)	0
C2	20(1)	36(1)	30(1)	0	2(1)	0
C5	34(1)	35(1)	27(1)	0	-3(1)	0
C9	32(1)	34(1)	43(1)	11(1)	6(1)	-3(1)

Table A.6. Bond lengths [Å] and angles [°] for Me_3PCH_2. Symmetry transformations used to generate equivalent atoms: #1 x,-y+1/2,z

P1-C2	1.678(2)	P1-C5	1.791(2)
P1-C9	1.808(1)	P1-C9#1	1.808(1)
C2-H3	0.92(3)	C2-H4	0.74(3)
C2-H4#1	0.74(3)	C5-H6	0.92(2)
C5-H6#1	0.92(2)	C5-H7	0.96(3)
C9-H10	0.94(2)	C9-H11	1.00(2)
C9-H12	0.94(2)	C2-P1-C5	110.7(1)
C2-P1-C9	115.69(6)	C5-P1-C9	105.40(7)
C2-P1-C9#1	115.69(6)	C5-P1-C9#1	105.40(7)
C9-P1-C9#1	102.9(1)	P1-C2-H3	110.5(17)
P1-C2-H4	118(3)	H3-C2-H4	118(3)
P1-C2-H4#1	118(3)	H3-C2-H4#1	118(3)
H4-C2-H4#1	71(5)	P1-C5-H6	111.7(12)
P1-C5-H6#1	111.7(12)	H6-C5-H6#1	105(2)
P1-C5-H7	111.2(16)	H6-C5-H7	108.3(15)
H6#1-C5-H7	108.3(15)	P1-C9-H10	106.6(11)
P1-C9-H11	110.9(12)	H10-C9-H11	109.2(16)
P1-C9-H12	110.3(13)	H10-C9-H12	112.3(17)
H11-C9-H12	107.7(18)		

A.2 Dimethylstannane

Data collection, structure solution and refinement were performed by Dr. Simon Parsons from a single crystal grown *in situ* from a sample prepared by the author.

Table A.7. Crystal Data

Empirical formula	C2 H8 Sn
Formula weight	150.77
Wavelength	0.71073 Å
Temperature	100(2) K
Crystal system	Triclinic
Space group	P -1
Unit cell dimensions	a = 6.1460(12) Å alpha = 102.68(3) deg.
	b = 6.4270(13) Å beta = 92.40(3) deg.
	c = 6.8310(14) Å gamma = 107.79(3) deg.
Volume	248.93(9) $Å^3$
Z	2
Density (calculated)	2.012 Mg/m^3
Absorption coefficient	4.932 mm^{-1}
F(000)	140

Table A.8. Data Collection

Crystal description	Colourless cylinder
Crystal size	0.23 x 0.19 x 0.19 mm
Theta range for data collection	3.08 to 27.50 deg.
Index ranges	-7<=h<=7, -8<=k<=8, -8<=l<=8
Reflections collected	2772
Independent reflections	1139 [R(int) = 0.0267]
Scan type	omega-theta

Table A.9. Solution and Refinement

Data / restraints / parameters	1139/1/39 (Full-matrix least-squares on F^2)
Goodness-of-fit on F^2	1.064
Conventional R [F>4sigma(F)]	R1 = 0.0249 [1075 data]
R indices (all data)	R1 = 0.0268, wR2 = 0.0720
Extinction coefficient	0.028(4)
Final maximum delta/sigma	0.003
Weighting scheme	calc $w=1/[s^2F_O{}^2+(0.0486P)^2+0.3553P]$ where $P=(F_O{}^2+2F_C{}^2)/3$
Largest diff. peak and hole	1.176 and -1.226 e.$Å^{-3}$

Table A.10. Atomic coordinates (x10^4), and equivalent isotropic displacement parameters (A^2 x 10^3) for Me_2SnH_2 U(eq) is defined as one third of the trace of the orthogonalized Uij tensor.

	x	y	z	U(eq)
Sn(1)	734(1)	2105(1)	2988(1)	25(1)
C(1)	-2900(7)	1479(8)	2709(8)	33(1)
C(2)	2486(8)	4782(9)	1659(8)	35(1)

Table A.11. Anisotropic displacement parameters (A^2 x 10^3) for Me_2SnH_2. The anisotropic displacement factor exponent takes the form: $-2\pi^2[h^2a^{*2}U_{11}+\ldots+2hka^*b^*U_{12}]$

	U11	U22	U33	U23	U13	U12
Sn(1)	21(1)	27(1)	29(1)	12(1)	3(1)	7(1)
C(1)	27(2)	31(2)	39(2)	6(2)	6(2)	8(2)
C(2)	28(2)	38(3)	43(3)	23(2)	9(2)	8(2)

Table A.12. Bond lengths [Å] and angles [°] for Me_2SnH_2.

Sn(1)-C(1)	2.138(4)
Sn(1)-C(2)	2.140(4)
Sn(1)-H(1)	1.63(5)
Sn(1)-H(2)	1.62(5)
C(1)-H(1A)	0.98
C(1)-H(1B)	0.98
C(1)-H(1C)	0.98
C(2)-H(2A)	0.98
C(2)-H(2B)	0.98
C(2)-H(2C)	0.98
C(1)-Sn(1)-C(2)	111.8(2)
C(1)-Sn(1)-H(1)	112(2)
C(2)-Sn(1)-H(1)	108(2)
C(1)-Sn(1)-H(2)	109(2)
C(2)-Sn(1)-H(2)	107(2)
H(1)-Sn(1)-H(2)	109(3)
Sn(1)-C(1)-H(1A)	109.47(14)
Sn(1)-C(1)-H(1B)	109.47(13)
H(1A)-C(1)-H(1B)	109.5
Sn(1)-C(1)-H(1C)	109.47(14)
H(1A)-C(1)-H(1C)	109.5
H(1B)-C(1)-H(1C)	109.5
Sn(1)-C(2)-H(2A)	109.47(15)
Sn(1)-C(2)-H(2B)	109.47(13)
H(2A)-C(2)-H(2B)	109.5
Sn(1)-C(2)-H(2C)	109.47(14)
H(2A)-C(2)-H(2C)	109.5
H(2B)-C(2)-H(2C)	109.5

Table A.13. Hydrogen coordinates (x10^4) and isotropic displacement parameters (Å^2 x 10^3) for Me_2SnH_2.

	x	y	z	U(eq)
H(1A)	-3333(12)	2188(58)	3987(21)	50
H(1B)	-3700(7)	-150(8)	2381(61)	50
H(1C)	-3334(12)	2110(60)	1630(42)	50
H(2A)	2244(60)	4240(22)	184(8)	52
H(2B)	4136(12)	5294(49)	2123(51)	52
H(2C)	1881(51)	6038(29)	2061(52)	52
H(1)	1373(106)	-120(93)	1917(96)	47(17)
H(2)	1722(112)	2852(114)	5368(77)	51(18)

A.3 Trimethylstannane

Data collection, structure solution and refinement were performed by Dr. Simon Parsons from a single crystal grown *in situ* from a sample prepared by the author.

Table A.14. Crystal Data

Empirical formula	C3 H10 Sn
Formula weight	164.80
Wavelength	0.71073 Å
Temperature	100(2) K
Crystal system	Triclinic twin
Space group	P -1
Unit cell dimensions	a = 6.2620(13) Å alpha = 67.41(3) deg.
	b = 6.8220(14) Å beta = 80.92(3) deg.
	c = 8.640(2) Å gamma = 62.62(3) deg.
Volume	302.52(11) $Å^3$
Z	2
Density (calculated)	1.809 Mg/m^3
Absorption coefficient	4.066 mm^{-1}
F(000)	156

Table A.15. Data Collection

Crystal description	Colourless needle
Crystal size	? x ? x ? mm
Theta range for data collection	2.55 to 24.98 deg.
Index ranges	-7<=h<=7, -8<=k<=8, -10<=l<=10
Reflections collected	2367
Independent reflections	2367 [R(int) = 0.0000]
Scan type	omega-theta

Table A.16. Solution and Refinement

Absorption correction	Psi-scans (Tmin= 0.277, Tmax=0.309)
Data / restraints / parameters	2349/0/41 (Full-matrix least-squares on F^2)
Goodness-of-fit on F^2	1.106
Conventional R [F>4sigma(F)]	R1 = 0.0556 [1997 data]
R indices (all data)	R1 = 0.0724, wR2 = 0.1516
Final maximum delta/sigma	0.003
Weighting scheme	calc w=1/[$s^2{F_O}^2$+(0.0122P)^2+8.3696P] where P=($F_O{}^2$+2$F_C{}^2$)/3
Largest diff. peak and hole	1.668 and -1.510 e.Å^{-3}

Table A.17. Atomic coordinates (x10^4), and equivalent isotropic displacement parameters (A^2 x 10^3) for Me_3SnH. U(eq) is defined as one third of the trace of the orthogonalized Uij tensor.

	x	y	z	U(eq)
Sn(1)	1417(1)	1491(1)	1934(1)	24(1)
C(1)	-2051(18)	1687(19)	1732(14)	38(2)
C(2)	3948(18)	-2117(16)	3068(15)	39(3)
C(3)	1197(20)	3441(21)	3431(16)	44(3)

Table A.18. Anisotropic displacement parameters (A^2 x 10^3) for Me_3SnH. The anisotropic displacement factor exponent takes the form: $-2\pi^2[h^2a^{*2}U_{11} + \ldots + 2hka^*b^*U_{12}]$

	U11	U22	U33	U23	U13	U12
Sn(1)	21(1)	25(1)	27(1)	-10(1)	-2(1)	-10(1)
C(1)	39(6)	25(5)	57(7)	-22(5)	-10(5)	-9(5)
C(2)	29(5)	21(5)	52(7)	-4(5)	-4(5)	-5(4)
C(3)	36(6)	48(7)	60(7)	-35(6)	0(5)	-17(5)

Table A.19. Bond lengths [Å] and angles [°] for Me_3SnH.

Sn(1)-C(3)	2.134(11)
Sn(1)-C(2)	2.140(10)
Sn(1)-C(1)	2.145(10)
C(3)-Sn(1)-C(2)	109.4(5)
C(3)-Sn(1)-C(1)	109.8(4)
C(2)-Sn(1)-C(1)	109.7(4)

Table A.20. Hydrogen coordinates (x10^4) and isotropic displacement parameters (Å^2 x 10^3) for Me_3SnH.

	x	y	z	U(eq)
H(1)	2321(1)	2623(1)	45(1)	49
H(1A)	-1892(27)	581(101)	1211(90)	57
H(1B)	-3131(44)	3296(39)	1041(81)	57
H(1C)	-2715(63)	1273(133)	2853(16)	57
H(2A)	4091(97)	-3001(32)	2361(47)	59
H(2C)	5520(38)	-2195(18)	3184(84)	59
H(3A)	278(113)	5133(22)	2815(40)	65
H(3B)	2821(20)	3120(102)	3687(79)	65
H(3C)	389(121)	2965(96)	4478(43)	65

A.4 Me_3PbH

This refinement was performed by Dr. Simon Parsons using data collected from a single crystal grown *in situ* from a sample prepared by Dr. Holger Fleischer.

Table A.21. Crystal Data

Empirical formula	C3 H10 Pb
Formula weight	253.30
Wavelength	0.71073 Å
Temperature	105(2) K
Crystal system	Monoclinic
Space group	P2(1)/n
Unit cell dimensions	a = 6.287(3) Å alpha = 90 deg.
	b = 15.859(10) Å beta = 115.96(4) deg.
	c = 6.850(3) Å gamma = 90 deg.
Volume	614.1(6) $Å^3$
Z	4
Density (calculated)	2.740 Mg/m^3
Absorption coefficient	27.320 $mm^{-}1$
F(000)	440

Table A.22. Data Collection

Crystal description	Colourless column
Crystal size	0.21 x 0.12 x 0.12 mm
Theta range for data collection	2.57 to 27.49 deg.
Index ranges	-8<=h<=7, 0<=k<=22, 0<=l<=9
Reflections collected	1629
Independent reflections	1403 [R(int) = 0.0270]
Scan type	omega-theta

Table A.23. Solution and Refinement

Data / restraints / parameters	1402/0/37 (Full-matrix least-squares on F^2)
Goodness-of-fit on F^2	1.044
Conventional R [F>4sigma(F)]	R1 = 0.0478 [1013 data]
R indices (all data)	R1 = 0.0761, wR2 = 0.1331
Final maximum delta/sigma	0.000
Weighting scheme	calc $w=1/[s^2F_O{}^2+(0.0796P)^2+0.2764P]$ where $P=(F_O{}^2+2F_C{}^2)/3$
Largest diff. peak and hole	1.232 and -1.560 e.Å^{-3}

Table A.24. U(eq) is defined as one third of the trace of the orthogonalized Uij tensor. Atomic coordinates (x10^4), equivalent isotropic displacement parameters (Å^2 x 10^3) and site occupancies for Me_3PbH. U(eq) is defined as one third of the trace of the orthogonalized Uij tensor.

	x	y	z	U(eq)
Pb	1353(1)	8459(1)	4970(1)	40(1)
C(1)	-2216(31)	8381(13)	5003(33)	55(5)
C(2)	995(31)	9097(14)	1959(29)	55(5)
C(3)	3864(27)	9192(15)	7806(30)	55(5)

Table A.25. Bond lengths [Å] and angles [°] for Me_3PbH

Pb-C(2)	2.22(2)
Pb-C(3)	2.22(2)
Pb-C(1)	2.26(2)
C(2)-Pb-C(3)	108.6(7)
C(2)-Pb-C(1)	109.7(7)
C(3)-Pb-C(1)	110.5(7)

Table A.26. Anisotropic displacement parameters (Å^2 x 10^3) for Me_3PbH. The anisotropic displacement factor exponent takes the form: $-2\pi^2[h^2a^{*2}U_{11} + \ldots + 2hka^*b^*U_{12}]$

	U11	U22	U33	U23	U13	U12
Pb	41(1)	40(1)	40(1)	1(1)	17(1)	-1(1)
C(1)	41(8)	66(12)	64(10)	-9(10)	27(8)	-22(9)
C(2)	47(9)	64(12)	54(10)	22(9)	24(8)	-6(9)
C(3)	32(8)	78(14)	56(10)	-16(10)	19(7)	-3(8)

Table A.27. Hydrogen coordinates (x10^4) and isotropic displacement parameters (Å^2 x 10^3) for Me_3PbH.

	x	y	z	U(eq)
H	2464(1)	7441(1)	5064(1)	50
H(1A)	-2050(31)	8099(13)	6335(33)	82
H(1B)	-3306(31)	8059(13)	3739(33)	82
H(1C)	-2843(31)	8951(13)	4949(33)	82
H(2A)	-110(31)	8780(14)	693(29)	82
H(2B)	2544(31)	9122(14)	1942(29)	82
H(2C)	393(31)	9670(14)	1913(29)	82
H(3A)	4039(27)	8917(15)	9150(30)	83
H(3B)	3256(27)	9765(15)	7746(30)	83
H(3C)	5406(27)	9217(15)	7775(30)	83

References

1. F. Paneth and K. Fürth *Ber.* **52B,** 2020–2029 (1919).

2. F. Paneth and E. Rabinowitsch *Ber.* **57B,** 1877–1890 (1924).

3. F. Paneth, W. Haken, and E. Rabinowitsch *Ber.* **57B,** 1891–1903 (1924).

4. W. H. Organisation *Tin and Organotin compounds : a preliminary review;* volume 15 of *Environmental health criteria* WHO: Geneva, 1980.

5. A. G. Davies and P. J. Smith "Tin". In *Comprehensive Organometallic Chemistry,* Vol. 2; G. I. Wilkinson, F. G. A. Stone, and E. W. Abel, Eds.; Pergamon: Oxford, 1982.

6. A. G. Davies "Tin". In *Comprehensive Organometallic Chemistry II : a review of the literature 1982–1994,* Vol. 2; E. W. Abel, F. G. Stone, and G. Wilkinson, Eds.; Pergamon: Oxford, 1995.

7. A. E. Finholt, A. C. Bond, Jr., K. E. Wilzbach, and H. I. Schlesinger *J. Am. Chem. Soc.* **69,** 2692–2696 (1947).

8. A. E. Finholt, A. C. Bond, and H. I. Schlesinger *J. Am. Chem. Soc.* **69,** 1199 (1947).

9. A. D. Norman, J. R. Webster, and W. L. Jolly *Inorganic Syntheses* **XI,** 170–181 (1968).

10. D. R. Lide, Ed.; *CRC Handbook of Chemistry and Physics;* CRC Press: Boca Raton, 74th ed.; 1994.

11. K. Tamaru *J. Phys. Chem.* **60,** 610–612 (1956).

12. G. W. Schaeffer and M. Emilius *J. Am. Chem. Soc.* **76,** 1203 (1954).

13. D. J. Aaserud and F. W. Lampe *J. Phys. Chem.* **101,** 4114–4116 (1997).

14. S. Masamune, L. R. Sita, and D. J. Williams *J. Am. Chem. Soc.* **105,** 630 (1983).

15. W. V. Farrar and H. A. Skinner *J. Organometal. Chem.* **1,** 434 (1964).

16. V. K. Belsky, N. N. Zemlyansky, N. D. Kolosova, and I. V. Borisova *J. Organometal. Chem.* **215,** 41 (1981).

17. M. F. Lappert, W. P. Leung, C. L. Raston, A. J. Thorne, B. W. Skelton, and A. W. White *J. Organometal. Chem.* **233,** C28 (1982).

18. H. Puff, C. Bach, W. Schuh, and R. Zinnmer *J. Organometal. Chem.* **312,** 313 (1986).

19. H. Puff, C. Bach, H. Reuter, and W. Schuh *J. Organometal. Chem.* **277,** 17 (1984).

20. S. Adams and M. Dräger *J. Organometal. Chem.* **288,** 295–304 (1985).

21. S. Adams and M. Dräger *Angew. Chem. Int. Ed. Engl.* **26,** 1255–1256 (1987).

22. L. R. Sita and R. D. Bickerstaff *J. Am. Chem. Soc.* **111,** 6454 (1989).

23. L. R. Sita and I. Kinoshita *J. Am. Chem. Soc.* **114,** 7024–7029 (1992).

24. P. Edwards and J. D. Corbett *Inorg. Chem.* **16,** 903–907 (1977).

25. J. D. Corbett and P. E. Edwards *J. Am. Chem. Soc.* **99,** 3313–3317 (1977).

26. C. A. Kraus and W. N. Greer *J. Am. Chem. Soc.* **44,** 2629–2632 (1922).

27. C. A. Kraus and W. N. Greer *J. Am. Chem. Soc.* **47,** 2568 (1925).

28. S. F. A. Kettle *J. Chem. Soc.* 2938–2941 (1959).

29. S. Masamune and L. R. Sita *J. Am. Chem. Soc.* **105,** 630 (1985).

30. C. A. Kraus and W. V. Sessions *J. Am. Chem. Soc.* **47,** 2361–2368 (1925).

31. B. Beagley, K. McAloon, and J. M. Freeman *Acta. Cryst.* **B30,** 444–449 (1974).

32. D. R. Lide *J. Chem. Phys.* **19,** 1605–1606 (1951).

33. T. Birchall and J. A. Vetrone *J. Chem. Soc., Chem. Comm.* 877 (1988).

34. D. Reed, D. Stalke, and D. S. Wright *Angew. Chem. Int. Ed. Engl.* **30,** 1459 (1991).

35. K. Kobayashi, M. Kawanisi, S. Kozima, T. Hitomi, H. Iwamura, and T. Sugawara *J. Organometal. Chem.* **217,** 315 (1981).

36. K. Kobayashi, M. Kawanisi, T. Hitomi, and S. Kozima *J. Organometal. Chem.* **233,** 299–311 (1982).

37. E. Amberger *Angew. Chem.* **72,** 494 (1960).

38. R. Duffy and A. K. Holliday *Proc. Chem. Soc.* 124 (1959).

39. W. E. Becker and S. E. Cook *J. Am. Chem. Soc.* **82,** 6264–6265 (1960).

40. R. Duffy, J. Feeney, and A. K. Holliday *J. Chem. Soc.* 1144–1147 (1962).

41. D. F. Shriver and M. A. Drezdon *The Manipulation of Air-Sensitive Compounds;* Wiley–Interscience: New York, Second ed.; 1986.

42. M. J. Frisch, G. W. Trucks, H. B. Schlegel, P. M. W. Gill, B. G. Johnson, M. A. Robb, J. R. Cheeseman, T. Keith, G. A. Petersson, J. A. Montgomery, K. Raghavachari, M. A. Al-Laham, V. G. Zakrzewski, J. V. Ortiz, J. B. Foresman, J. Cioslowski, B. B. Stefanov, A. Nanayakkara, M. Challacombe, C. Y. Peng, P. Y. Ayala, W. Chen, M. W. Wong, J. L. Andres, E. S. Replogle, R. Gomperts, R. L. Martin, D. J. Fox, J. S. Binkley, D. J. Defrees, J. Baker, J. P. Stewart, M. Head-Gordon, C. Gonzalez, and J. A. Pople "Gaussian 94, Revision C.2", Gaussian, Inc., Pittsburgh PA, 1995.

43. P. J. Hay and W. R. Wadt *J. Chem. Phys.* **82,** 284 (1985).

44. P. J. Hay and W. R. Wadt *J. Chem. Phys.* **82,** 270 (1985).

45. P. J. Hay and W. R. Wadt *J. Chem. Phys.* **82,** 299 (1985).

46. T. H. Dunning and P. J. Hay *Modern Theoretical Chemistry;* Plenum: New York, 1976.

47. T. H. Dunning *J. Chem. Phys.* **66,** 1382 (1977).

48. A. J. Sadlej *Theor. Chim. Acta* **81,** 339–354 (1992).

49. A. C. McLean and G. S. Chandler *J. Phys. Chem.* **72,** 5639 (1980).

50. T. H. Dunning *J. Chem. Phys.* **55,** 716–723 (1971).

51. S. Huzinaga *J. Chem. Phys.* **42,** 1293–1302 (1965).

52. P. A. A. Klusener, L. Brandsma, H. D. Verkruijsse, P. von Ragué Schleyer, T. Friedl, and R. Pi *Angew. Chem. Int. Ed. Engl.* **25,** 465 (1986).

53. K. W. Greenlee and A. L. Henne *Inorganic Syntheses* **2,** 128–135 (1946).

54. W. Wolfsberger and H. Schmidbaur *Synth. Inorg. Metal-Org. Chem.* **4,** 149 (1974).

55. H. F. Klein *Inorganic Syntheses* **18,** 138 (1978).

56. W. Sawodny *Z. Anorg. Allg. Chem.* **368,** 284–292 (1969).

57. R. Köster, D. Simić, and M. A. Grassberger *Liebigs Ann. Chem.* **739,** 211–219 (1970).

58. H. Schmidbaur, H. Stühler, and W. Vornberger *Chem. Ber.* **105,** 1084–1086 (1972).

59. N. Flitcroft and H. D. Kaesz *J. Am. Chem. Soc.* **85,** 1377 (1963).

60. E. Krause *Ber. dtsch. Chem. Ges.* **62,** 1877 (1929).

61. H. Gilman and R. G. Jones *J. Am. Chem. Soc.* **72,** 1760 (1950).

62. G. Grüttner and E. Krause *Ber. dtsch. Chem. Ges.* **49,** 1415 (1916).

63. J. D. Kennedy, W. McFarlane, and G. S. Pyne *J. Chem. Soc., Dalton Trans.* 2332 (1977).

64. R. F. Chambers and P. C. Scherer *J. Am. Chem. Soc.* **48,** 1054 (1926).

65. W. C. Still *J. Am. Chem. Soc.* **100,** 1481 (1978).

66. R. E. Dessey, W. Kitching, and T. Chivers *J. Am. Chem. Soc.* **88,** 453 (1966).

67. H. J. Emeléus and S. F. A. Kettle *J. Am. Chem. Soc.* 2444–2448 (1958).

68. C. Tamborski, F. E. Ford, and E. J. Soloski *J. Org. Chem.* **28,** 237–239 (1963).

69. C. Tamborski, F. E. Ford, and E. J. Soloski *J. Org. Chem.* **28,** 181 (1963).

70. T. Birchall and A. Pereira *J. Chem. Soc., Chem. Comm.* 1150 (1972).

71. R. E. Wasylishen and N. Burford *Can. J. Chem.* **65,** 2707 (1987).

72. T. Birchall and A. R. Pereira *J. Chem. Soc., Dalton Trans.* 1087–1092 (1975).

73. H. Schumann and S. Ronecker *Z. Naturforsch.* **22,** 452–3 (1967).

74. A. J. Cormack "The Hydrides of Tin", Fourth Year Project Report, Department of Chemistry, The University of Edinburgh, 1993.

75. T. N. Mitchell and G. Walter *J. Organometal. Chem.* **121,** 177–184 (1976).

76. J. B. Foresman and Æ. Frisch *Exploring Chemistry with Electronic Structure Methods;* Gaussian, Inc.: Pittsburgh, 2nd ed.; 1996.

77. C. R. Pulham *Studies of the Hydrides of the Heavier Group III Elements,* Thesis, The University of Oxford, 1991.

78. J. D. Kennedy, W. McFarlane, G. S. Pyne, and B. Wrackmeyer *J. Chem. Soc., Dalton Trans.* 386–390 (1975).

79. T. N. Mitchell and G. Walter *J. Chem. Soc., Perkin II* 1842–1847 (1977).

80. J. B. Hendrickson, M. L. Maddox, J. J. Sims, and H. D. Kaesz *Tetrahedron* **20,** 449–459 (1964).

81. H. Schmidbaur, W. Buchner, and D. Scheutzow *Chem. Ber.* **106,** 1251–1255 (1973).

82. K. Hildenbrand and H. Dreeskamp *Z. Naturforsch.* **28B,** 128 (1973).

83. B. E. Mann *J. Chem. Soc., Perkin II* **1,** 30–34 (1972).

84. C. J. Pouchert and J. Behnke, Eds.; *The Aldrich Library of C and H FT NMR spectra;* Aldrich Chemical Co.: Milwaukee, 1993.

85. T. A. K. Al-Allaf *J. Organometal. Chem.* **306,** 337–346 (1986).

86. M.-R. Kula, E. Amberger, and K.-K. Mayer *Chem. Ber.* **98,** 634–637 (1965).

87. J. R. Webster, M. M. Millard, and W. L. Jolly *Inorg. Chem.* **10,** 879–883 (1971).

88. E. Amberger *Angew. Chem.* **72,** 78–79 (1960).

89. W. L. Jolly and J. R. Webster *Inorg. Chem.* **10,** 877–879 (1971).

90. B. J. Aylett *Progr. Stereochem.* **4,** 213 (1969).

91. H. Bürger and M. Betzel *Z. Naturforsch.* **40a,** 989–994 (1985).

92. M. Betzel, H. Bürger, and A. Rahner *Z. Naturforsch.* **41a,** 1009–1014 (1986).

93. H. Bürger, M. Betzel, and P. Schulz *J. Mol. Struct.* **121,** 218–235 (1987).

94. L. C. Krisher, R. A. Gsell, and J. M. Bellama *J. Chem. Phys.* **54,** 2287–2288 (1971).

95. S. N. Wolf, L. C. Krisher, and R. A. Gsell *J. Chem. Phys.* **54,** 4605–4611 (1971).

96. S. N. Wolf, L. C. Krisher, and R. A. Gsell *J. Chem. Phys.* **55,** 2106–2114 (1971).

97. D. C. McKean *J. Mol. Struct.* **113,** 251–266 (1984).

98. T. Birchall and V. Manivannan *J. Chem. Soc., Dalton Trans.* 2671–2675 (1985).

99. N. A. Matwiyoff and R. S. Drago *Inorg. Chem.* **3,** 337 (1964).

100. J. R. Holmes and H. D. Kaesz *J. Am. Chem. Soc.* **83,** 3904 (1961).

101. W. L. Jolly *J. Am. Chem. Soc.* **83,** 335–337 (1961).

102. A. G. Davies and P. J. Smith "Tin". In *Comprehensive Organometallic Chemistry,* Vol. 2; E. W. Abel, G. Wilkinson, and F. G. A. Stone, Eds.; Pergamon Press: Oxford, 1982.

103. G. Güttner *Chem. Ber.* **50,** 1808 (1917).

104. G. Wittig, E. J. Meyer, and G. Lange *Liebigs Ann. Chem.* **571,** 167 (1951).

105. C. Radek "Mass Spectrum Pattern Simulation, version 1.2", 1994.

106. M. Fink and A. Ross *International Tables for Crystallography;* International Union of Crystallography: Reidel, Dordrecht, 1983.

107. H. C. Clark, R. J. O'Brien, and J. Trotter *J. Chem. Soc.* 2332-2337 (1964).

108. E. O. Schlemper and W. C. Hamilton *Inorg. Chem.* **5,** 995 (1966).

109. J. Cosier and A. M. Glazer *J. Appl. Crystallogr.* **19,** 105 (1986).

110. R. C. B. Copley, A. C. Goeta, C. W. Lehmann, J. C. Cole, D. S. Yuft, J. A. K. Howard, and J. M. Archer *J. Appl. Crystallogr.* **30,** 413 (1997).

111. G. M. Sheldrick "SHELXTL V.5", University of Gottingen, 1995.

112. D. A. Fletcher, R. F. McMeeking, and D. Parkin *Chem. Inf. Comput. Sci.* **36,** 746–749 (1996) We wish to acknowledge the use of the EPSRC's Chemical Database Service at Daresbury.

113. F. H. Allen and O. Kennard *Chemical Design Automation News* **8,** 1 & 31–37 (1993) 3D Search and Research using the Cambridge Structural Database.

114. A. G. Davies, H. J. Milledge, D. C. Puxley, and P. J. Smith *J. Chem. Soc. A* 2862 (1970).

115. V. I. Shcherbakov, I. K. Grigoreva, G. A. Razuvaev, L. N. Zakharov, R. I. Bochkova, and Y. T. Struchkov *J. Organometal. Chem.* **319,** 41 (1987).

116. E. Krause *Chem. Ber.* **51,** 1447 (1918).

117. J. L. Lefferts, K. C. Molloy, M. B. Hossain, D. van der Helm, and J. J. Zuckerman *J. Organometal. Chem.* **240,** 349–361 (1982).

118. H.-J. Bestmann and R. Zimmermann . In *Methoden der Organischen Chemie*; Houben-Weyl-Müller, Ed.; Thieme-Verlag: Stuttgart, 1982.

119. I. Gosney and A. G. Rowley . In *Organophosphorus Reagents in Organic Synthesis*; J. I. Cadogan, Ed.; Academic: London, 1979.

120. B. E. Maryanoff and A. B. Reitz *Chem. Rev.* **89,** 863–927 (1989).

121. S. M. Bachrach *J. Org. Chem.* **57,** 4367–4373 (1992).

122. H. Schmidbaur, J. Jeong, A. Schier, W. Graf, D. L. Wilkinson, and G. Müller *New J. Chim.* **13,** 341 (1989).

123. A. S. Batsanov, M. G. Davidson, J. A. K. Howard, S. Lamb, and C. Lustig *J. Chem. Soc., Chem. Comm.* 1791 (1996).

124. H. Schmidbaur and W. Trönich *Chem. Ber.* **101,** 595–603 (1968).

125. H. Schmidbaur, A. Schier, C. M. F. Frazao, and G. Müller *J. Am. Chem. Soc.* **108,** 976 (1986).

126. E. A. V. Ebsworth, T. E. Fraser, and D. W. H. Rankin *Chem. Ber.* **110,** 3494–3500 (1977).

127. N. W. Mitzel, D. H. Brown, S. Parsons, P. T. Brain, C. R. Pulham, and D. W. H. Rankin *in press* (1997).

128. A. J. Blake, P. T. Brain, H. McNab, J. Miller, C. A. Morrison, S. Parsons, D. W. H. Rankin, H. E. Robertson, and B. A. Smart *J. Chem. Phys.* **100,** 12280–12287 (1996).

129. N. W. Mitzel, B. A. Smart, A. J. Blake, H. E. Robertson, and D. W. H. Rankin *J. Chem. Phys.* **100,** 9339–9347 (1996).

130. R. M. Ibberson, W. I. F. David, and K. S. Knight "The High Resolution Neutron Powder Diffractometer (HRPD) at ISIS - A User Guide", Technical Report RAL-92-031, Rutherford Appleton Laboratory, 1992.

131. A. K. Cheetham "*Ab initio* Structure Solution with Powder Diffraction Data". In *The Rietveld Method*; R. A. Young, Ed.; Oxford University Press: Oxford, 1993.

132. D. Louër and R. Vargas *J. Appl. Crystallogr.* **15,** 542 (1982).

133. G. S. Pawley *J. Appl. Crystallogr.* **14,** 357 (1981).

134. H. M. Rietveld *Acta. Cryst.* **22,** 151-2 (1967).

135. H. M. Rietveld *J. Appl. Crystallogr.* **2,** 65–71 (1969).

136. R. A. Young "Introduction to the Rietveld Method". In *The Rietveld Method*; R. A. Young, Ed.; Oxford University Press: Oxford, 1993.

137. H. Fleischer, C. R. Pulham, and S. Parsons Unpublished data.

138. A. C. Larson and R. B. von Dreele "GSAS – Generalised Structure Analysis System", LANSCE, MS-H805, Los Alamos National Laboratory Los Alamos, NM 87545 USA.

139. R. B. V. Dreele "Combined X-ray and Neutron Rietveld Refinement". In *The Rietveld Method*; R. A. Young, Ed.; Oxford University Press: Oxford, 1993.

140. E. Dowty "ATOMS for Windows Version 3.2", .

141. D. Viterbo "Solution and Refinement of Crystal Structures". In *Fundamentals of Crystallography*; C. Giacovazzo, Ed.; International Union of Crystallography texts on Crystallography, Oxford University Press: Oxford, 1992; Chapter 5, page 366.

142. Siemens "XP - Interactive Molecular Graphics, Version 5.03", 1994.

143. H. Fleischer and C. R. Pulham Unpublished data.

144. C. J. Holwill Thesis, University of Reading, U. K., 1987.

145. K. Tamagawa, T. Iijima, and M. Kimura *J. Mol. Struct.* **30,** 243 (1976).

146. S. Gundersen and T. G. Strand *J. Appl. Cryst.* **29,** 638 (1996).

147. K. Hagen, R. J. Hobson, C. J. Holwill, and D. A. Rice *Inorg. Chem.* **25,** 3659 (1986).

Courses and Conferences Attended

Postgraduate Lecture Courses :

- Prof. Donald McKean - 'Infra-red Spectroscopy : Practice and Theory'
- University of Edinburgh Inorganic Section meetings 1995-7

Conferences :

- 6th European Symposium on Gas-Phase Electron Diffraction, Firbush Point, Scotland, 19th–23rd June, 1995
- University of Strathclyde Inorganic Chemistry Conference, University of St. Andrews, September, 1996
- Chemistry Research for Britain, London, February 1997
- 7th European Symposium on Gas-Phase Electron Diffraction, Prague, Czech Republic, June 1997
- Universities of Scotland Inorganic Club Conference, University of Edinburgh, September 1997